Nuclear structure and statistical decay properties of closed and near closed shell nuclei

Naeem Ul Hasan Syed

Department of Physics
University of Oslo
February, 2009

Dissertation presented for the degree of
Philosophia Doctor (PhD) in Physics

Series of dissertations submitted to the
Faculty of Mathematics and Natural Sciences, University of Oslo
Nr. 826

ISSN 1501-7710

Cover: Inger Sandved Anfinsen.
Printed in Norway: AiT e-dit AS, Oslo, 2009.

Produced in co-operation with Unipub AS.
The thesis is produced by Unipub AS merely in connection with the
thesis defence. Kindly direct all inquiries regarding the thesis to the copyright
holder or the unit which grants the doctorate.

Unipub AS is owned by
The University Foundation for Student Life (SiO)

Acknowledgement

First and foremost I offer my sincerest gratitude to my supervisors Magne Guttormsen and Sunniva Siem for their continuous guidance and encouragement. They helped me a lot in developing scientific skills, and were always available to provide guidance and discussion whenever needed. Without their advice and persistent help this dissertation would not have been possible.

The nuclear physics group at the University of Oslo deserves my deep appreciation. Within the group I am much indebted to the Ann-Cecilie Larsen for her contributions and suggestions. She nourished the progress of this work at both scientific and personal level. Special thanks to John Rekstad, Finn Ingebretsen and Stein Ødegård for taking shifts during the experiments. I thank also other members of the group; Alexander Bürger, Hilde T. Nyhus, and Heidi K. Toft who were involved in the discussion process of this thesis.

Outside the University of Oslo I am very thankful to Alexander Voinov and Andreas Schiller from Ohio University. They have been involved in the discussion and the proofreading phase of this work. I would also like to thank Tom Lönnroth from Åbo Akademi for his contribution during the experiments.

The Oslo Cyclotron Laboratory is the main experimental apparatus used in this thesis. To the operation engineers of the laboratory, Eivind A. Olsen and Jon C. Wikne, I express my gratitude for their efforts in making the cyclotron running smoothly and continuously during the experiments.

I am grateful to my cousin Aamer M. Syed and my friends Akbar A. Khan, Asif Hassan, and Munib Sarwar for their moral support and for keeping the enthusiasm alive in me.

I wish to thank my parents M. Afzal Shah and Anees Akhtar, my father- and mother-in-law G. Musa Syed and Memmona Syed, my sister Sadia Najaf, and my brother Suleman A. Syed for their affectionate love and all their prayers for me. Last, but not least, I would like to thank my wife Rubab Syed and my one year old daughter Manahil F. Syed. Your love, understanding, and patience sustained me through to the end of my PhD. Thank you.

Contents

List of Figures

Chapter 1

Introduction

Understanding the structure of the nucleus from its basic constituents is a great challenge. The nuclear structure can be interpreted in terms of nucleon-nucleon interactions (derived from nucleon-nucleon scattering phase shifts and effective field theory) applied to the nuclear many-body problem. Exciting the nucleus from the regime where one can follow the configurations and the dynamics of individual nucleons in the nucleus to a regime where a statistical approach is more appropriate, is an important way to understand more complicated structures. The experimental techniques for heating the nuclei may include the light ion reactions with one charged ejectile and heavy ion collision reactions. The light ion reaction is preferable over heavy ion collision since the populated excited states lie in a narrower spin window and thus prevents large admixtures of collective contributions.

At the low excitation energy the nucleus is excited to levels, characterized by energy, spin and parity. These levels are discrete and the level density can be determined by direct counting. However, at higher excitation energy regions (so called quasi-continuum regime) the levels become so dense that the individual levels cannot be resolved and become undeterminable by direct spectroscopic methods. Instead, it is more appropriate to employ statistical models by averaging the number of levels at a given excitation energy. Hans Bethe, in his work [1] described the simplest expression for the level density in the Fermi-gas model by considering the nucleus as a cloud of non-interacting fermions. A number of phenomenological extensions were made to incorporate the shortcomings of the Bethe's approach like the back-shifted Fermi gas model, which simulates the shell and pair correlation effects.

The closed shell nuclei, within the description of the shell model [2], have filled major shells, corresponding to the proton and neutron numbers equal to magic numbers: Z or N = 2, 8, 20, 28, 50, 82, and 126. Nuclei close to these magic numbers change their nuclear structure abruptly, and the statistical description of

their properties may be less favorable.

The nuclear level density is an important quantity for revealing the statistical properties of the nucleus. This is a basic parameter in the Hauser-Feshbach calculations of reaction cross-sections [3], and in the models of accelerator driven transmutation of nuclear waste. The counting of discrete levels [4] is restricted to the low excitation energies, where the experimental resolution is high enough to resolve the individual lines in the spectra. At energies close to the neutron separation energy, the level density can be extracted from the average level spacings observed in neutron-resonance capture [5]. However, at other excitation energies the experimental information is scarce.

The γ-ray strength function is another important statistical quantity describing the average electromagnetic properties of an excited nucleus. In general, the γ-ray emission in an excited nucleus has to compete with other decay modes like particle-emission and fission. However, our focus will mainly be on the γ-decay in the excitation regions below the particle threshold. The strength functions can be deduced from the neutron capture and photonuclear reactions. Since the γ-decay depends on the number of accessible levels, the results are dependent on our knowledge of the level density.

The nuclear physics group at the Oslo Cyclotron Laboratory has developed a method (the Oslo method) to extract level density and γ-ray strength function, simultaneously. The extraction of these quantities is based on the γ-ray energy distribution from initial excitation energies. The experimental method covers an excitation energy region between the ground state and the neutron (proton) binding energy [6, 7, 8]. This unique technique has provided experimental evidence for the sequential breaking of nucleon Cooper pairs [9] and an M1 scissors mode pygmy resonance in rare-earth nuclei [10, 11]. Also, a strongly enhanced strength function at low γ energies has been discovered in several Fe and Mo isotopes [12, 13].

The main aim of the present thesis is to extend the application of the Oslo method to the closed and near closed shell nuclei. It is known that in general the level densities are significantly lower for light nuclei and nuclei in the vicinity of closed shells. Here, the large γ-ray intensity fluctuations and the insufficient averaging over nuclear levels may introduce non-statistical effects. Therefore, exploring the level densities and γ-ray strength functions in these nuclei would be interesting. It is also desirable to investigate the development of these average quantities while going away from doubly magic to single magic nuclei. The nuclei that have been studied in the present thesis are ^{44,45}Sc [14], ^{45}Ti [15], ^{50,51}V [16], and $^{205-208}$Pb [17]. The chain of $A = 205 - 208$ lead isotopes are of special interest due to their large $N = 126$ and $Z = 82$ shell gaps. For ^{208}Pb, the gaps prevent the protons and neutrons to participate in creating the level density until the excitation energy is high enough to cross these gaps.

The lighter nuclei investigated in this thesis (^{44,45}Sc, ^{45}Ti, and ^{50,51}V), are

interesting for several reasons. The primary motives are to (i) confirm the low-energy γ-ray enhancements of the strength functions in the light nuclei, and (ii) study the level density dependence of the interplay between crossing shell gaps and breaking Cooper pairs. The light nuclei studied are situated between the 20 and 28 shell gaps, where nuclear structure and dynamics may change considerably as functions of mass number and excitation energy. The scandium nuclei are close to both the $Z = N = 20$ shell gaps. In addition, α-cluster structures are expected to play a role in these nuclei. The vanadium nuclei are influenced by the $Z = 20$ and $N = 28$ shell gaps. The titanium nuclei, on the other hand, are well deformed and are not expected to show large shell effects.

In Chapter 2 a brief description of the experimental setup and data analysis are given. The main steps of the Oslo method and their application to physical spectra are discussed in Chapter 3. The normalization of the Oslo data using the available data from other experiments is described in Chapter 4. In Chapters 5 and 6 a brief description of the level density and the γ-ray strength function are given. Chapter 7 presents three published articles, one accepted article and one draft. Finally, summary and conclusions are given in Chapter 8.

Chapter 2

Experimental Details and Data Analysis

The experiments were performed at the Oslo Cyclotron Laboratory (OCL), University of Oslo, where the MC-35 Scanditronix cyclotron delivered the pulsed proton and ^{3}He-ion beams. A lay-out of the beam lines and target stations is shown in Fig. 2.1. In the present experiments the proton beam was used on the ^{46}Ti target and beams of ^{3}He ions were used on the ^{45}Sc, ^{51}V and ^{206,208}Pb targets. The details on the applied reactions and target specifications are listed in Table 2.1.

In our investigation, the neutron pick-up and inelastic scattering reactions are used. These reactions populate states in a narrow spin window at high intrinsic excitation energies and with only one charged ejectile. This allows the accurate determination of excitation energy of the residual nuclei. The particle-γ coincidence events were recorded for ^{44,45}Sc, ^{45}Ti, ^{50,51}V, and $^{205-208}$Pb nuclei with the CACTUS [18] γ-ray detector system in combination with eight silicon particle telescopes.

The arrangement of the 28 $5'' \times 5''$ NaI(Tl) detectors in a spherical frame is shown in Fig. 2.2. The detectors have a distance of 22 cm to the target, and in order to obtain a good peak-to-total ratio, each detector is collimated as shown in Fig. 2.3. The CACTUS multi-detector array extends a total solid angle of 15% of 4π.

The particle telescopes are placed in vacuum inside the CACTUS detector. They are composed of ΔE and E detectors having a thickness of 140 μm and 1500 μm, respectively. The eight telescopes are placed at a distance of 5 cm from the target in the forward direction, making an angle of 45° with respect to the beam axis. A schematic setup of the particle telescopes is shown in Fig. 2.4. The energy loss per unit length of charged particles in the particle detector depends on both the charge state and the mass of the penetrating particle. Therefore, particles with equal charges and different masses, e.g. ^{3}He, and α and particles having

Target	Enrichment %	Thickness (mg/cm^2)	Reaction	Beam energy (MeV)
^{206}Pb	99.8	4.7	^{206}Pb(^{3}He,^{3}He$'$)^{206}Pb ^{206}Pb(^{3}He,α)^{205}Pb	38
^{208}Pb	99.9	1.4	^{208}Pb(^{3}He,^{3}He$'$)^{208}Pb ^{208}Pb(^{3}He,α)^{207}Pb	38
^{45}Sc†	99.9	3.4	^{45}Sc(^{3}He,α)^{44}Sc ^{45}Sc(^{3}He,^{3}He$'$)^{45}Sc	38
^{51}V†	99.8	2.3	^{51}V(^{3}He,α)^{50}V ^{51}V(^{3}He,^{3}He$'$)^{51}V	30
^{46}Ti†	86.4	1.8	^{46}Ti(p,d)^{45}Ti	32

† Natural targets.

Table 2.1: Targets and reactions used for the experiments studied in this thesis.

equal q/m ratio e.g. deuterons and α's, can easily be distinguished by plotting the energy loss in the ΔE vs. the E detector, as shown in Fig. 2.5. The reaction ejectiles are collimated in order to reduce the uncertainty in the reaction angle and the energy spread. An Al foil of 15 μm thickness is placed in front of the particle detectors to stop low-energy δ electrons. The beam current was limited to $\sim 1-2$ nA to prevent pile-up events in the detectors.

For the runs on the titanium target, a 60% HPGe detector was placed in the backward direction in order to monitor the range of spins populated in the (p,d) reaction, and also to ensure that the correct nuclei were studied by looking for the appearance of well-known γ transitions in the specific nuclei.

2.1 Data analysis

The excited residual nuclei after the direct reaction are assumed to thermalize before the subsequent γ-ray emission. From the known Q-values and reaction kinematics, the ejectile energy can be transformed into the initial excitation energy of the residual nuclei. Using the particle-γ coincidence technique, each γ-ray is assigned to a cascade depopulating the nucleus at given excitation energy. The methodology and data analysis performed are briefly described below.

Each particle and γ-detector is calibrated linearly as:

$$E = a_0 + a_1 \cdot ch, \tag{2.1}$$

where E is the energy corresponding to channel number ch, and a_0 and a_1 are the calibration coefficients. The particle spectra obtained from the front and end

particle detectors are calibrated from the known states in the final nuclei. The particle identification is made from a two dimensional $\Delta E - E$ matrix, as shown in Fig. 2.5. An important feature of this plot is that particles like proton, deuteron, triton, ^{3}He, and α are well separated. By gating on a specific particle type in the $\Delta E - E$ matrix, the particle-γ coincidences for a specific reaction channel are obtained. Gates are also set in the timing spectra of all the NaI(Tl) detectors. The true coincident events are found by gating the prompt time peak and subtracting the random events. A time spectrum for the NaI(Tl) detector in a ^{208}Pb(^{3}He,α)^{207}Pb reaction is shown in Fig. 2.6, where the prompt and random gates are shown. The events falling into the prompt region are incremented, and those that fall into the random region are decremented.

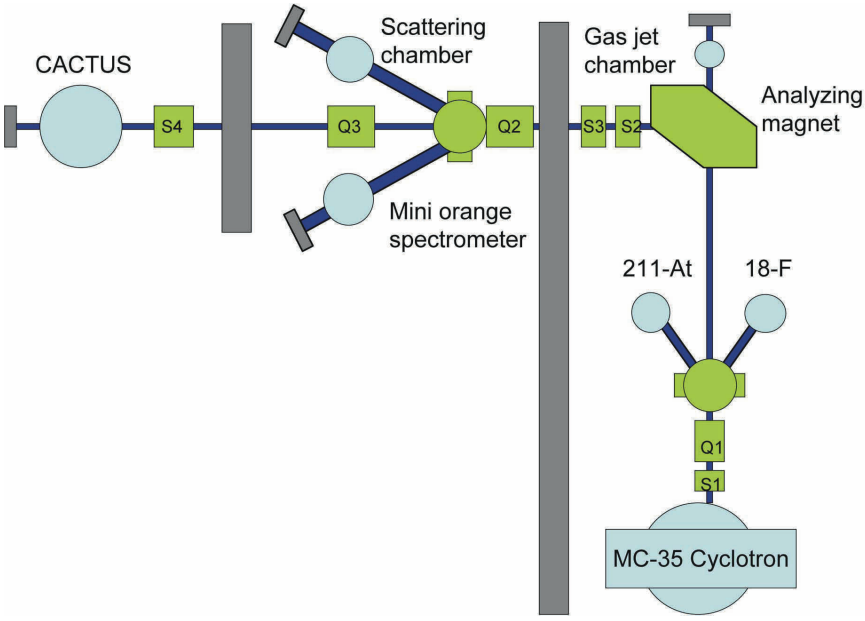

Figure 2.1: Experimental setup at the Oslo Cyclotron Laboratory.

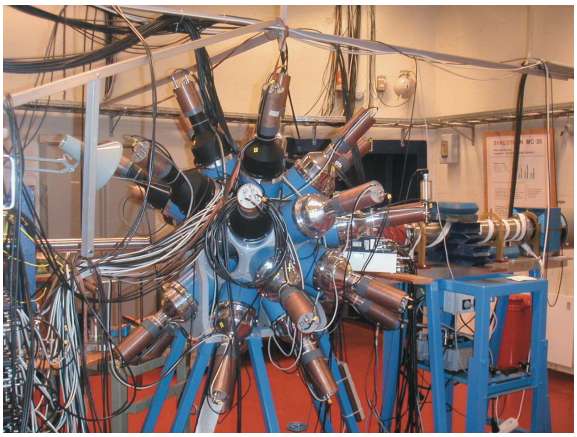

Figure 2.2: The CACTUS multi-detector array, showing the positions of the NaI(Tl) γ-ray detectors.

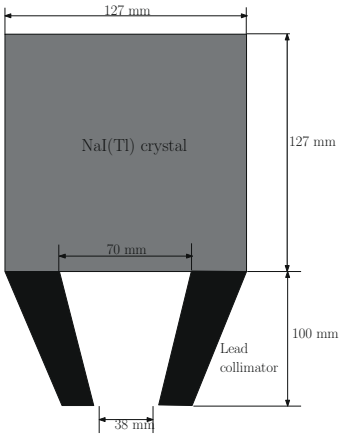

Figure 2.3: A collimated NaI(Tl) detector. The collimator is used so that a better peak-to-total ratio can be achieved.

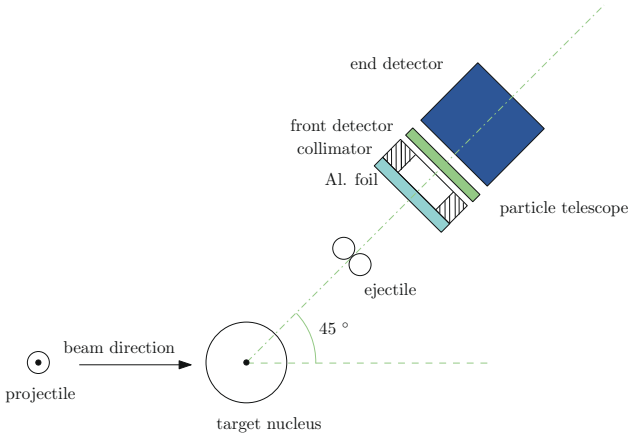

Figure 2.4: Schematic drawing of a Si particle telescope.

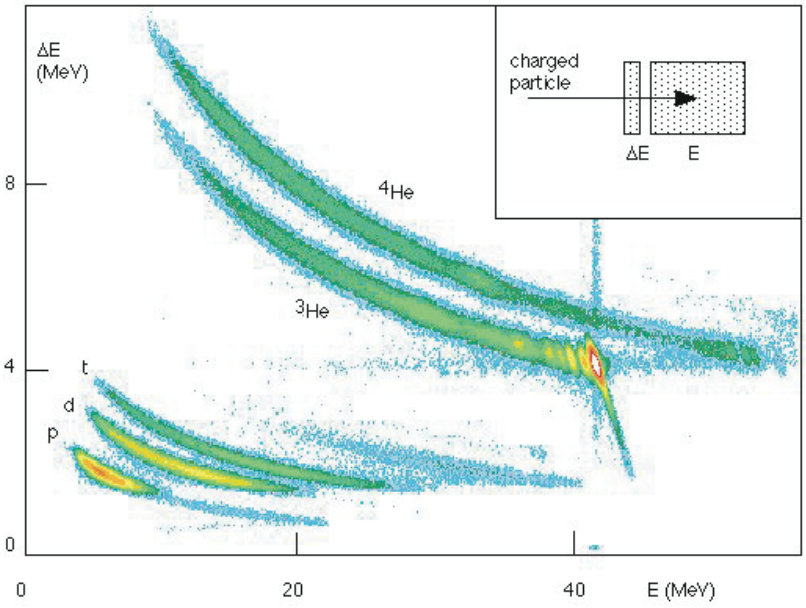

Figure 2.5: A typical $\Delta E - E$ matrix used to identify the ejectile particles in a nuclear reaction.

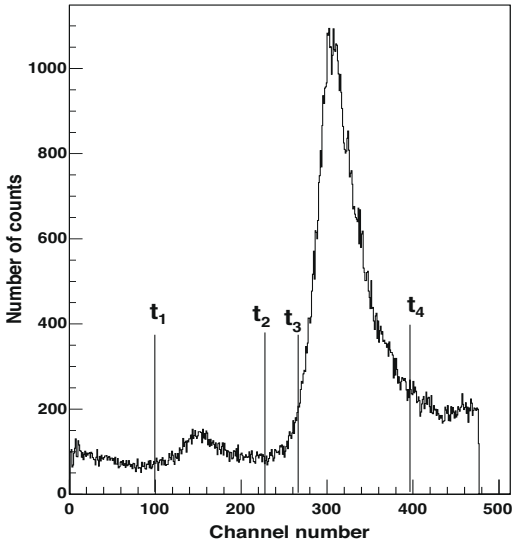

Figure 2.6: Time spectrum between the particle and the NaI(Tl) detector. The true coincident events are the prompt events, which are sorted out by putting gate between the markers t_3 and t_4. The random events are obtained by gating between the t_1 and t_2 markers.

Chapter 3

The Oslo Method

In the previous chapter the method of recording the raw data in a coincidence matrix of ejectile and γ-ray energies, has been briefly described. These coincidence measurements for all excitation energy bins provide us the particle-γ matrix which is the starting point of the Oslo method. The three main steps of the method are; unfolding the γ-ray spectra, extraction of the first generation γ-rays and the factorization of the distribution of primary γ-rays into level density and γ-ray strength function. In the following, these procedures will be briefly discussed.

3.1 Unfolding the γ-ray spectra

The observed γ-ray spectra are not a true representative of the γ-emission. The incident γ-ray that hits a detector interacts mainly in three ways: Compton scattering, photoelectric absorption and pair production. Among these interactions the photoelectric absorption is the one where the incident γ-ray deposits its full energy. The detector response function includes the contributions from all these processes. Therefore, we need to correct for the response functions of the NaI(Tl) γ-ray detectors in order to get true γ-ray spectra.

The response functions of the CACTUS detector array are obtained by doing measurements at monoenergetic γ-ray energies: 122, 245, 344, 662, 1173, 1333, 1836, 4439, 6130 and 15110 keV. For other γ energies the response functions are interpolated. The interpolation of peak structures like photoelectric peak, single and double escape peaks and back-scattered peaks and Compton scattering continuum is made separately and the method has been described in Ref. [6].

In order to unfold the observed γ spectra, the folding iteration method [19] is

used. The folding can be expressed by

$$\begin{pmatrix} f_1 \\ f_2 \\ \vdots \\ f_n \end{pmatrix} = \begin{pmatrix} R_{11} & R_{12} & \cdots & R_{1n} \\ R_{21} & R_{22} & \cdots & R_{2n} \\ \vdots & \vdots & \ddots & \vdots \\ R_{n1} & R_{n2} & \cdots & R_{nn} \end{pmatrix} \times \begin{pmatrix} u_1 \\ u_2 \\ \vdots \\ u_n \end{pmatrix}, \tag{3.1}$$

where f and u represent the folded and unfolded spectra, respectively and the matrix element R_{ij} represents the response in channel i when the detector is hit by γ-rays having energy corresponding to channel j. The iteration procedure takes the raw spectrum as a first trial function. The spectrum is then folded and a new trial function is obtained by adding the difference spectrum to the original trial function. The new trial function is folded again to obtain a new trial function. The iteration is continued until the folded spectrum becomes equivalent to the raw spectrum, subsequently giving us the unfolded γ-ray spectrum. A straight forward way to unfold is by inversion of $\mathbf{R}$ and solving $u = \mathbf{R}^{-1} f$. However, this way of unfolding gives large fluctuations due to unstabilities in $\mathbf{R}^{-1}$.

Instead we adopt an iteration proceedure, the Compton subtraction method [6], that subtracts the Compton background from the observed spectrum while preserving the fluctuations in the original spectra without introducing any further spurious fluctuations. The method takes the unfolded spectrum u, resulting from the previous folding iteration method, as input. The contributions from full energy u_f, single escape u_s, double escape u_d and annihilation process u_a are separated from the unfolded spectrum. Each of these contributions is then smoothed with appropriate energy resolution in order to achieve the experimental energy resolution. The Compton-scattering events $u_c(i)$ in corresponding channel i are obtained by subtracting the peak structures spectra from the observed spectrum $r(i)$;

$$u_c(i) = r(i) - [u_f(i) + u_s(i - i_{511}) + u_d(i - i_{1022}) + u_a(i_{511})]. \tag{3.2}$$

Here i_{511} and i_{1022} represent the channels with energies 511 and 1022 keV, respectively. It is notable that all annihilation events are registered in i_{511} since these 511 keV annihilation γ-ray originate in the detector surroundings. The Compton background makes large contribution to the detector response. Its extraction from the raw spectrum reduces the fluctuations caused by the folding iteration method. However, the extracted Compton spectrum $u_c(i)$ shows strong oscillations due to statistical fluctuations in the observed spectrum. So, it is smoothed with a large energy resolution as Compton scattering process varies slowly with γ-ray energy.

The unfolded spectrum is obtained by subtracting the unwanted peak structures and Compton background from the total raw spectrum:

$$u_{un}(i) = r(i) - [u_c(i) + u_s(i - i_{511}) + u_d(i - i_{1022}) + u_a(i_{511})] \tag{3.3}$$

This new unfolded spectrum has the same staistical fluctuations as the observed spectrum. Finally, including the detector efficiency η_{tot} we get,

$$U_{un}(i) = \frac{u_{un}(i)}{\eta_{tot}} \tag{3.4}$$

An application of the unfolding method described above is shown in Fig. 3.1 for ^{207}Pb. The similarity of the folded and the raw spectra shows the good quality of the method for the specified nucleus.

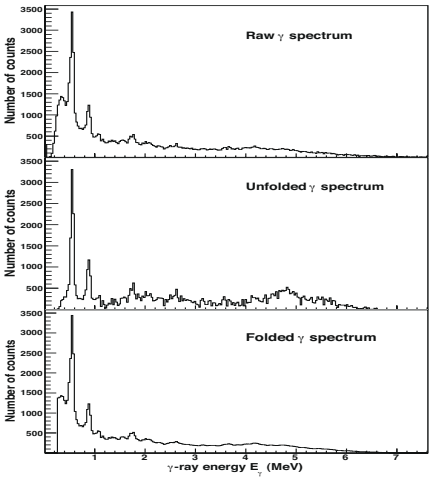

Figure 3.1: Unfolding of the γ-ray spectrum for ^{207}Pb in the excitation region $E = 4.5 - 6.7$ MeV.

3.2 Extraction of the first generation γ-ray spectra

The unfolded spectra contain all generation γ-rays in cascades starting at a certain initial excitation energy E. The OCL group has developed a method [7] to isolate the first generation γ-rays from the decay cascades whose energy distribution reveals essential information on the nuclear structure in the quasi-continuum region.

The method of extraction of primary γ-ray spectra [7] for every excitation energy bin from the unfolded total γ-ray spectra is based on some assumptions. The most important of these is that the γ-ray decay pattern from any excitation energy

bin is independent of the population mechanism of states, i.e. direct population by a nuclear reaction, or population by the γ-decay.

Figure 3.2 illustrates the subtraction method. For each excitation energy bin in a particle-γ matrix there is a γ-ray spectrum f_i. The first generation γ-ray spectrum of a specific excitation energy bin 1 is estimated by subtracting the weighted sum of all lower excitation energy spectra g from the total, unfolded γ-ray spectrum of bin 1 :

$$h = f_1 - g, \tag{3.5}$$

or equivalently,

$$h = f_1 - \sum_i n_i w_i f_i, \tag{3.6}$$

where w_i is the weighting function representing the decay probability from bin 1 to i and corresponds to the first generation γ-ray spectrum. The normalization coefficient n_i can mainly be determined by two methods; singles and multiplicity normalization methods. The singles normalzation uses the singles particle cross-

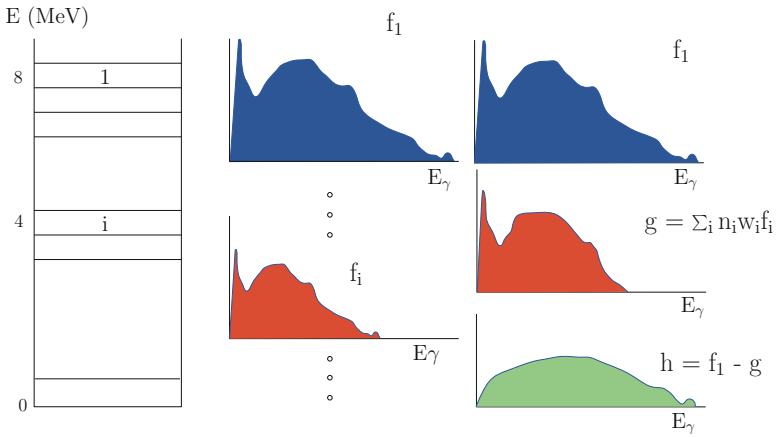

Figure 3.2: The method of first generation γ-rays extraction.

sections such that for bin i the n_i can be written as:

$$n_i = \frac{\sigma_1}{\sigma_i}, \tag{3.7}$$

where σ is the particle cross-section. In the multiplicity normalization, the γ-ray multiplicity M is used to find the normalization coefficient

$$n_i = \frac{M_i A(f_1)}{M_1 A(f_i)}, \tag{3.8}$$

where $A(f_i)$ represents the area of spectrum f_i. Further details of these normalization methods can be found in Ref. [7].

The close relation between the h and w_i allows us to use a trial weight function to find h through a converging iteration proceedure. It has been shown [7] that the shape of the first generation spectrum remains the same after a few iterations for different choices of the trial weight functions. So, the choice of the trial weighting function does not effect the results.

The basic assumption that the γ-decay pattern from an excitation energy bin is independent of the population mechanism, may not be fulfilled if the direct reaction at lower excitation bins do not favour some levels within the excitation energy bin that are populated from above. This situation may cause that some γ-rays are not fully subtracted from the total γ-ray spectrum. The influence of a possible different selectivity of levels at one excitation energy in the direct reaction compared to γ-decay from the higher levels, is expected to be most pronounced when only few levels are present in the excitation bin. These considerations are considerably important in the vicinity of closed shell nuclei, where the level densities are low. Therefore, one must show cautions while applying the Oslo method in such cases.

An unfolded, first generation, and higher generation spectra are shown in Fig. 3.3 for ^{207}Pb in the excitation energy region $E = 4.5 - 6.7$ MeV.

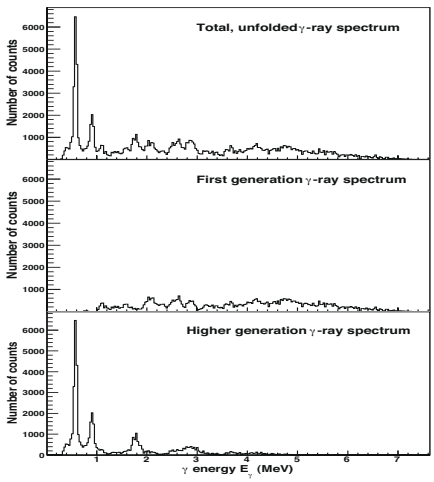

Figure 3.3: Extraction of first generation γ-rays (middle panel) from the total, unfolded spectrum (top panel) by subtracting the second and higher generation γ-rays (bottom panel).

3.3 Disentanglement of level density and γ-ray strength function

The primary γ-ray matrix $P(E,E_\gamma)$ is normalized to unity for every excitation energy bin E. Thus, $P(E,E_\gamma)$ represents the γ-decay probability. This normalized matrix contains information on both the level density and the γ-ray strength function.

The generalized Fermi's golden rule states that the decay probability can be factorized into state density of final states, and a factor depending on the transition matrix element between the initial and final state. Following this rule, we express the γ-decay probabilty from an initial excitation energy E in terms of level density $\rho(E-E_\gamma)$ and γ-ray transmission coefficient $\mathcal{T}(E_\gamma)$:

$$P(E,E_\gamma) \propto \rho(E-E_\gamma) \times \mathcal{T}(E_\gamma). \tag{3.9}$$

According to the Brink-Axel hypothesis [20, 21], the transmission coefficient $\mathcal{T}$ is assumed to be independent of temperature (or excitation energy). The hypothesis states that collective excitations built on excited states have the same properties as those built on the ground state. The average temperature for the nuclei studied is typically below 2 MeV. In addition, the temperature is believed to vary slowly as a function of excitation energy $T \sim \sqrt{E_f}$. Thus, the constant temperature approximation for $\mathcal{T}$ in Eq. (3.9) is a reasonable approximation.

The factorization of the primary γ-ray matrix into ρ and $\mathcal{T}$ is determined by a global least χ^2 fit to the primary γ-ray matrix. An example to illustrate the quality of the fit is shown in Fig. 3.4, where a least χ^2 fit has been compared with the experimental primary γ-ray matrix in the ^{208}Pb(^{3}He,α)^{207}Pb reaction. The calculated primary γ-ray spectra are obtained by:

$$P_{\mathrm{th}}(E,E_\gamma) = \frac{\rho(E-E_\gamma)\mathcal{T}(E_\gamma)}{\sum_{E_\gamma=E_\gamma^{min}}^{E} \rho(E-E_\gamma)\mathcal{T}(E_\gamma)}. \tag{3.10}$$

The error bars of the data points in Fig. 3.4 take into account only statistical uncertainties. This means that any systematic error occurring as a result of possible shortcomings of the first generation method and a weak dependence of $\mathcal{T}$ on the excitation energy is not included. In this context the comparison shown in Fig. 3.4 works satisfactorily for the ^{207}Pb nucleus.

Equation (3.9) gives an infinite number of solutions for ρ and $\mathcal{T}$. Applying the transformation to one arbitrary solution [8]

$$\tilde{\rho}(E-E_\gamma) = A\exp[\alpha(E-E_\gamma)]\rho(E-E_\gamma), \tag{3.11}$$

$$\tilde{\mathcal{T}}(E_\gamma) = B\exp(\alpha\, E_\gamma)\, \mathcal{T}(E_\gamma), \tag{3.12}$$

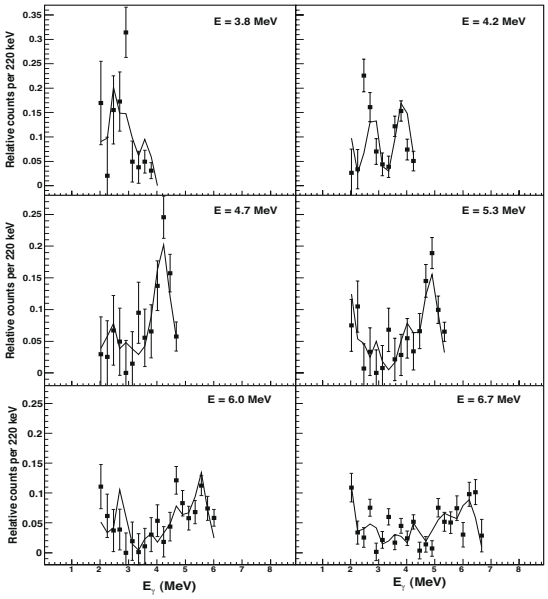

Figure 3.4: Comparison of the normalized experimental primary γ-ray spectra for the ^{208}Pb(^{3}He,α)^{207}Pb reaction (data points) at various excitation energies and the fit (solid lines) using the factorization of Eq. (3.9). The excitation energy bins are 220 keV.

one can construct all the solutions. Here A, B and α are the generators of the transformation and are undetermined. These parameters have to be determined using independent experimental information to get the physically most relevant solution.

Chapter 4

Absolute Normalization of the Experimental Results

The $\rho(E)$ and $\mathcal{T}(E_\gamma)$ functions in the previous chapter are obtained from the χ^2 minimization, giving only one solution out of many possible solutions that could reproduce the primary γ-ray matrix. In order to get the most relevant solutions, the determination of the transformation generators α, A, and B of Eqs. (3.11) and (3.12) are necessary.

4.1 Normalization of level density

The parameters α and A correspond to the slope and the absolute value of the level density, respectively. The level density ρ is normalized to the known discrete levels at low excitation energies [4] and to the level density deduced from neutron resonance spacing data at the neutron separation energy S_n. In Fig. 4.1 the normalization procedure for ^{205}Pb has been illustrated. The level density at S_n has been deduced from the Fermi-gas expression [22] using the available proton or neutron-resonance spacing data [5] and assuming that positive and negative parities contribute equally to the level density at S_n. For $\ell = 0$ capture (s-waves), the level density ρ_0 becomes:

$$\rho_0(S_n) = \frac{2\sigma^2}{D_0}[I_t \exp(-I_t^2/2\sigma^2) + (I_t+1)\exp(-(I_t+1)^2/2\sigma^2)]^{-1}. \qquad (4.1)$$

For $\ell = 1$ capture (p-waves), the above equation is modified as:

$$\begin{aligned}\rho_1(S_n) = \frac{2\sigma^2}{D_1}[&(I_t-1)\exp(-(I_t-1)^2/2\sigma^2)\\ &+ I_t\exp(-I_t^2/2\sigma^2)\\ &+ (I_t+1)\exp(-(I_t+1)^2/2\sigma^2)\\ &+ (I_t+2)\exp(-(I_t+2)^2/2\sigma^2)]^{-1}.\end{aligned} \tag{4.2}$$

The quantities D_0 and D_1 are the average s- and p-wave resonances spacing. The parameter I_t is the spin of the target nucleus. For target spin $I_t = 0$, the first two

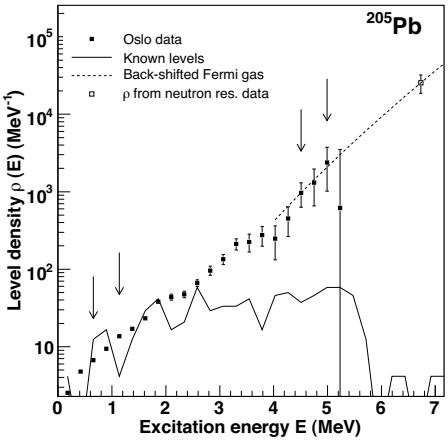

Figure 4.1: Normalization of the level density (data points) for ^{205}Pb. At low excitation energies the data points are normalized between the arrows, to the known levels (solid lines). At higher excitation energies the data points are normalized with the Fermi-gas level density (dotted lines) scaled to the level density at S_n (open square) deduced from Eq. (4.2).

terms inside the bracket of Eq. (4.2) should be omitted and for spin $I_t = 1/2$ and 1, only the first term should be omitted. The σ is the spin-cut off parameter, which accounts for the spin distribution and can either be determined by [23]:

$$\sigma^2 = 0.0146A^{5/3}\frac{1+\sqrt{1+4a(E-E_1)}}{2a} \tag{4.3}$$

or by combining the Eqs. (9) and (11) of Ref. [22] i.e.

$$\sigma^2 = 0.0888A^{2/3}\sqrt{a(E-E_{\rm pair})}, \tag{4.4}$$

where E_1 is the back shift parameter (values taken from [23]) and E_{pair} is the pairing energy correction parameter, evaluated following the description of Ref. [24].

In Fig. 4.1, the excitation energy regions between the arrows are used for normalization. Below E_γ^{min} ($\sim$2 MeV in the present case) the γ-rays are omitted in the extraction procedure such that our data points reach up to $\sim S_n - E_\gamma^{min}$. An interpolation is made to fill the gap between the data points and the deduced level density at S_n using the Fermi-gas level density:

$$\rho_{\text{FG}}(U) = \eta \frac{\exp(2\sqrt{aU})}{12\sqrt{2}a^{1/4}U^{5/4}\sigma}, \tag{4.5}$$

where a is the level density parameter, $U = E - E_1$ is the intrinsic excitation energy and η is a constant introduced to adjust ρ_{FG} to the deduced level density at S_n.

4.2 Normalization of the transmission coefficient

The γ-ray transmission coefficient $\mathcal{T}(E_\gamma)$ is connected to the electromagnetic decay properties of the nucleus. It is expressed as the sum of all the γ-ray strength functions f_{XL} for transitions having energy E_γ, electromagnetic character X, and multipolarity L

$$\mathcal{T}_{XL}(E_\gamma) = 2\pi \sum_{XL} f_{XL} E_\gamma^{2L+1}. \tag{4.6}$$

The slope correction $\exp(\alpha E_\gamma)$ of Eq. (3.12) is already included in $\mathcal{T}$ during the normalization of level density. However, the absolute normalization of the transmission coefficient $\mathcal{T}$ is determined by the parameter B. The determination of B requires other experimental data and will be described below.

In Fig. 4.2 is shown the transmission coefficient $\mathcal{T}$ in arbitray units for ^{205}Pb. By assuming that the γ-decay in the quasi-continuum region is mainly governed by dipole transitions and that the number of accessible levels of positive and negative parity are equal for any energy and spin, $\mathcal{T}$ can be expressed as

$$B\mathcal{T}(E_\gamma) = 2\pi(f_{E1} + f_{M1})E_\gamma^3. \tag{4.7}$$

The experimental data on the average total radioactive width $\langle\Gamma_\gamma\rangle$ of neutron resonances at S_n can be used to determine B. In Ref. [25] the average total radiative width $\langle\Gamma_\gamma(E,I,\pi)\rangle$ of levels with excitation energy E, spin I, and parity π is given by

$$\langle\Gamma_\gamma(E,I,\pi)\rangle = \frac{1}{2\pi\rho(E,I,\pi)} \sum_{XL} \sum_{I_f,\pi_f} \int_0^E \mathrm{d}E_\gamma \mathcal{T}_{XL}(E_\gamma)\rho(E - E_\gamma, I_f, \pi_f). \tag{4.8}$$

The summations and integration run over all final levels with spin I_f and parity π_f, accessible by the γ-decay with energy E_γ, electromagnetic character X and multipolarity L. By assuming the dipole radiation as a significant contributor and equal-parity distribution, one can determine the average total radiative width $\langle\Gamma_\gamma\rangle$ for neutron resonances by combining Eqs. (4.7) and (4.8). For s-wave neutron resonances the populated spins are $I = |I_t \pm 1/2|$ and for p-wave neutron resonances the populated spins are $|I_t \pm 1/2 \pm 1|$, where I_t represents the spin of the target nucleus in the (n,γ) reaction. The parity is determined by the target parity π_t as $\pi = \pi_t(-1)^l$. The $\langle\Gamma_\gamma\rangle$ at S_n can now be written as

$$\langle\Gamma_\gamma(S_n,I)\rangle = \frac{1}{4\pi\rho(S_n,I,\pi)}\int_0^{S_n} \mathrm{d}E_\gamma B\mathcal{T}(E_\gamma)\rho(S_n-E_\gamma)\sum_{J=-1}^{1} g(S_n-E_\gamma,I+J). \tag{4.9}$$

The spin distribution of level density is given by [22]

$$g(E,I) = \frac{2I+1}{2\sigma^2}\exp[-(I+1/2)^2/2\sigma^2], \tag{4.10}$$

which is normalized to $\sum_I g(E,I) \sim 1$. The experimental value of $\langle\Gamma_\gamma(S_n,I)\rangle$ is then the weighted sum of contributions with I according to Eq. (4.9).

The methodological difficulties in the primary γ-ray extraction prevent the determination of $\mathcal{T}$ below a certain E_γ^{min}. The extrapolation of $\mathcal{T}$ is made by an exponential form, as shown in Fig. 4.2, in order to calculate the integral of Eq. (4.9). The contribution of this extrapolation in Eq. (4.9) is not more than 15%, so the possible error induced by the extrapolation is of minor importance.

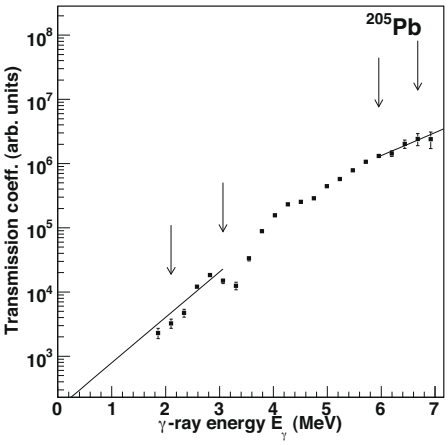

Figure 4.2: Transmission coefficient $\mathcal{T}$ in arbitrary units for ^{205}Pb. An exponential function (solid line) is fitted to the data points between the arrows at low and high excitation energies.

Chapter 5

Level Density and Thermodynamic Properties

5.1 Level density

The nuclear level density is defined as the number of energy levels accessible at a specific excitation energy, within a given energy bin. It is a characteristic property of every nucleus that the level density increases rapidly with excitation energy. Bethe [1] introduced his Fermi-gas description of level density $\rho(E)$ to predict the experimental data by

$$\rho(E) = \frac{\sqrt{\pi}\exp(2\sqrt{aE})}{12a^{1/4}E^{5/4}}, \tag{5.1}$$

where a is the level density parameter given by

$$a = \frac{\pi^2}{6}(g_p + g_n). \tag{5.2}$$

Here, g_p and g_n are single particle level density parameters for protons and neutrons, respectively. The major assumptions of the model include independent particle motion and equidistant spacings of single-particle states. Bethe's formula predicts the general exponential increase in level density with excitation energy and with mass number A. However, it did not consider the shell effects and odd-even effects of the nuclei. Therefore, the phenomenological modifications were proposed to this model, which take into account features like shell effects and residual interactions. The standard Fermi-gas level density is expressed by

$$\rho(U,J) = \frac{\exp(2\sqrt{aU})}{12\sigma\sqrt{2}a^{1/4}U^{5/4}}\frac{(2J+1)}{2\sigma^2}\exp\left(\frac{-(J+1/2)^2}{2\sigma^2}\right), \tag{5.3}$$

where U is the effective shifted excitation energy, and σ is the spin-cut off parameter (see Eqs. (4.3) and (4.4). Gilbert and Cameron [22] proposed a pairing correction parameter E_{pair} as a shift in excitation energy, such that $U = E - E_{\text{pair}}$.

Gilbert and Cameron [22] also developed a constant temperature level density formula, given by

$$\rho(E) = \frac{1}{T} \exp\left(\frac{E - E_0}{T}\right) \tag{5.4}$$

for low excitation energies. The constant nuclear temperature T and energy shift E_0 are the free parameters, fitted to the experimental data at low and high excitation energies in order to give absolute values of the level density.

Another approach of describing the experimental data is the back-shifted Fermi-gas model (BSFG). The level density parameter a and energy shift E_1 are considered as free parameters in this model. This approach covers a wider range of energies allowing a reasonable fit to the experimental data. T. von Egidy and D. Bucurescu [23] determined a new set of phenomenological level density parameters for the BSFG and CT level density models, by fitting experimental data to levels at low excitation energy and to neutron resonance spacings at the neutron binding energies.

All the above approaches of determining level densities are semi-empirical and based on experimental data. Although they give reasonable agreement with the experimental data, yet they are unable to predict any fine structures in the level density caused by pair breaking, shell effects etc.

5.2 Thermodynamics

Thermodynamic quantities in nuclear physics depend on statistical properties in the nuclear many body system and may reveal phase transitions. In a microscopic system there are fewer particles that make up the system compared to a macroscopic system. Therefore, the application of thermodynamical and statistical methods must be done with care.

The level density as a function of excitation energy is the starting point to establish the thermal quantities like entropy and nuclear temperature, of a nuclear system. The multiplicity of states Ω_s, the number of physically accessible microstates, is related to the level density and average spin $\langle J(E) \rangle$ by

$$\Omega_s(E) \propto \rho(E) \left[2\langle J(E) \rangle + 1\right]. \tag{5.5}$$

The $2J+1$ degeneracy of magnetic sub-states is not included during the extraction of our level density. Therefore, it does not correspond to the true multiplicity of

states, and we use multiplicity Ω_l based on experimental level density as:

$$\Omega_l(E) \propto \rho(E). \tag{5.6}$$

The micro-canonical ensemble describes an isolated nuclear system with fixed energy and size. Due to the short range of the nuclear force, the nucleus does not exchange its excitation energy with the external environment. According to Ref. [26], the micro-canonical ensemble is the most appropriate statistical ensemble for isloated systems like the nucleus. The entropy $S(E)$ in the micro-canonical ensemble is related to the multiplicity of levels $\Omega_l(E)$ by

$$S(E) = k_B \ln \Omega_l(E), \tag{5.7}$$

where k_B is Boltzmann's constant. The multiplicity can be written as $\Omega_l(E) = \rho(E)/\rho_0$. The normalization constant ρ_0 is adjusted to fulfill the condition of the third law of thermodynamics; $S \to 0$ for $T \to 0$, T being the nuclear temperature. Temperature is assumed to be zero for the ground state of the even-even nucleus, so that $S(E) = 0$ for $E = 0$ in even-even nucleus. The nuclear temperature in a micro-canonical system is defined as:

$$\frac{1}{T(E)} = \frac{\partial S}{\partial E}. \tag{5.8}$$

A finite many-body system, like a nucleus, is characterized by large fluctuations in the thermodynamic observables. It is obvious that small statistical deviations in the entropy S will be enhanced due to the derivation in Eq. (5.8), giving large contributions to the temperature $T(E)$.

Chapter 6

Models of γ-Ray Strength Functions

The γ-ray strength function represents the distribution of average decay probabilities between levels in quasi-continuum as a function of γ-ray energy. It is the measure of average electromagnetic properties of the nucleus. The charge of the protons (Ze) and the magnetic dipole moments of the protons (μ_p) and neutrons (μ_n) are the basic elements for these properties.

Blatt and Weisskopf [27] showed that the square of the γ-ray transition matrix element connecting the compound states is related directly to the average level spacing of the initial states with equal spin and parity. This lead to the description of γ-ray strength function in terms of average partial radiative width $\langle\Gamma_{\gamma if}\rangle$, average level spacing D_i of initial states, and transition energy E_γ, by

$$f_{XL} = \frac{\langle\Gamma_{\gamma if}\rangle}{E_\gamma^{2L+1} D_i}. \tag{6.1}$$

Here f_{XL} is the strength function for electromagnetic character X and multipolarity L. The relation between the γ-ray strength function f_{XL} and transition coefficient $\mathcal{T}_{XL}$ is given by

$$f_{XL} = \frac{1}{2\pi} \frac{\mathcal{T}_{XL}(E_\gamma)}{E_\gamma^{2L+1}}. \tag{6.2}$$

Several models have been developed to determine the γ-ray strength function f_{XL}. The simplest of these is the Standard Lorentzian model (SLO). This model is used to describe the giant electric dipole resonance (GEDR) $E1$, giant magnetic dipole resonance (GMDR) [28] $M1$, and isoscalar giant resonance $E2$ radiations. The SLO model uses the Brink-Axel approach [20, 21], which has been widely used to describe the giant dipole resonances. The SLO model describes the dominant $E1$ strength function by

$$f_{E1}^{\mathrm{SLO}}(E_\gamma) = \frac{1}{3\pi^2\hbar^2c^2} \frac{\sigma_{E1} E_\gamma \Gamma_{E1}^2}{(E_\gamma^2 - E_{E1}^2)^2 + E_\gamma^2 E_{E1}^2}, \tag{6.3}$$

where σ_{E1}, E_{E1}, and Γ_{E1} are the GEDR parameters derived from photoabsorption experiments. The model is independent of the excitation energy and depends only on the transition energy, in accordance with the Brink-Axel hypothesis.

The magnetic dipole $M1$ strength function also plays an important role in the determination of the total γ-ray strength function. The SLO model describes the $M1$ radiation by

$$f_{M1}^{\mathrm{SLO}}(E_\gamma) = \frac{1}{3\pi^2 h^2 c^2} \frac{\sigma_{M1} E_\gamma \Gamma_{M1}^2}{(E_\gamma^2 - E_{M1}^2)^2 + E_\gamma^2 \Gamma_{M1}^2}. \tag{6.4}$$

The contribution from isoscalar $E2$ transition strength is of minor importance, but can be included to the total γ-ray strength function. The $E2$ strength is described in Ref. [5] by

$$f_{E2}^{\mathrm{SLO}}(E_\gamma) = \frac{1}{5\pi^2 \hbar^2 c^2 E_\gamma^2} \frac{\sigma_{E2} E_\gamma \Gamma_{E2}^2}{(E_\gamma^2 - E_{E2}^2)^2 + E_\gamma^2 \Gamma_{E2}^2}. \tag{6.5}$$

The resonance parameters of $M1$ and $E2$ resonances are deduced from the systematics given in Ref. [5].

The experimental data [29] have shown the presence of a non-zero finite strength function at the tail of the GEDR below 2 MeV. The SLO model underestimates extensively the $E1$ strength function for the γ-ray energy $E_\gamma < 1 - 2$ MeV.

Kadmenskiĭ, Markushev, and Furman (KMF) suggested an improved model [30] for the determination of the $E1$ strength function. The KMF model includes the temperature dependent width $\Gamma_k(E_\gamma, T)$ of the GEDR and give a non-zero strength function for $E_\gamma \to 0$. The KMF model describes the $E1$ strength functions at the tail of GEDR by

$$f_{E1}^{\mathrm{KMF}}(E_\gamma) = \frac{1}{3\pi^2 \hbar^2 c^2} \frac{0.7 \sigma_{E1} \Gamma_{E1} E_\gamma \Gamma_k(E_\gamma, T)}{(E_\gamma^2 - E_{E1}^2)^2}, \tag{6.6}$$

where $T = \sqrt{(U/a)}$ is the temperature of the final state, and Γ_k is the energy and temperature dependent width of the GEDR given by

$$\Gamma_k(E_\gamma, T) = \frac{\Gamma_{E1}}{E_\gamma^2}(E_\gamma^2 + 4\pi^2 T^2). \tag{6.7}$$

The KMF model is singular at the resonance energies and is only valid for lower γ energies.

The Generalized Lorentzian model (GLO) [31] is a combined model which describes the GEDRs both at resonance energies and at low γ energies. The model

is described as:

$$f_{E1}^{\mathrm{GLO}}(E_\gamma) = \frac{1}{3\pi^2\hbar^2c^2}\sigma_{E1}\Gamma_{E1} \left\{ \frac{E_\gamma\Gamma_k(E_\gamma,T)}{(E_\gamma^2-E_{E1}^2)^2+(E_\gamma\Gamma_k(E_\gamma,T_f))^2} + 0.7\frac{\Gamma_k(E_\gamma=0,T)}{E_{E1}^3} \right\}. \tag{6.8}$$

In Ref. [32] it has been shown that the GLO model gives a good agreement with the data on average resonance capture (ARC) data and capture cross-sections for selected spherical nuclei. However, in the mass region of strongly deformed nuclei $A = 150-170$, the GLO model underestimates the observed strength functions. Therefore, the enhanced generalized Lorentzian model (EGLO) [5] is developed to determine the γ-ray strength function for the whole mass region. In the EGLO model the temperature and energy dependent width $\Gamma_k(E_\gamma,T)$ of Eq. (6.7) is modified by

$$\Gamma_k(E_\gamma,T) = K(E_\gamma)\frac{\Gamma_{E1}}{E_\gamma^2}[E_\gamma^2+4\pi^2T^2], \tag{6.9}$$

where the empirical function $K(E_\gamma)$ is given by

$$K(E_\gamma) = \kappa + (1-\kappa)\frac{E_\gamma - E_0}{E_{E1}-E_0}. \tag{6.10}$$

Here we use $E_0 = 4.5$ MeV and the enhancement factor κ, given by [33]

$$\kappa = \begin{cases} 1 & \text{if } A < 148, \\ 1+0.09(A-148)^2\exp(-0.18(A-148)) & \text{if } A \geq 148. \end{cases} \tag{6.11}$$

These expressions are developed in the framework of the collisional damping model for $E_\gamma < E_{E1}$ and hold for $T < 2$ MeV.

The theoretical expressions discussed above have to be modified for deformed nuclei. The GEDR in deformed nuclei is split into two components corresponding to two oscillation frequencies, one for each principal axis. Therefore, the experimental data are best described by adding the strength functions with the corresponding resonance parameters.

Chapter 7

Papers

The following papers are included in this thesis:

1. A. C. Larsen, R. Chankova, M. Guttormsen, F. Ingebretsen, T. Lönnroth, S. Messelt, J. Rekstad, A. Schiller, S. Siem, N. U. H. Syed, A. Voinov, and S. W. Ødegård, *Microcanonical entropies and radiative strength functions of* ^{50,51}V, Phys. Rev. C **73**, 064301 (2006).

2. A. C. Larsen, M. Guttormsen, R. Chankova, F. Ingebretsen, T. Lönnroth, S. Messelt, J. Rekstad, A. Schiller, S. Siem, N. U. H. Syed, and A. Voinov, *Nuclear level densities and γ-ray strength functions in* ^{44,45}Sc, Phys. Rev. C **76**, 044303 (2007).

3. A. V. Voinov, S. M. Grimes, A. C. Larsen, C. R. Brune, M. Guttormsen, T. Massey, A. Schiller, S. Siem, and N. U. H. Syed, *Level densities of* ^{44}Sc *and* ^{47}Ti *from different experimental techniques*, Phys. Rev. C **77**, 034613 (2008).

4. N. U. H. Syed, M. Guttormsen, F. Ingebretsen, A. C. Larsen, T. Lönnroth, J. Rekstad, A. Schiller, S. Siem, and A. Voinov, *Level density and γ-decay properties of closed shell* Pb *nuclei*, accepted to be published in Phys. Rev. C.

5. N.U.H. Syed, *Extraction of thermal and electromagnetic properties in* ^{45}Ti, submitted to the Oslo Collaboration.

7.1 Survey of papers

Paper I

The level densities and γ-ray strength functions are measured for the ^{50,51}V from particle-γ coincidence spectra of the (^{3}He, ^{3}He$'\gamma$) and (^{3}He, $\alpha\gamma$) reactions with

45 MeV ^{3}He ions. The extracted level densities in ^{51}V show bump structures at excitation energies up to $E \sim 4.5$ MeV. These structures of ^{51}V are partly due to the closed proton shell and partly due to the breaking of nucleon pairs. The presence of a valance proton vacancy in ^{50}V produces some freedom of space, causing the bump structures in the level density to be damped out. The extracted level densities are used to deduce the thermodynamic quantities of ^{50,51}V nuclei in the micro-canonical ensemble. The entropy difference between the two isotopes is found to be 1.2 k_B, which is close to the value ($0.9k_B$) obtained in the lead region.

The experimental radiative strength function is nicely described by the KMF model. However, an enhancement in the strength function below 3 MeV is observed, in total disagreement with the theoretical models. The physical explanation of this enhancement is not yet understood.

Paper II

The motivation of this paper is to investigate the nuclear structure of scandium isotopes in the quasi-continuum region. The ^{44,45}Sc isotopes lie in the vicinity of light near closed shell nuclei where one would expect low and fluctuating level densities. The presence of upbend in the γ-ray strength function at low γ energies in ^{56,57}Fe, $^{93-98}$Mo, and ^{50,51}V isotopes, suggests that upbend occurs in certain nuclear mass regions due to a so far unknown collective resonances. Therefore, studying the presence of enhancement in the γ-ray strength function of Sc isotopes at low γ-ray energies are interesting.

The Oslo method is applied to primary γ-ray spectra of ^{44,45}Sc nuclei to extract the level densities and γ-ray strength functions, simultaneously. The extracted level densities display fine structures, however, these are less prominent compare to those seen in closed shell lead and vanadium nuclei. The level densities are compared to a combinatorial microscopic model. The agreement between the model and the experimental level densities is satisfactory, especially for ^{44}Sc. The γ-ray strength functions of the ^{44,45}Sc isotopes are normalized using the (γ, n) and (γ, p) nuclear cross-sections data. The normalized strength functions are found to be described well by the KMF model at the tail of the GEDR, except for γ-ray energies below 4 MeV. The expected upbend in the γ-ray strength function below 4 MeV is confirmed for the Sc isotopes. This work also shows that the upbend structure in the strength function is independent of the chosen excitation region.

Paper III

The two well-known approaches for the level density extraction above the known discrete levels are the Oslo method and the modeling of the particle-evaporation spectra from a compound nuclear reaction. In this paper the consistency of two

level density extraction approaches have been investigated for the ^{44}Sc nucleus. Previously, such a consistency has been established for the level densities in ^{56}Fe.

The level densities in ^{44}Sc are determined from the evaporation spectra of α particles in a (^{3}He,α) reaction. The experiment was conducted at the Edwards Accelerator Laborattories, Ohio University and the results are compared with the level density determined by the Oslo method in a (^{3}He,α) reaction, of the experiment performed at the OCL, Oslo University. The consistency of the two approaches is confirmed for the ^{44}Sc nucleus. The level densities of the ^{47}Ti populated by ^{45}Sc(^{3}He,p) reaction are extracted as well.

Paper IV

Extracting the level densities by the Oslo method in the vicinity of closed shell lead nuclei is the primary motive of this paper. From a statistical point of view, the level densities in the closed shell nuclei are low and one can expect large Porter-Thomas fluctuations on the γ-transition intensities. Therefore, non-statistical effects are expected to influence the results of the Oslo method in the closed shell nuclei. It is therefore interesting to investigate if these non-statistical effects make the Oslo method non-applicable in the region of closed shell nuclei.

The Oslo method is applied to data from the (^{3}He, ^{3}He$'\gamma$) and (^{3}He, $\alpha\gamma$) reactions on ^{206}Pb and ^{208}Pb targets. In spite of the possible non-statistical effects, the extracted level densities are consistent with the known discrete levels. In ^{208}Pb the very good agreement between our data and previously known data indicates the robustness of the Oslo method for its use for the closed shell nuclei. The level densities of the lead nuclei show pronounced bump structures due to the shell effects. However, these step structures are damped out by gradual opening of the neutron shell closure at $N = 126$ in the $^{205-207}$Pb nuclei.

The micro-canonical entropies are deduced from the experimental level densities. An average entropy difference of $\Delta S \sim 0.9 k_B$ has been observed between ^{205,206}Pb. The micro-canonical temperatures are deduced for ^{205,206}Pb with an average temperature of $T \sim 1.0$ MeV. The violent fluctuations in the entropy of ^{207,208}Pb nuclei make their use unreliable for the determination of other thermodynamic quantities.

The γ-ray strength functions in the $^{205-208}$Pb are also extracted and compared with the (γ, n) reaction cross-section data. The Oslo data for the lead nuclei are also compared with the SLO and EGLO γ-ray strength functions models. However, these models do not describe the data adequately. Intermediate structures in the γ-ray strength functions for all the Pb nuclei have been observed at the tail of the GEDR. These structures become less pronounced by gradual moving from the doubly closed shell ^{208}Pb to the single closed shell ^{205}Pb.

Paper V

In this work the Oslo method is used for the first time to extract the level density and the γ-ray strength function from a (p,d) reaction. The proton beam is used on the ^{46}Ti target to populate ^{45}Ti. The experimental level density confirm the quenching of number of levels per MeV due to few interplaying valence nucleons. The Oslo data for the ^{45}Ti are compared with the level density of ^{47}Ti, determined by the proton-evaporation technique, described in paper III. The slope of these two level densities from different techniques is similar, confirming our results. The experimental level density of ^{45}Ti is further investigated by a combinatorial theoretical model. The model is based on BCS quasi-particles, scattered randomly into the Nilsson single-particle levels, where collective states are schematically added. The agreement between the model and the experimental level densities is very good. The average number of broken Cooper pairs and the parity asymmetry are calculated as well.

The γ-ray strength function is compared with the (γ, abs) reaction cross-section data and with the GLO model. The γ-ray strength function is well described by the model, however, below $E_\gamma < 2.5$ MeV the observed strength is higher than the GLO model predictions. This enhancement of the γ-ray strength function at low γ-ray energies, called upbend, has been observed previously in Fe, Mo, V and Sc nuclei. The presence of upbend in Ti isotopes also strengthens the argument made in paper II, that this structure might be due to some sort of low energy resonances in the mass region $A < 100$.

7.2 Paper 1: Microcanonical entropies and radiative strength functions of ^{50,51}V

PHYSICAL REVIEW C **73**, 064301 (2006)

Microcanonical entropies and radiative strength functions of ^{50,51}V

A. C. Larsen,* R. Chankova, M. Guttormsen, F. Ingebretsen, S. Messelt, J. Rekstad, S. Siem, N. U. H. Syed, and S. W. Ødegård
Department of Physics, University of Oslo, P.O. Box 1048, Blindern, N-0316 Oslo, Norway

T. Lönnroth
Department of Physics, Åbo Akademi University, FIN-20500 Åbo, Finland

A. Schiller
National Superconducting Cyclotron Laboratory, Michigan State University, East Lansing, Michigan 48824, USA

A. Voinov
Department of Physics and Astronomy, Ohio University, Athens, Ohio 45701, USA
(Received 23 November 2005; published 7 June 2006)

The level densities and radiative strength functions (RSFs) of ^{50,51}V have been extracted using the (^{3}He,$\alpha\gamma$) and (^{3}He,^{3}He$'\gamma$) reactions, respectively. From the level densities, microcanonical entropies are deduced. The high γ-energy part of the measured RSF fits well with the tail of the giant electric dipole resonance. A significant enhancement over the predicted strength in the region of $E_\gamma \lesssim 3$ MeV is seen, which at present has no theoretical explanation.

DOI: 10.1103/PhysRevC.73.064301 PACS number(s): 21.10.Ma, 24.10.Pa, 25.55.Hp, 27.40.+z

I. INTRODUCTION

The structure of the vanadium isotopes is based on simple shell-model configurations at low excitation energies. The valence protons and neutrons occupy the single-particle $\pi f_{7/2}$ and $\nu f_{7/2}$ orbitals, respectively. These shells are isolated from other orbitals by the N, $Z = 20$ and 28 shell gaps, making the vanadium isotopes interesting objects for studying various nuclear shell effects. In particular, it is well known that the number of available singe-particle levels is significantly reduced for nuclei at closed shells.

The density of states or, equivalently, the entropy in these systems depends on the number of broken Cooper pairs and single-particle orbitals made available by crossing the shell gaps. The ^{50,51}V nuclei are of special interest because the neutrons are strongly blocked in the process of creating entropy; ^{50}V and ^{51}V have seven and eight neutrons in the $\nu f_{7/2}$ orbital, respectively. Thus, the configuration space of the three protons in the $\pi f_{7/2}$ shell is of great importance.

These particular shell-model configurations are also expected to govern the γ-decay routes. Specifically, as within every major shell, the presence of only one parity for single-particle orbitals in the low-spin domain means that transitions of $E1$ type will be suppressed. The low mass of the investigated nuclei causes the centroid of the giant electric dipole resonance (GEDR) to be relatively high, while the integrated strength according to the Thomas-Reiche-Kuhn sum rule is low; both observations work together to produce a relatively weak low-energy tail when compared to heavier nuclei. Hence, possible nonstatistical effects in the radiative strength function (RSF) might stand out more in the present investigation.

The Oslo Cyclotron group has developed a method to extract first-generation (primary) γ-ray spectra at various initial excitation energies. From such a set of primary spectra, the nuclear level density and the RSF can be extracted simultaneously [1,2]. These two quantities reveal essential information on nuclear structure such as pair correlations and thermal and electromagnetic properties. In the last five years, the Oslo group has demonstrated several fruitful applications of the method [3–7].

In Sec. II an outline of the experimental procedure is given. The level densities and microcanonical entropies are discussed in Sec. III, and in Sec. IV the RSFs are presented. Finally, concluding remarks are given in Sec. V.

II. EXPERIMENTAL METHOD

The experiment was carried out at the Oslo Cyclotron Laboratory using a beam of 30-MeV ^{3}He ions. The self-supporting natural V target had a purity of 99.8% and a thickness of 2.3 mg/cm^2. Particle-γ coincidences for ^{50,51}V were measured with the CACTUS multidetector array [8]. The charged ejectiles were detected using eight Si particle telescopes placed at an angle of 45° relative to the beam direction. Each telescope consists of a front ΔE detector and a back E detector with thicknesses of 140 and 1500 μm, respectively. An array of 28 collimated NaI γ-ray detectors with a total efficiency of ∼15% surrounded the target and the particle detectors. The reactions of interest were the pick-up reaction ^{51}V(^{3}He, $\alpha\gamma$)^{50}V, and the inelastic scattering ^{51}V(^{3}He,^{3}He$'\gamma$)^{51}V. The typical spin range is expected to be $I \sim 2$–$4\hbar$. The experiment ran for about one week, with beam currents of ∼1 nA.

The experimental extraction procedure and the assumptions made are described in Refs. [1,2]. The data analysis is based

*Electronic address: a.c.larsen@fys.uio.no

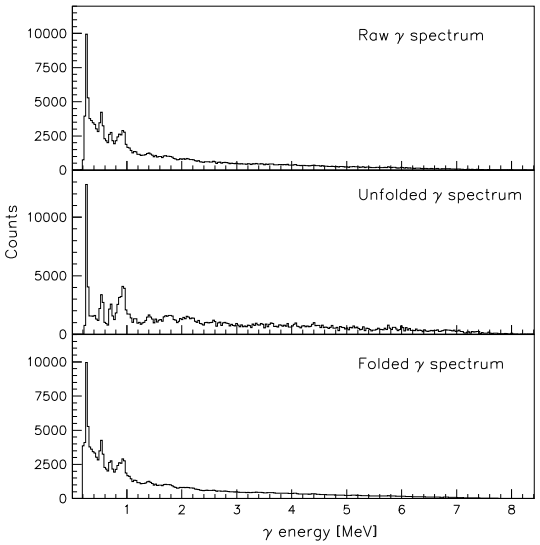

FIG. 1. γ spectra of ^{50}V for excitation energy $E = 6$–8 MeV.

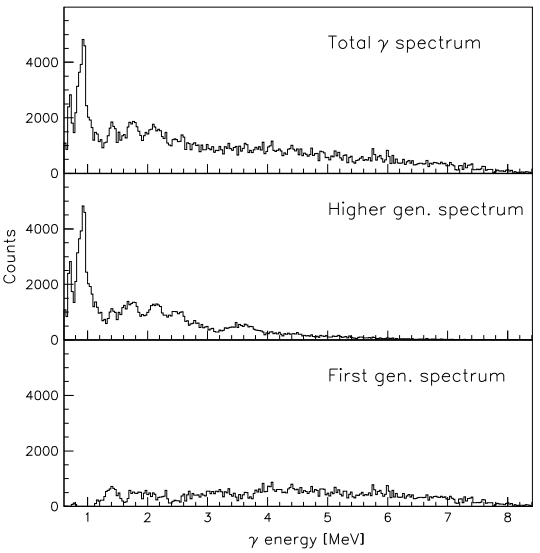

FIG. 2. Unfolded γ spectra of ^{50}V for excitation energy $E = 6$–8 MeV.

on three main steps: (1) preparing the particle-γ coincidence matrix, (2) unfolding the γ-ray spectra, and (3) constructing the first-generation matrix.

In the first step, for each particle-energy bin, total spectra of the γ-ray cascades are obtained from the coincidence measurement. The particle energy measured in the telescopes is transformed to excitation energy of the residual nucleus, using the reaction kinematics. Then each row of the coincidence matrix corresponds to a certain excitation energy E, while each column corresponds to a certain γ energy E_γ.

In the next step, the γ-ray spectra are unfolded using the known response functions of the CACTUS array [9]. The Compton-subtraction method described in Ref. [9] preserves the fluctuations in the original spectra without introducing further spurious fluctuations. A typical raw γ spectrum is shown in the top panel of Fig. 1, taken from the ^{50}V coincidence matrix gating on the excitation energies between $E = 6$–8 MeV. The middle panel shows the unfolded spectrum, and in the bottom panel this spectrum has been folded with the response functions. The top and bottom panels are in excellent agreement, indicating that the unfolding method works very well.

The third step is to extract the γ-ray spectra containing only the first γ rays in a cascade. These spectra are obtained for each excitation-energy bin through a subtraction procedure as described in Ref. [10]. The main assumption of this method is that the γ-decay spectrum from any excitation-energy bin is independent of the method of formation, either directly by the nuclear reaction or populated by γ decay from higher-lying states following the initial reaction. This assumption is automatically fulfilled when the same states are equally populated by the two processes, since γ branching ratios are properties of the levels themselves. Even if different states are populated, the assumption is still valid for statistical γ decay, which only depends on the γ-ray energy and the number of accessible final states. In Fig. 2, the total unfolded γ spectrum, the γ spectrum of second and higher generations, and the first-generation spectrum of ^{50}V with excitation-energy gates $E = 6$–8 MeV are shown. The first-generation spectrum is obtained by subtracting the higher-generation γ rays from the total γ spectrum.

When the first-generation matrix is properly normalized [2], the entries of it are the probabilities $P(E, E_\gamma)$ that a γ ray of energy E_γ is emitted from an excitation energy E. The probability of γ decay is proportional to the product of the level density $\rho(E - E_\gamma)$ at the final energy $E_f = E - E_\gamma$ and the γ-ray transmission coefficient $\mathcal{T}(E_\gamma)$, that is,

$$P(E, E_\gamma) \propto \rho(E - E_\gamma)\mathcal{T}(E_\gamma). \quad (1)$$

This factorization is the generalized form of the Brink-Axel hypothesis [11,12], which states that any excitation modes built on excited states have the same properties as those built on the ground state. This means that the γ-ray transmission coefficient is independent of excitation energy and thus of the nuclear temperature of the excited states. There is evidence that the width of the giant dipole resonance varies with the nuclear temperature of the state on which it is built [13,14]. However, the temperature corresponding to the excitation-energy range covered in this work is rather low and changes slowly with excitation energy ($T \sim \sqrt{E_f}$); thus, we assume that the temperature is constant and that the γ-ray transmission coefficient does not depend on the excitation energy in the energy interval under consideration.

The ρ and $\mathcal{T}$ functions can be determined by an iterative procedure [2], with which each data point of these two functions is simultaneously adjusted until a global χ^2 minimum with the experimental $P(E, E_\gamma)$ matrix is reached. No *a*

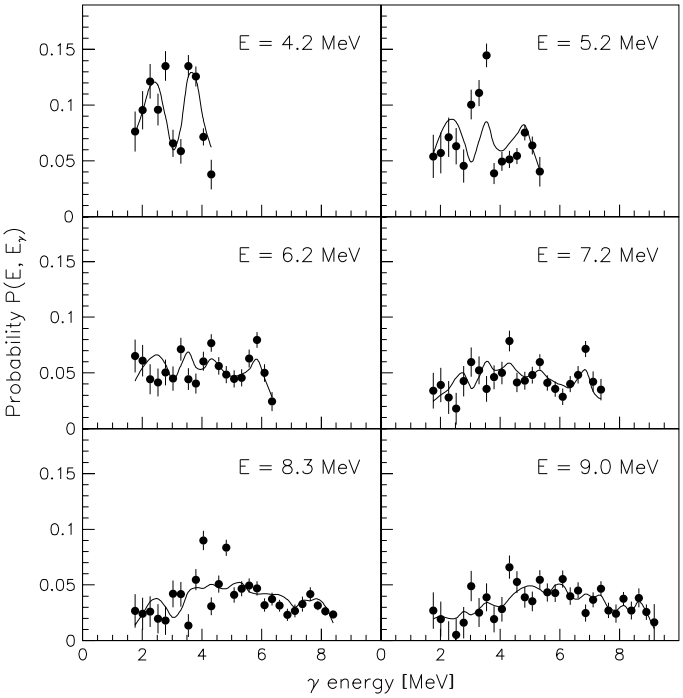

FIG. 3. Experimental first-generation γ spectra (data points with error bars) at six different initial excitation energies compared to the least-χ^2 fit (solid lines) for ^{50}V. The fit is performed simultaneously on the entire first-generation matrix of which the six displayed spectra are a fraction. The first-generation spectra are normalized to unity for each excitation-energy bin.

priori assumptions about the functional form of either the level density or the γ-ray transmission coefficient are used. An example to illustrate the quality of the fit is shown in Fig. 3, where we compare for the ^{51}V(^{3}He, $\alpha\gamma$)^{50}V reaction the experimental first-generation spectra to the least-χ^2 solution for six different initial excitation energies.

The globalized fitting to the data points determines the functional form of ρ and $\mathcal{T}$; however, it has been shown [2] that if one solution for the multiplicative functions ρ and $\mathcal{T}$ is known, one may construct an infinite number of other functions, which give identical fits to the P matrix by

$$\tilde{\rho}(E - E_\gamma) = A \exp[\alpha(E - E_\gamma)]\rho(E - E_\gamma), \quad (2)$$

$$\mathcal{T}(E_\gamma) = B \exp(\alpha E_\gamma)\mathcal{T}(E_\gamma). \quad (3)$$

Thus, the transformation parameters α, A, and B, which correspond to the physical solution, remain to be determined.

III. LEVEL DENSITY AND MICROCANONICAL ENTROPY

The parameters A and α can be obtained by normalizing the level density to the number of known discrete levels at low excitation energy [15] and to the level density estimated from neutron-resonance spacing data at the neutron binding energy $E = B_n$ [16]. The procedure for extracting the total level density ρ from the resonance energy spacing D is described in Ref. [2]. Since our experimental level-density data points only reach up to an excitation energy of $E \sim B_n - 1$ MeV, we extrapolate with the back-shifted Fermi-gas model with a global parametrization [17,18]

$$\rho_{\mathrm{BS}}(E) = \eta \frac{\exp(2\sqrt{aU})}{12\sqrt{2}a^{1/4}U^{5/4}\sigma_I}, \quad (4)$$

where a constant attenuation coefficient η is introduced to adjust ρ_{BS} to the experimental level density at B_n. The intrinsic excitation energy is estimated by $U = E - C_1 - E_{\mathrm{pair}}$, where $C_1 = -6.6A^{-0.32}$ MeV is the back-shift parameter and A is the mass number. The pairing energy E_{pair} is based on pairing gap parameters Δ_p and Δ_n evaluated from even-odd mass differences [19] according to [20]. The level-density parameter a and the spin-cutoff parameter σ_I are given by $a = 0.21A^{0.87}\mathrm{MeV}^{-1}$ and $\sigma_I^2 = 0.0888TA^{2/3}$, respectively. The nuclear temperature T is described by $T = \sqrt{U/a}$. The parameters used for ^{50,51}V in Eq. (4) are listed in Table I.

Unfortunately, ^{49}V is unstable, and no information exists on the level density at $E = B_n$ for ^{50}V. Therefore, we estimate the values from the systematics of other nuclei in the same mass region. In order to put these data on the same footing, we plot the level densities as a function of intrinsic energy U. Due to the strongly scattered data of Fig. 4, the estimate is rather uncertain. We chose a rough estimate of $\rho(B_n) = 5400 \pm 2700$ MeV^{-1} for ^{50}V. This value gives an attenuation $\eta = 0.46$, which is in good agreement with the obtained value of $\eta = 0.51$ for the ^{51}V nucleus. Figure 5 demonstrates the level-density normalization procedure for the ^{50}V case, i.e., how parameters A and α of Eq. (3) are determined to obtain a level-density function consistent with known experimental data.

TABLE I. Parameters used for the back-shifted Fermi-gas level density.

Nucleus	E_{pair} (MeV)	a (MeV^{-1})	C_1 (MeV)	B_n (MeV)	D (keV)	$\rho(B_n)$ (10^3 MeV^{-1})	η
^{50}V	0	6.31	−1.89	9.33	-	5.4(16)[a]	0.46
^{51}V	1.36	6.42	−1.88	11.05	2.3(6)	8.4(26)	0.51

[a]Estimated from systematics.

The experimentally extracted and normalized level densities of ^{50}V and ^{51}V are shown in Fig. 6 for excitation energies up to ∼8 and 9 MeV, respectively. The level density of ^{50}V is relatively high and has a rather smooth behavior due to the effect of the unpaired proton and neutron, while the level density of ^{51}V displays distinct structures for excitation energies up to ∼4.5 MeV. This effect is probably caused by the closed $f_{7/2}$ neutron shell in this nucleus.

The level densities of ^{50,51}V obtained with the Oslo method are compared to the number of levels from spectroscopic experiments [21]. The ^{51}V nucleus has relatively few levels per energy bin because of its closed neutron shell, so using spectroscopic methods to count the levels seems to be reliable up to ∼4 MeV excitation energy in this case. For higher excitations, the spectroscopic data are significantly lower compared to the level density obtained with the Oslo method. This means that many levels are not accounted for in this excitation region by using standard methods. The same can be concluded for ^{50}V, and in this case the spectroscopic level density drops off at an excitation energy of about 2.5 MeV.

The level densities of ^{50,51}V are also compared to the constant-temperature formula

$$\rho_{\text{fit}} = C\exp(E/T), \tag{5}$$

which is drawn as a solid line in Fig. 6. Here the parameters C and T are the level density at about zero excitation energy and the average temperature, respectively; both are estimated from the fit of the exponential to the region of the experimental level density indicated by arrows. From this model, a constant temperature of about 1.3 MeV is found for both nuclei.

The level density of a system can give detailed insight into its thermal properties. The multiplicity of states $\Omega_s(E)$, which is the number of physically obtainable realizations available at a given energy, is directly proportional to the level density and a spin-dependent factor $(2\langle J(E)\rangle + 1)$, thus

$$\Omega_s(E) \propto \rho(E)(2\langle J(E)\rangle + 1), \tag{6}$$

where $\langle J(E)\rangle$ is the average spin at excitation energy E. Unfortunately, the experimentally measured level density in this work does not correspond to the true multiplicity of states, since the $(2J + 1)$ degeneracy of magnetic substates

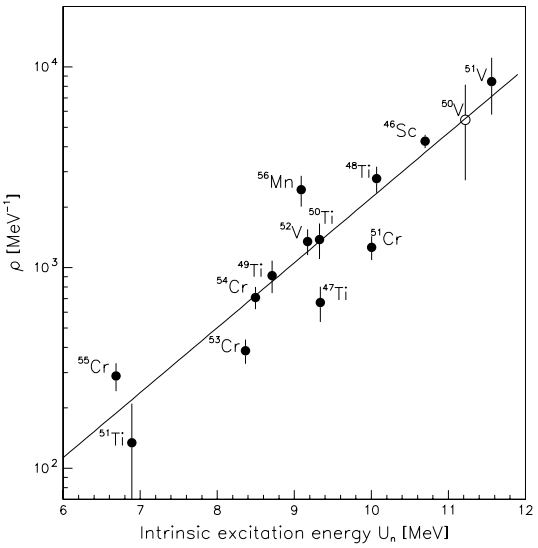

FIG. 4. Level densities estimated from neutron resonance level spacings at B_n and plotted as a function of intrinsic excitation energy $U_n = B_n - C_1 - E_{\text{pair}}$. The unknown level density for ^{50}V (open circle) is estimated from the line determined by a least-χ^2 fit to the data points.

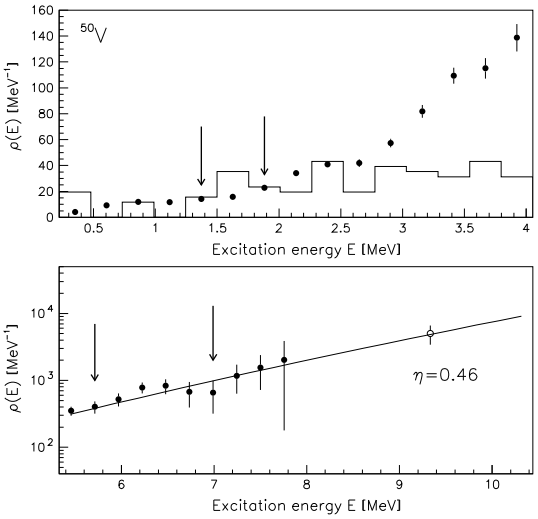

FIG. 5. Normalization procedure of the experimental level density (data points) of ^{50}V. The data points between the arrows are normalized to known levels at low excitation energy (histograms) and to the level density at the neutron-separation energy (open circle) using a Fermi-gas level-density extrapolation (solid line).

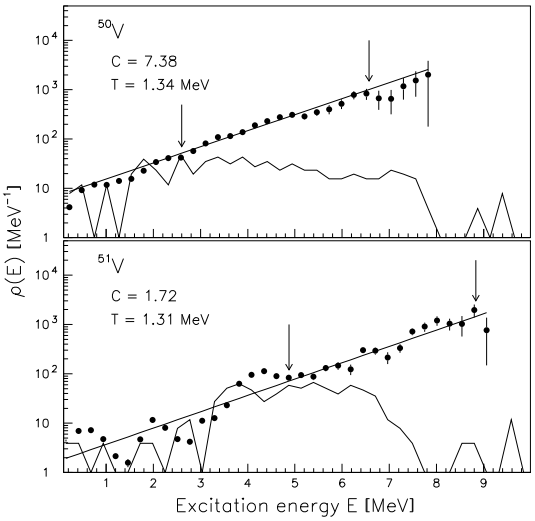

FIG. 6. Normalized level density of ^{50,51}V compared to known discrete levels (jagged line) and a constant temperature model (straight line). The fits are performed in the region between the arrows.

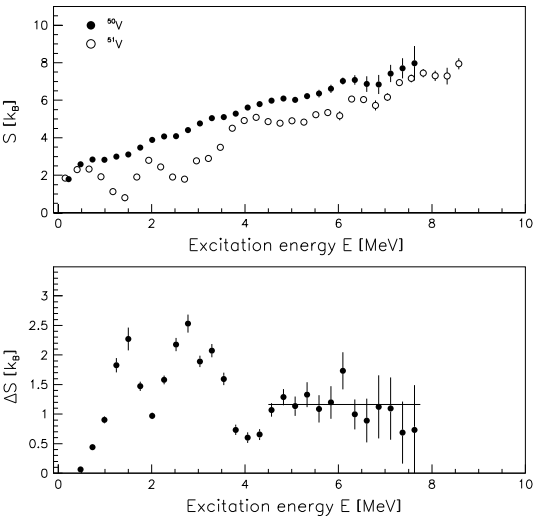

FIG. 7. Entropies of ^{50,51}V (upper panel), and entropy difference between the two vanadium isotopes (lower panel).

is not included. If the average spin of levels $\langle J \rangle$ at any excitation energy were known, this problem could be solved by multiplying an energy-dependent factor $(2\langle J(E)\rangle + 1)$ by the experimental level density. However, little experimental data exist on the spin distribution. Therefore, we choose in this work to use a multiplicity $\Omega_l(E)$ based on the experimental level density alone:

$$\Omega_l(E) \propto \rho(E). \tag{7}$$

The entropy $S(E)$ is a measure of the degree of disorder of a system at a specific energy. The microcanonical ensemble in which the system is completely isolated from any exchange with its surroundings, is often considered as the appropriate one for the atomic nucleus since the strong force has such a short range, and because the nucleus normally does not share its excitation energy with the external environment.

According to our definition of the multiplicity of levels $\Omega_l(E)$ obtained from the experimental level density, we define a "pseudo" entropy

$$S(E) = k_{\mathrm{B}} \ln \Omega_l(E), \tag{8}$$

which is utilized in the following discussion. For convenience, Boltzmann's constant k_B can be set to unity.

In order to normalize the entropy, the multiplicity is written as $\Omega_l(E) = \rho(E)/\rho_0$. The normalization denominator ρ_0 is to be adjusted such that the entropy approaches a constant value when the temperature approaches zero in order to fullfill the third law of thermodynamics: $S(T \to 0) = S_0$. In the case of even-even nuclei, the ground state represents a completely ordered system with only one possible configuration. This means that the entropy in the ground state is $S = \ln 1 = 0$, and the normalization factor $1/\rho_0$ is chosen such that this is the case. Since the vanadium nuclei have an odd number of protons, a ρ_0 which is typical for even-even nuclei in this mass region is used for both the ^{50}V and the ^{51}V nucleus. The normalization factor ρ_0 used is 0.7 MeV^{-1}, found from averaging data on ^{50}Ti and ^{52}Cr.

The entropies of ^{50,51}V extracted from the experimental level densities are shown in the upper panel of Fig. 7. Naturally, they show the same features as the level-density plot, with the odd-odd ^{50}V displaying higher entropy than the odd-even ^{51}V. Since the neutrons are almost (^{50}V) or totally (^{51}V) blocked at low excitation energy, the multiplicity and thus the entropy is made primarily by the protons in this region.

At 4 MeV of excitation energy, a relatively large increase in entropy is found in the case of ^{51}V. This is probably because the excitation energy is large enough to excite a nucleon across the $N, Z = 28$ shell gap to other orbitals.

In the excitation region above ~4.5 MeV, the entropies show similar behavior, which is also expressed by the entropy difference ΔS displayed in the lower panel of Fig. 7. We assume here that the two systems have an approximately statistical behavior and that the neutron hole in ^{50}V acts as a spectator to the ^{51}V core. The entropy of the hole can be estimated from the entropy difference $\Delta S = S(^{50}\mathrm{V}) - S(^{51}\mathrm{V})$. From the lower panel of Fig. 7, we find $\Delta S \sim 1.2 k_B$ for $E >$ 4.5 MeV. This is slightly less than the quasiparticle entropy found in rare-earth nuclei, which is estimated to be $\Delta S \sim 1.7 k_B$ [5]. This is not unexpected since the single-particle levels are more closely spaced for these nuclei; they have therefore more entropy.

The naive configurations of ^{50,51}V at low excitations are $\pi f_{7/2}^3 \nu f_{7/2}^7$ and $\pi f_{7/2}^3 \nu f_{7/2}^8$, respectively. Thus, by counting the possible configurations within the framework of the BCS model [22] in the nearly degenerate $f_{7/2}$ shell, one can estimate the multiplicity of levels and thus the entropy when no Cooper

pairs are broken in the nucleus, one pair is broken, and so on. We assume a small deformation that gives four energy levels with Nilsson quantum numbers $\Omega = 1/2, 3/2, 5/2, 7/2$. Furthermore, we neglect the proton-neutron coupling and hence assume that the protons and neutrons can be considered as two separate systems; the total entropy based on the number of energy levels can then be written as $S = S_p + S_n$. This gives $S = 2.8k_B$ for the nucleus ^{50}V, and $S = 1.4k_B$ for ^{51}V when two protons are coupled in a Cooper pair. These values are in fair agreement with the data of Fig. 7 at an excitation energy below ~2 MeV. It is gratifying that these crude estimates give an entropy of the neutron hole in ^{50}V of $\Delta S = 1.4k_B$, in good agreement with the experimental value for the entropy difference of $1.2k_B$ found from Fig. 7.

With the three $f_{7/2}$ protons unpaired, we obtain a total entropy of $S = 3.5$ and $2.1k_B$ for ^{50,51}V, respectively. This means that the process of just breaking a proton pair within the same shell does not contribute much to the total entropy, but when a nucleon has enough energy to cross the shell gap a significant increase of the entropy is expected. As already mentioned, at excitation energies above ~4 MeV, it is very likely that configurations from other shells will participate in building the total entropy.

IV. RADIATIVE STRENGTH FUNCTIONS

The γ-ray transmission coefficient $\mathcal{T}$ in Eq. (1) is expressed as a sum of all the RSFs f_{XL} of electromagnetic character X and multipolarity L:

$$\mathcal{T}(E_\gamma) = 2\pi \sum_{XL} E_\gamma^{2L+1} f_{XL}(E_\gamma). \tag{9}$$

The slope of the experimental γ-ray transmission coefficient $\mathcal{T}$ has been determined through the normalization of the level densities, as described in Sec. III. The remaining constant B in Eq. (3) is determined using information from neutron resonance decay, which gives the absolute normalization of $\mathcal{T}$. For this purpose, we utilize experimental data [16] on the average total radiative width $\langle\Gamma_\gamma\rangle$ at $E = B_n$.

We assume here that the γ decay taking place in the quasicontinuum is dominated by $E1$ and $M1$ transitions and that the number of positive and negative parity states is equal. For initial spin I and parity π at $E = B_n$, the expression of the width [23] reduces to

$$\langle\Gamma_\gamma\rangle = \frac{1}{4\pi\rho(B_n, I, \pi)} \sum_{I_f} \int_0^{B_n} dE_\gamma B\mathcal{T}(E_\gamma) \times \rho(B_n - E_\gamma, I_f), \tag{10}$$

where $D_i = 1/\rho(B_n, I, \pi)$ is the average spacing of s-wave neutron resonances. The summation and integration run over all final levels with spin I_f, which are accessible by dipole ($L = 1$) γ radiation with energy E_γ. From this expression, the normalization constant B can be determined as described in Ref. [6]. However, some considerations have to be made before normalizing according to Eq. (10).

Methodical difficulties in the primary γ-ray extraction prevent determination of the function $\mathcal{T}(E_\gamma)$ in the interval $E_\gamma < 1$ MeV. In addition, the data at the highest γ energies, above $E_\gamma \sim B_n - 1$ MeV, suffer from poor statistics. We therefore extrapolate $\mathcal{T}$ with an exponential form, as demonstrated for ^{51}V in Fig. 8. The contribution of the extrapolation to the total radiative width given by Eq. (10) does not exceed 15%, thus the errors due to a possibly poor extrapolation are expected to be of minor importance [6].

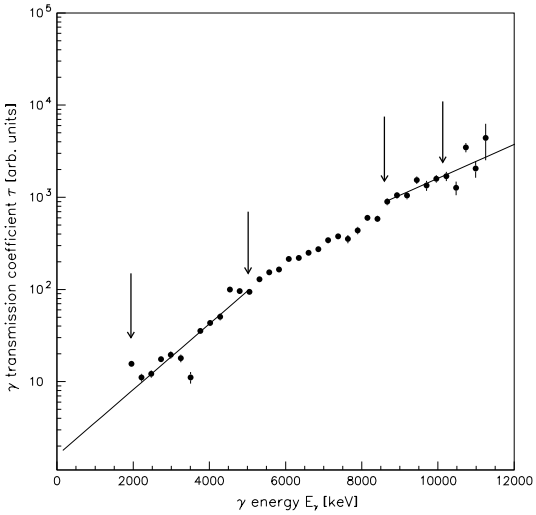

FIG. 8. Unnormalized γ-ray transmission coefficient for ^{51}V. Lines are extrapolations needed to calculate the normalization integral of Eq. (10). Arrows indicate the lower and upper fitting regions for the extrapolations.

Again, difficulties occur when normalizing the γ-ray transmission coefficient in the case of ^{50}V because of the lack of neutron resonance data. Since the average total radiative width $\langle\Gamma_\gamma\rangle$ at $E = B_n$ does not seem to show any clear systematics for nuclei in this mass region, we choose the same absolute value of the GEDR tail for ^{50}V as the one found for ^{51}V from photoabsorption experiments. The argument for this choice is that the GEDR should be similar for equal number of protons provided that the two nuclei have the same shapes.

Since it is assumed that the radiative strength is dominated by dipole transitions, the RSF can be calculated from the normalized transmission coefficient by

$$f(E_\gamma) = \frac{1}{2\pi} \frac{\mathcal{T}(E_\gamma)}{E_\gamma^3}. \tag{11}$$

We would now like to decompose the RSF into its components from different multipolarities to investigate how the $E1$ and $M1$ radiation contribute to the total strength.

The Kadmenskiĭ, Markushev, and Furman (KMF) model [13] is employed for the $E1$ strength. In this model, the Lorentzian GEDR is modified in order to reproduce the nonzero limit of the GEDR for $E_\gamma \to 0$ by means of a temperature-dependent width of the GEDR. The $E1$ strength

TABLE II. Parameters used for the radiative strength functions.

Nucleus	$E_{E1,1}$ (MeV)	$\sigma_{E1,1}$ (mb)	$\Gamma_{E1,1}$ (MeV)	$E_{E1,2}$ (MeV)	$\sigma_{E1,2}$ (mb)	$\Gamma;_{E1,2}$ (MeV)	E_{M1} (MeV)	σ_{M1} (mb)	Γ_{M1} (MeV)	$\langle\Gamma_\gamma\rangle$ (meV)	T (MeV)	κ
^{50}V	17.93	53.3	3.62	20.95	40.7	7.15	11.1	0.532	4.0	–	1.34	0.75
^{51}V	17.93	53.3	3.62	20.95	40.7	7.15	11.1	0.563	4.0	600(80)	1.31	0.74

in the KMF model is given by

$$f_{E1}(E_\gamma) = \frac{1}{3\pi^2\hbar^2c^2}\frac{0.7\sigma_{E1}\Gamma_{E1}^2\left(E_\gamma^2+4\pi^2T^2\right)}{E_{E1}\left(E_\gamma^2-E_{E1}^2\right)^2}, \quad (12)$$

where σ_{E1} is the cross section, Γ_{E1} is the width, and E_{E1} is the centroid of the GEDR determined from photoabsorption experiments.

We adopt the KMF model with temperature T taken as a constant to be consistent with our assumption that the RSF is independent of excitation energy. The possible systematic uncertainty caused by this assumption is estimated to have a maximum effect of 20% on the RSF [24]. The values used for T are the ones extracted from the constant-temperature model in Eq. (5).

The GEDR is split into two parts for deformed nuclei. Data of ^{51}V from photoabsorption experiments show that the GEDR is best fitted with two Lorentzians, indicating a splitting of the resonance and a non-zero ground-state deformation of this nucleus. Indeed, $B(E2)$ values [16] suggest a deformation of $\beta \sim 0.1$ for ^{50,51}V. Therefore, a sum of two modified Lorentzians each described by Eq. (12) is used (see Table II).

For f_{M1}, which is supposed to be governed by the spin-flip $M1$ resonance [6], the Lorentzian giant magnetic dipole resonance (GMDR)

$$f_{M1}(E_\gamma) = \frac{1}{3\pi^2\hbar^2c^2}\frac{\sigma_{M1}E_\gamma\Gamma_{M1}^2}{\left(E_\gamma^2-E_{M1}^2\right)^2+E_\gamma^2\Gamma_{M1}^2} \quad (13)$$

is adopted.

The GEDR and GMDR parameters are taken from the systematics of Ref. [16] and are listed in Table II. Thus, we fit the total RSF given by

$$f = \kappa(f_{E1,1} + f_{E1,2} + f_{M1}) \quad (14)$$

to the experimental data using the normalization constant κ as a free parameter. The value of κ generally deviates from unity because of theoretical uncertainties in the KMF model and the evaluation of the absolute normalization in Eq. (10). The resulting RSFs extracted from the two reactions are displayed in Fig. 9, where the data have been normalized with parameters from Tables I and II.

The γ-decay probability is governed by the number and character of available final states and by the RSF. A rough inspection of the experimental data of Fig. 9 indicates that the RSFs are increasing functions of γ energy, generally following the tails of the GEDR and GMDR resonances in this region.

At low γ energies ($E_\gamma \lesssim 3$ MeV), an enhancement of a factor of $\sim$5 over the KMF estimate of the strength appears in the RSFs. This increase has also been seen in some Fe [25] and Mo [24] isotopes, where it has been shown to be present in the whole excitation-energy region. In the case of the ^{57}Fe RSF, the feature has been confirmed by an $(n, 2\gamma)$ experiment [25]. However, it has not appeared in the RSFs of the rare-earth nuclei investigated earlier by the Oslo group. The physical origin of the enhancement has not, at present, any satisfying explanation, as none of the known theoretical models can account for this behavior.

So far, we have not been able to detect any technical problems with the Oslo method. The unfolding procedure with the NaI response functions gives reliable results, as demonstrated in Fig. 1. Also, Fig. 2 indicates that the low-energy γ intensity

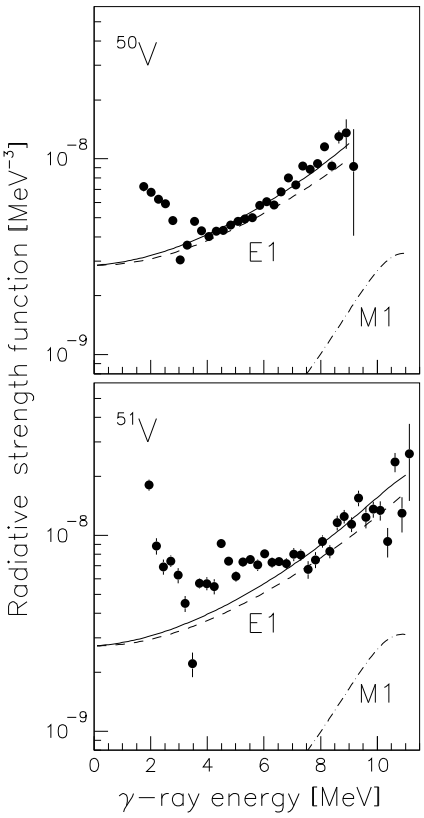

FIG. 9. Normalized RSFs of ^{50,51}V. Dashed and dash-dotted lines show the extrapolated tails of the giant electric and giant magnetic dipole resonances, respectively. Solid line is the summed strength for the giant dipole resonances.

is subtracted correctly; if not, one would find less intensity in the higher-generation spectrum at these γ energies. Figure 3 shows the final test, where the result from the least-χ^2 fit nicely reproduces the experimental data. In addition, investigations in ^{27,28}Si [26] showed that our method produced γ-transition coefficients in excellent agreement with average decay widths of known, discrete transitions. Hence, we do not believe that the enhancement is caused by some technical or methodical problems. Still, independent confirmation of the increasing RSF from, e.g., $(n, 2\gamma)$ experiments on the V and Mo isotopes, is highly desirable.

V. SUMMARY AND CONCLUSIONS

The Oslo method has been applied to extract level densities and RSFs of the vanadium isotopes ^{50,51}V. From the measured level densities, microcanonical entropies have been derived. The entropy carried by the neutron hole in ^{50}V is estimated to be $\sim 1.2\ k_B$, which is less than the quasiparticle entropy of $\sim 1.7\ k_B$ found in rare-earth nuclei.

The experimental RSFs are generally increasing functions of γ energy. The main contribution to the RSFs is the GEDR; also the GMDR is present. At low γ energies, an increase in the strength functions is apparent. A similar enhancement has also been seen in iron and molybdenum isotopes. There is still no explanation for the physics behind this very interesting behavior.

ACKNOWLEDGMENTS

A.V. acknowledges support from a NATO Science Fellowship under Project Number 150027/432 given by the Norwegian-Research Council (NFR) and from the Stewardship Science Academic Alliances, Grant Number DE-FG03-03-NA0074. Financial support from the NFR is gratefully acknowledged.

[1] L. Henden, L. Bergholt, M. Guttormsen, J. Rekstad, and T. S. Tveter, Nucl. Phys. **A589**, 249 (1995).
[2] A. Schiller, L. Bergholt, M. Guttormsen, E. Melby, J. Rekstad, and S. Siem, Nucl. Instrum. Methods Phys. Res. A **447**, 498 (2000).
[3] E. Melby, L. Bergholt, M. Guttormsen, M. Hjorth-Jensen, F. Ingebretsen, S. Messelt, J. Rekstad, A. Schiller, S. Siem, and S. W. Ødegård, Phys. Rev. Lett. **83**, 3150 (1999).
[4] A. Schiller, A. Bjerve, M. Guttormsen, M. Hjorth-Jensen, F. Ingebretsen, E. Melby, S. Messelt, J. Rekstad, S. Siem, and S. W. Ødegård, Phys. Rev. C **63**, 021306(R) (2001).
[5] M. Guttormsen, M. Hjorth-Jensen, E. Melby, J. Rekstad, A. Schiller, and S. Siem, Phys. Rev. C **63**, 044301 (2001).
[6] A. Voinov, M. Guttormsen, E. Melby, J. Rekstad, A. Schiller, and S. Siem, Phys. Rev. C **63**, 044313 (2001).
[7] S. Siem, M. Guttormsen, K. Ingeberg, E. Melby, J. Rekstad, A. Schiller, and A. Voinov, Phys. Rev. C **65**, 044318 (2002).
[8] M. Guttormsen, A. Atac, G. Løvhøiden, S. Messelt, T. Ramsøy, J. Rekstad, T. F. Thorsteinsen, T. S. Tveter, and Z. Zelazny, Phys. Script. T **32**, 54 (1990).
[9] M. Guttormsen, T. S. Tveter, L. Bergholt, F. Ingebretsen, and J. Rekstad, Nucl. Instrum. Methods Phys. Res. A **374**, 371 (1996).
[10] M. Guttormsen, T. Ramsøy, and J. Rekstad, Nucl. Instrum. Methods Phys. Res. A **255**, 518 (1987).
[11] D. M. Brink, Ph.D. thesis, Oxford University, 1955.
[12] P. Axel, Phys. Rev. **126**, 671 (1962).
[13] S. G. Kadmenskiĭ, V. P. Markushev, and V. I. Furman, Yad. Fiz. **37**, 277 (1983) [Sov. J. Nucl. Phys. **37**, 165 (1983)].
[14] G. Gervais, M. Thoennessen, and W. E. Ormand, Phys. Rev. C **58**, R1377 (1998).
[15] Data extracted using the NNDC On-Line Data Service from the ENSDF database, www.nndc.bnl.gov/ensdf.
[16] Data extracted using the Reference Input Parameter Library, http://www-nds.iaea.org/RIPL-2/
[17] A. Gilbert and A. G. W. Cameron, Can. J. Phys. **43**, 1446 (1965).
[18] T. von Egidy, H. H. Schmidt, and A. N. Behkami, Nucl. Phys. **A481**, 189 (1988).
[19] G. Audi and A. H. Wapstra, Nucl. Phys. **A595**, 409 (1995).
[20] A. Bohr and B. Mottelson, *Nuclear Structure* (Benjamin, New York, 1969), Vol. I, p. 169.
[21] R. Firestone and V. S. Shirley, *Table of Isotopes*, 8th ed. (Wiley, New York, 1996), Vol. II.
[22] J. Bardeen, L. N. Cooper, and J. R. Schrieffer, Phys. Rev. **108**, 1175 (1957).
[23] J. Kopecky and M. Uhl, Phys. Rev. C **41**, 1941 (1990).
[24] M. Guttormsen, R. Chankova, U. Agvaanluvsan, E. Algin, L. A. Bernstein, F. Ingebretsen, T. Lönnroth, S. Messelt, G. E. Mitchell, J. Rekstad, A. Schiller, S. Siem, A. C. Sunde, A. Voinov, and S. Ødegård, Phys. Rev. C **71**, 044307 (2005).
[25] A. Voinov, E. Algin, U. Agvaanluvsan, T. Belgya, R. Chankova, M. Guttormsen, G. E. Mitchell, J. Rekstad, A. Schiller, and S. Siem, Phys. Rev. Lett. **93**, 142504 (2004).
[26] M. Guttormsen, E. Melby, J. Rekstad, A. Schiller, S. Siem, T. Lönnroth, and A. Voinov, J. Phys. G **29**, 263 (2003).

7.3 Paper 2: Nuclear level densities and γ-ray strength functions in ^{44,45}Sc

Nuclear level densities and γ-ray strength functions in ^{44,45}Sc

A. C. Larsen,[1,*] M. Guttormsen,[1] R. Chankova,[2] F. Ingebretsen,[1] T. Lönnroth,[3] S. Messelt,[1] J. Rekstad,[1] A. Schiller,[4] S. Siem,[1] N. U. H. Syed,[1] and A. Voinov[5]

[1]*Department of Physics, University of Oslo, P. O. Box 1048 Blindern, N-0316 Oslo, Norway*

[2]*North Carolina State University, Raleigh, North Carolina 27695, USA and Triangle Universities Nuclear Laboratory, Durham, North Carolina 27708, USA*

[3]*Department of Physics, Åbo Akademi University, FIN-20500 Åbo, Finland*

[4]*National Superconducting Cyclotron Laboratory, Michigan State University, East Lansing, Michigan 48824, USA*

[5]*Department of Physics and Astronomy, Ohio University, Athens, Ohio 45701, USA and Frank Laboratory of Neutron Physics, Joint Institute for Nuclear Research, RU-141980 Dubna, Moscow region, Russia*

(Received 29 May 2007; published 4 October 2007)

The scandium isotopes ^{44,45}Sc were studied with the ^{45}Sc(^{3}He, $\alpha\gamma$)^{44}Sc and ^{45}Sc(^{3}He, ^{3}He$'\gamma$)^{45}Sc reactions, respectively. The nuclear level densities and γ-ray strength functions have been extracted using the Oslo method. The experimental level densities are compared to calculated level densities obtained from a microscopic model based on BCS quasiparticles within the Nilsson level scheme. This model also gives information about the parity distribution and the number of broken Cooper pairs as a function of excitation energy. The experimental γ-ray strength functions are compared to theoretical models of the $E1$, $M1$, and $E2$ strength and to data from (γ,n) and (γ,p) experiments. The strength functions show an enhancement at low γ energies that cannot be explained by the present standard models.

DOI: 10.1103/PhysRevC.76.044303 PACS number(s): 21.10.Ma, 24.10.Pa, 25.55.Hp, 27.40.+z

I. INTRODUCTION

The energy levels of an atomic nucleus and the decay probability of each level contain essential information on the nuclear structure. When the nucleus is excited to levels just above the ground state, spectroscopic measurements are able to give accurate information on the energy, spin, parity, and transition rates of the levels. However, as the excitation energy increases, the number of levels quickly becomes so high that all levels cannot be found with present state-of-the art spectroscopy methods. The nucleus leaves the discrete region and enters the region of quasicontinuum and continuum, where it is regarded as more appropriate to use average quantities to describe the behavior of the nucleus.

The nuclear level density and the γ-ray strength function give a measure of the gross properties of the nucleus. These average quantities are indispensable in practical applications of nuclear physics, such as calculations of nuclear reaction rates in astrophysical processes, the design and operation of fission reactors, and transmutation of nuclear waste. When it comes to fundamental nuclear structure, the level density can reveal information on, e.g., pair correlations and thermodynamic quantities such as entropy and temperature [1,2], whereas the average electromagnetic properties are characterized by the γ-ray strength function [3].

Neutron (and proton) resonance experiments provide data on the level density at or above the nucleon binding energy [4], and fluctuation analysis of total neutron cross sections [5] gives level density at excitation energies well above the nucleon binding energy. However, in the intermediate region between the nucleon binding energy and the discrete regime (the quasicontinuum) relatively little is known. To fill in this gap, the Oslo Cyclotron group has developed the so-called Oslo method, which enables the extraction of both level density and γ-ray strength function from the distribution of primary γ rays at various initial excitation energies. The method has been thoroughly tested on nuclei in the rare-earth region [6–8] and has also been successfully extended to other mass regions [9–12].

The present work reports on new results from an experiment on the scandium isotopes ^{44,45}Sc. The ^{45}Sc nucleus has one unpaired proton in the $\pi f_{7/2}$ orbital, whereas ^{44}Sc has an unpaired proton and a neutron in the $\pi f_{7/2}$, $\nu f_{7/2}$ orbitals. If one naively assumes that only the $f_{7/2}$ orbital is dominant in the model space, one would expect a majority of positive-parity states in the case of ^{44}Sc and negative-parity states for ^{45}Sc. However, it is well known that states with different parity appear already at very low excitation energy in these nuclei. Early attempts on reproducing the states both with particle-plus-rotor models [13] and shell-model calculations [14] had relatively little success. More recent works have shown that these nuclei exhibit both collective and single-particle character even at low excitation energy, and they have been considered as a good case for studying the interplay between the single-particle and the collective degrees of freedom in medium-mass nuclei near the closed shell [15,16]. These scandium isotopes are therefore of special interest to test the Oslo method further.

In Sec. II an outline of the experimental procedure and the Oslo method is given. The level densities and the γ-ray strength functions are discussed in Secs. III and IV, respectively. Finally, concluding remarks are given in Sec. V.

*a.c.larsen@fys.uio.no

II. EXPERIMENTAL DETAILS AND THE OSLO METHOD

The experiment was performed at the Oslo Cyclotron Laboratory (OCL) using a beam of ^{3}He ions with energy 38 MeV. The self-supporting natural target of 99.9% ^{45}Sc had a thickness of 3.4 mg/cm^2. Eight Si ΔE-E telescopes were arranged close to the target at an angle of 45° relative to the beam. The γ-detector array CACTUS [17], consisting of 28 collimated NaI crystals with a total efficiency of ~15%, surrounded the target and the particle detectors. The experimental setup enabled particle-γ coincidence measurements of the reactions (^{3}He, $\alpha\gamma$) and (^{3}He, ^{3}He$'\gamma$). These reactions populate states with spin range $I \sim 2$–$6\hbar$, which means that most of the energy transferred to the target nucleus is intrinsic excitation energy. The experiment ran for about 5 days, with a typical beam current of ~1 nA.

The recorded coincidences were sorted into two-dimensional particle-γ matrices. From the reaction kinematics, the measured energy of the outgoing ^{3}He or α particle were converted into excitation energy of the residual nucleus. With particle-energy bins of 240 keV/channel, total γ-ray spectra were obtained for each bin. These γ spectra were then unfolded using a well-tested unfolding procedure based on the known response functions of the CACTUS array [18]. The unfolding method described in Ref. [18] preserves the fluctuations in the original spectra without introducing further, spurious fluctuations. In Fig. 1 an original γ spectrum, an unfolded spectrum, and the unfolded spectrum convoluted with the response functions are shown for ^{44}Sc with gate on the excitation-energy bins between 5.5 and 6.5 MeV. The original and the convoluted spectrum show excellent agreement, giving strong confidence in the unfolding method. The unfolded particle-γ matrix of the ^{45}Sc(^{3}He, $\alpha\gamma$)^{44}Sc data is displayed in Fig. 2, where the sharp diagonal $E = E_\gamma$ is clearly seen. Apart from the prominent peak at $E \sim 1$ MeV and $E_\gamma \sim 0.75$ MeV, the matrix is without outstanding structures.

The energy distribution of the first emitted γ rays from the decay cascades reveals essential information on the nuclear structure. To extract these primary γ rays from the total γ spectra, a subtraction procedure described in Ref. [19] is applied for each excitation-energy bin. The main assumption of this method is that the γ decay from any excitation-energy bin is independent on how the nucleus was excited to this bin. In other words, the decay routes are the same whether they were initiated directly by the nuclear reaction or by γ decay from higher-lying states. This assumption is automatically fulfilled when the same states are equally populated by the two processes, because γ branching ratios are properties of the levels themselves. Even if different states are populated, the assumption is still valid for statistical γ decay, which depends only on the γ-ray energy and the number of accessible final states. Figure 3 shows the total, unfolded γ spectrum, the second and higher generations γ spectrum and the first-generation spectrum of ^{45}Sc for excitation energy between $E = 5.5$ and 6.5 MeV. The first-generation spectrum is obtained by subtracting the higher-generation γ rays from the total γ spectrum. By looking at the lower panel of Fig. 3, it is clear that the main assumption of the subtraction method is

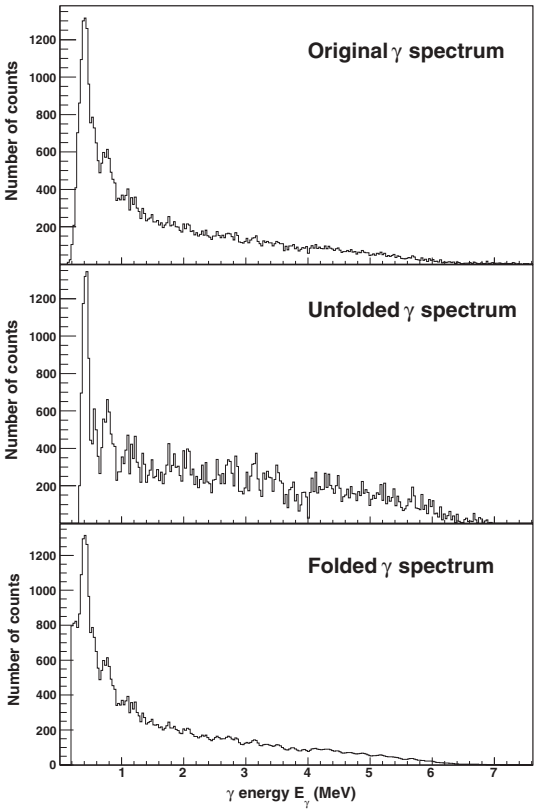

FIG. 1. Original (top), unfolded (middle) and folded γ spectrum of ^{44}Sc for excitation energy between 5.5 and 6.5 MeV.

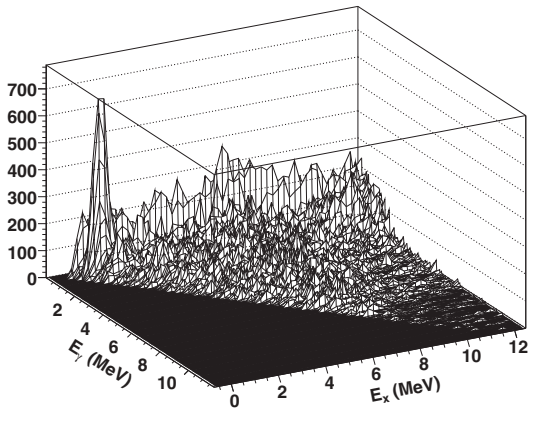

FIG. 2. Unfolded particle-γ matrix for the ^{45}Sc(^{3}He, α)^{44}Sc reaction.

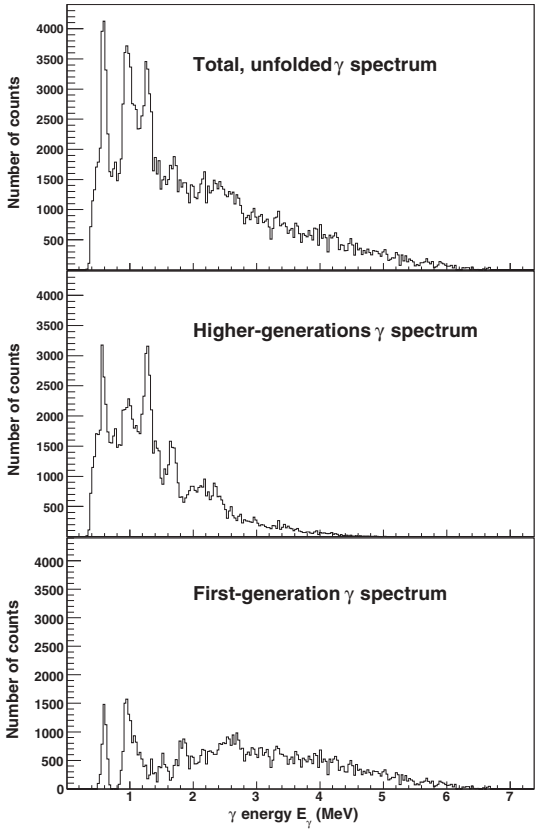

FIG. 3. Unfolded, total γ spectrum, second and higher-generation γ spectrum and first-generation γ spectrum of ^{45}Sc for excitation energy between 5.5 and 6.5 MeV.

not fulfilled for $E_\gamma \lesssim 1.4$ MeV. In this region, some strong, low-energy transitions were not subtracted correctly. This means that the levels from which these transitions originate are populated more strongly from higher excited levels through γ emission than directly by inelastic ^{3}He scattering. Therefore, only data for $E_\gamma > 1.6$ MeV are used in the further analysis. Similar considerations were done for ^{44}Sc.

The experimental matrix of first-generation γ rays is then normalized [20] such that for every excitation-energy bin E, the sum over all γ energies E_γ from some minimum value $E_\gamma^{\min}$ to the maximum value $E_\gamma^{\max} = E$ at this excitation-energy bin is unity:

$$\sum_{E_\gamma = E_\gamma^{\min}}^{E} P(E, E_\gamma) = 1. \tag{1}$$

For statistical γ decay in the continuum region, the γ-decay probability from an excitation energy E to $E_f = E - E_\gamma$ is proportional to the γ-ray transmission coefficient $\mathcal{T}(E_\gamma)$ and the level density at the final excitation energy $\rho(E_f)$:

$$P(E, E_\gamma) \propto \rho(E - E_\gamma)\mathcal{T}(E_\gamma). \tag{2}$$

The essential assumption underlying the above relation is that the reaction can be described as a two-stage process, where a compound state is first formed, before it decays in a manner that is independent of the mode of formation [21,22]. Equation (2) could also be regarded as a generalization[1] of Fermi's golden rule, where the decay rate is proportional to the density of final states and the square of the matrix element between the initial state and the final state.

The experimental normalized first-generation γ matrix can theoretically be approximated by

$$P_{\text{th}}(E, E_\gamma) = \frac{\rho(E - E_\gamma)\mathcal{T}(E_\gamma)}{\sum_{E_\gamma = E_\gamma^{\min}}^{E} \rho(E - E_\gamma)\mathcal{T}(E_\gamma)}. \tag{3}$$

The γ-ray transmission coefficient $\mathcal{T}$ is independent of excitation energy according to the generalized Brink-Axel hypothesis [23,24], which states that collective excitation modes built on excited states have the same properties as those built on the ground state. There is evidence that the width of the giant dipole resonance (GDR) varies with the nuclear temperature of the state on which it is built [25,26]. However, the temperature corresponding to the excitation-energy range covered in this work is rather low and changes slowly with excitation energy ($T \sim \sqrt{E_f}$). The temperature is therefore assumed to be approximately constant, and the Brink-Axel hypothesis is recovered in the energy region of interest.

To extract the level density and the γ-ray transmission coefficient, an iterative procedure [20] is applied to the first-generation γ matrix $P(E, E_\gamma)$. The basic idea of this method is to minimize

$$\chi^2 = \frac{1}{N_{\text{free}}} \sum_{E=E^{\min}}^{E^{\max}} \sum_{E_\gamma = E_\gamma^{\min}}^{E} \left[\frac{P_{\text{th}}(E, E_\gamma) - P(E, E_\gamma)}{\Delta P(E, E_\gamma)} \right]^2, \tag{4}$$

where N_{free} is the number of degrees of freedom and $\Delta P(E, E_\gamma)$ is the uncertainty in the experimental first-generation γ matrix. Every point of the ρ and $\mathcal{T}$ functions is assumed as an independent variable, so the reduced χ^2 is minimized for every argument $E - E_\gamma$ and E. The quality of the procedure when applied to the ^{44}Sc data is shown in Fig. 4, where the experimental first-generation spectra for various initial excitation energies are compared to the least-χ^2 solution. In general, the agreement between the experimental data and the fit is very good.

The globalized fitting to the data points only gives the functional form of ρ and $\mathcal{T}$. In fact, it has been shown [20] that if one solution for the multiplicative functions ρ and $\mathcal{T}$ is known, one may construct an infinite number of other

[1] A generalization in the sense that the present work deals with an ensemble of initial and final states and therefore considers the average decay properties in each excitation-energy bin.

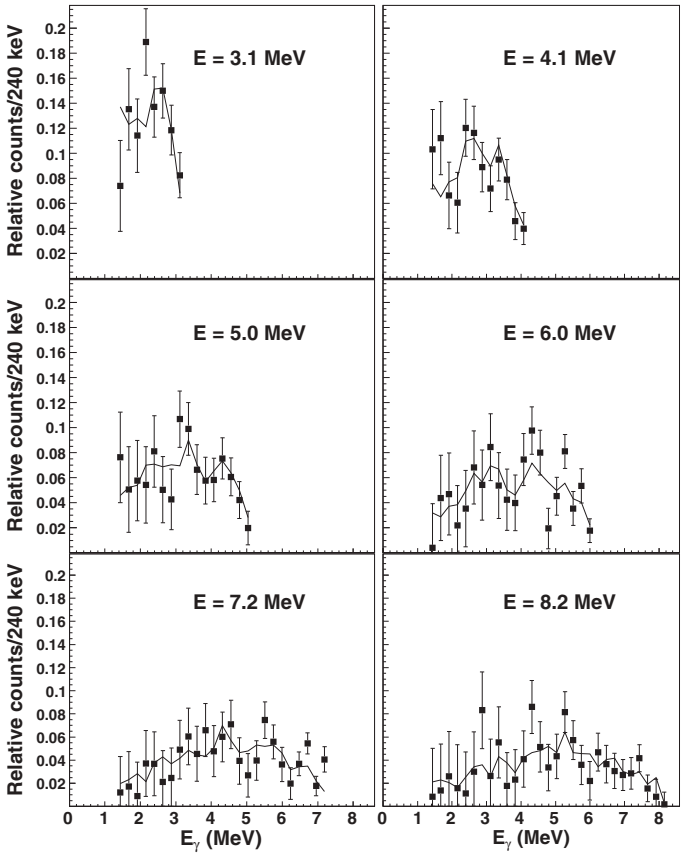

FIG. 4. A sample of the experimental first-generation spectra of ^{44}Sc (data points with error bars) are plotted with the least-χ^2 fit (lines).

functions, which give identical fits to the $P(E, E_\gamma)$ matrix by

$$\tilde{\rho}(E - E_\gamma) = A \exp[\alpha(E - E_\gamma)]\, \rho(E - E_\gamma), \quad (5)$$

$$\tilde{\mathcal{T}}(E_\gamma) = B \exp(\alpha E_\gamma) \mathcal{T}(E_\gamma). \quad (6)$$

Therefore the transformation parameters α, A, and B, which correspond to the physical solution, remain to be found.

III. THE LEVEL DENSITIES

A. Normalization

As described in the previous section, only the shape of the level density is found through the least χ^2 procedure of Ref. [20]. To determine the slope α and the absolute value A in Eq. (5), the ρ function is adjusted to match the number of known discrete levels at low excitation energy [27] and proton-resonance data [28,29] at high excitation energy. The procedure for extracting the total level density ρ from the resonance spacing D is described in Ref. [20]. Because the proton beam energy had a range of $E_p(^{44}\mathrm{Sc})$ = 0.90–1.50 MeV and $E_p(^{45}\mathrm{Sc})$ = 2.50–3.53 MeV in Refs. [28,29], respectively, the level density estimated from the proton resonances is not at the proton binding energy B_p, but rather at approximately $B_p + (\Delta E)/2$, where ΔE is the energy range of the proton beam, assuming that the resonances are approximately equally distributed over ΔE. Also, the authors of Ref. [28] do not distinguish between s- and p-wave resonances, so the calculation of the total level density is rather uncertain in the case of ^{44}Sc. However, by comparing with preliminary level-density data from an experiment done on ^{44}Sc at Ohio University, the slope α seems to be correct [30].

Because our experimental data points of the level density only reach up to an excitation energy of ~7.2 and ~8.0 MeV for ^{44,45}Sc, respectively, we extrapolate with the back-shifted Fermi gas model [31,32]

$$\rho_{\mathrm{BS}}(E) = \eta \frac{\exp(2\sqrt{aU})}{12\sqrt{2}a^{1/4}U^{5/4}\sigma}, \quad (7)$$

where a constant η is introduced to ensure that ρ_{BS} has the same value as the level density calculated from the proton-resonance experiments. The intrinsic excitation energy is estimated by $U = E - E_1$, where E_1 is the back-shift parameter.

TABLE I. Parameters used for the back-shifted Fermi gas level density and the parameters from Ref. [32].

Nucleus	E_1 (MeV)	a (MeV^{-1})	σ	E_1^{a} (MeV)	a^{a} (MeV^{-1})	σ^{a}	B_p (MeV)	$B_p+(\Delta E)/2$ (MeV)	D^{b} (eV)	ρ (proton res.) (MeV^{-1})	η
^{44}Sc	−2.91	5.13	3.53	−2.06	5.68	3.37	6.696	7.896	3243(324)	1855(392)	1.12
^{45}Sc	−2.55	4.94	3.75	−0.61	6.07	3.41	6.889	9.904	7874(496)	3701(760)	1.26

[a]Calculated with the method of Ref. [32].
[b]Calculated from proton-resonance data.

The spin-cutoff parameter is given by[2]

$$\sigma^2 = 0.0146A^{5/3}\frac{1+\sqrt{1+4aU}}{2a}, \quad (8)$$

where A is the mass number. Because the level-density parameter a and the back-shift parameter E_1 calculated with the method of Ref. [32] did not seem to give reliable results for ^{45}Sc, these parameters were extracted by fitting the Fermi gas to the known levels at ∼1.75 MeV and ∼2 MeV for ^{44,45}Sc, respectively, and to the known resonance-spacing data at $B_p+(\Delta E)/2$. The parameters used for ^{44,45}Sc in Eq. (7) are listed in Table I, where also the Fermi-gas parameters from Ref. [32] are shown. As the authors demonstrate in Fig. 5 in Ref. [32], the difference between the calculated parameters and the empirically extracted ones might be large in the mass region $A \leqslant 50$. The normalization procedure is pictured in Fig. 5; note that only statistical errors are shown. Above ∼2 MeV, there are more than 30 levels per MeV, giving the present limit to make complete spectroscopy in these nuclei.

The normalized level densities of ^{44}Sc and ^{45}Sc are displayed in Fig. 6. As one would expect, the odd-odd nucleus ^{44}Sc has an overall higher level density than its odd-even neighbor ^{45}Sc due to its two unpaired nucleons. The difference in level density between the odd-odd (^{44}Sc) and the odd-even (^{45}Sc) nucleus is seen to be approximately constant, except in the area between $E \sim 4$–5 MeV, where the level densities are almost the same. This is in agreement with earlier findings in the rare-earth region. However, here the odd-odd system has approximately a factor of 2 higher level density compared to the odd-even nucleus, whereas for rare-earth nuclei the difference was found to be a factor of 5.

Bump structures in the level densities of the scandium nuclei are observed. Standard models such as the back-shifted Fermi gas give a smooth ρ function and are unable to describe the structures that appear in the experimental level density in this excitation-energy region.

B. Comparison with microscopic model

To further investigate the level density at high excitation energy, a microscopic model has been developed. The model is based on combining all possible proton and neutron configurations within the Nilsson energy scheme, and the concept of Bardeen-Cooper-Schrieffer (BCS) quasiparticles [33] is utilized.

The model is described within the microcanonical ensemble, where the excitation energy E is well defined. The single-particle energies e_{sp} are taken from the Nilsson model for an axially deformed core described by the quadrupole deformation parameter ϵ_2. Furthermore, the model depends on the spin-orbit and centrifugal parameters κ and μ. The oscillator quantum energy $\hbar\omega_0 = 41A^{-1/3}$ MeV between the harmonic oscillator shells is also input to the code. Within the BCS model, the single-quasiparticle energies are defined by

$$e_{qp} = \sqrt{(e_{sp}-\lambda)^2+\Delta^2}, \quad (9)$$

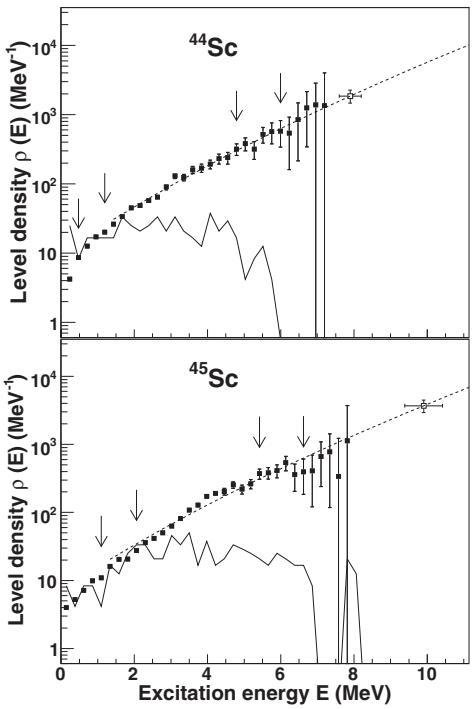

FIG. 5. Normalization procedure of the experimental level density (data points) of ^{44,45}Sc. The data points between the arrows are normalized to known levels at low excitation energy (solid line) and to the level density at the proton-separation energy (open square) using the Fermi-gas level density (dashed line).

[2]The authors of Ref. [32] found this expression to be the most adequate in the low-energy region, even though it is connected to the (mathematically incorrect) relation $U = aT^2 - T$ and not the standard one $U = aT^2$ (see Ref. [31] for more details).

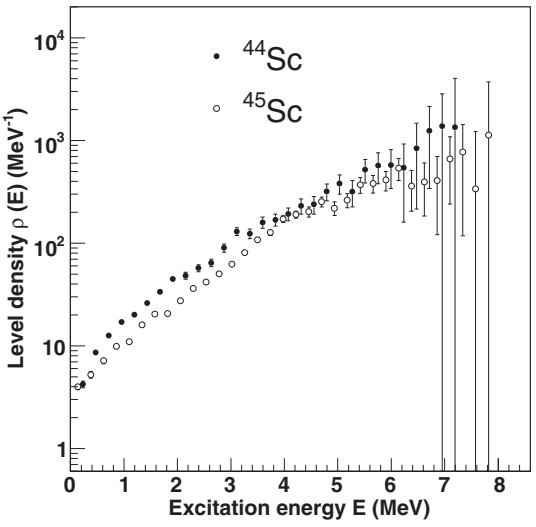

FIG. 6. Normalized level densities for ^{44,45}Sc.

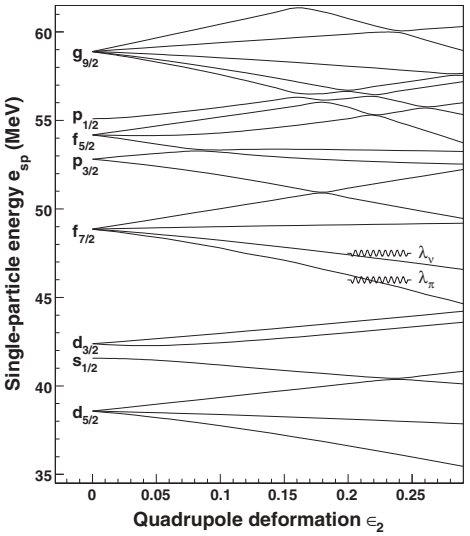

FIG. 7. The Nilsson level scheme for ^{45}Sc with parameters $\kappa = 0.066$ and $\mu = 0.32$.

where the Fermi level λ is adjusted to reproduce the number of particles in the system and Δ is the pair-gap parameter, which is kept constant.

The double-degenerated proton and neutron quasiparticle orbitals are characterized by their spin projections on the symmetry axis Ω_π and Ω_ν, respectively. The energy due to quasiparticle excitations is given by

$$E_{\rm qp}(\Omega_\pi, \Omega_\nu) = \sum_{\{\Omega'_\pi \Omega'_\nu\}} [e_{\rm qp}(\Omega'_\pi) + e_{\rm qp}(\Omega'_\nu) + V(\Omega'_\pi, \Omega'_\nu)]. \tag{10}$$

Between the aligned and antialigned levels of the proton and neutron projections, i.e., $\Omega_\pi + \Omega_\nu$ and $|\Omega_\pi - \Omega_\nu|$, a residual interaction V is defined as a random Gaussian distribution centered at zero energy with a width of 50 keV. The sets of proton and neutron orbitals $\{\Omega'_\pi \Omega'_\nu\}$ are picked out by using a random generator. The total number of broken Cooper pairs are set to 3, making a maximum number of 8 participating quasiparticles for odd-odd nuclear systems. Technically, this process is repeated until all possible energies $E_{\rm qp}(\Omega_\pi, \Omega_\nu)$ have been obtained. An indicator that this saturation is reached, is that all energies are reproduced at least ten times in the simulation.

Collective energy terms are schematically added by

$$E = E_{\rm qp}(\Omega_\pi, \Omega_\nu) + A_{\rm rot} R(R+1) + \hbar\omega_{\rm vib} v, \tag{11}$$

where $A_{\rm rot} = \hbar^2/2\mathcal{J}$ is the rotational parameter and $R = 0, 1, 2, 3 \ldots$ is the rotational quantum number. The vibrational motion is described by the phonon number $v = 0, 1, 2, \ldots$ and the oscillator quantum energy $\hbar\omega_{\rm vib}$.

The advantage of the present model is a fast algorithm that may include a large model space of single-particle states. Because level density is a gross property, the detailed knowledge of the many-particle matrix elements through large diagonalizing algorithms is not necessary. No level inversion is observed, as frequently seen for microscopic models with single-particle orbital truncations. In the sum of Eq. (10), all orbitals with energy up to the maximum energy ($e_{\rm qp} < E$) are included. Typically, for excitation energies up to ~10 MeV, about 20 proton and 20 neutron orbitals are taken into account (~10 orbitals below the Fermi level and ~10 orbitals above).

In the calculation we adopted the Nilsson parameters $\kappa = 0.066$ and $\mu = 0.32$ from Ref. [34] with oscillator quantum energy of $\hbar\omega_{\rm vib} = 1.904$ MeV, found from the 0^+ vibrational state in ^{44}Ti [35]. The Nilsson levels used in the calculations for ^{45}Sc are shown in Fig. 7, with the Fermi levels for the protons and neutrons. The value of the deformation parameter ϵ_2 was set to 0.23, which is in agreement with values suggested in Ref. [15]. The rotational and vibrational terms contribute only significantly to the total level density in the lower excitation region. To reproduce the transition energy from the $11/2^- \rightarrow 7/2^-$ transition in the ground-state rotational band of ^{45}Sc [35], the rotational parameter $A_{\rm rot}$ was set to 0.135 MeV. The adopted pairing gap parameters Δ_π and Δ_ν are taken from the calculations of Dobaczewski *et al.* [36] for the even-even ^{42}Ca for ^{44}Sc and ^{44}Ca for ^{45}Sc. A list of the input data for the model calculations can be found in Table II.

The experimental and calculated level densities are shown in Fig. 8. The result is satisfactory, especially for the nucleus

TABLE II. Model parameters.

Nucleus	ϵ_2	Δ_π (MeV)	Δ_ν (MeV)	$A_{\rm rot}$ (MeV)	$\hbar\omega_0$ (MeV)	$\hbar\omega_{\rm vib}$ (MeV)	λ_π (MeV)	λ_ν (MeV)
^{44}Sc	0.23	1.234	1.559	0.135	11.61	1.904	45.96	47.47
^{45}Sc	0.23	1.353	1.599	0.135	11.53	1.904	45.60	47.91

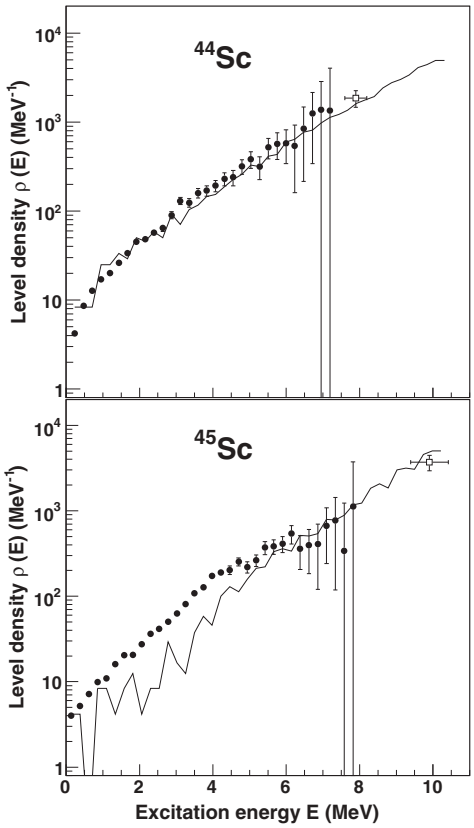

FIG. 8. Calculated level densities (solid lines) compared with the experimental ones (data points with error bars) for ^{44,45}Sc.

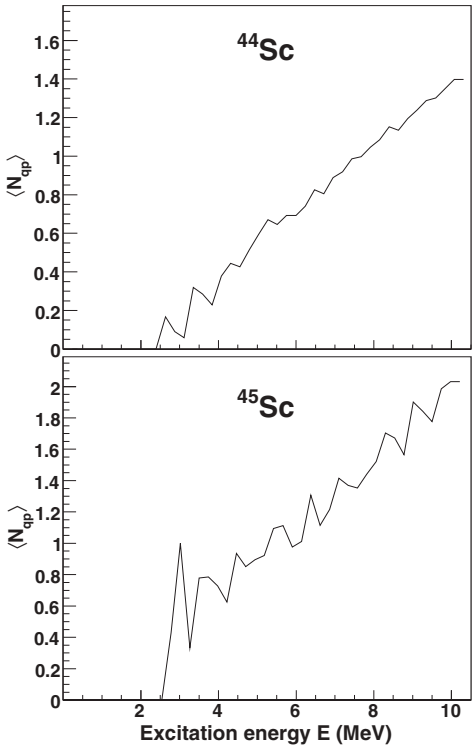

FIG. 9. The average number of broken Cooper pairs as function of excitation energy for ^{44,45}Sc.

^{44}Sc where there is a good agreement between the model calculation and the experimental level density. The general decrease in level density for the odd-even system compared to the odd-odd nucleus as well as the level densities found from the proton-resonance experiments are well reproduced. However, it is seen that the model misses many low-lying levels in the excitation-energy region $E = 1$–5 MeV for ^{45}Sc. This can, at least partially, be explained by the well-established shape coexistence determined from the negative-parity and positive-parity bands in this nucleus [15]. Only one shape is included in our model, and thus only one potential, which results in an undershoot of bandheads of about a factor of 2.

The pairing parameters Δ_π and Δ_ν are important inputs of the model, because the slope of the level density (in log scale) increases with decreasing pairing parameters in the energy region considered here. It can be seen from Fig. 8 that the adopted values give a nice agreement of the log slope of the level densities for both isotopes.

Figure 9 shows the average number of broken Cooper pairs $\langle N_{\rm qp}\rangle$ as a function of excitation energy. This is calculated by looking at all configurations obtained in each 240-keV excitation-energy bin, and finding the number of configurations with one broken pair, two broken pairs and so on. Both neutron and proton pairs are taken into account. From this information the average number of broken Cooper pairs is calculated. From Fig. 9, the pair-breaking process is seen to start at $E \sim 2.5$ MeV for both nuclei, in accordance with the values used for Δ_π (see Table II). The average number of broken pairs seems to have a relatively linear increase, giving an exponential growth in the level density. This behavior also indicates that there is no abrupt change in seniority as a function of excitation energy. For example, in the region $E = 9$–10 MeV, the model predicts 1% states with no pairs broken, 34% states with one broken pair, 61% states with two broken pairs, and 4% of the states have three pairs broken.

The location of the proton and neutron Fermi levels of ^{44,45}Sc in the Nilsson level scheme gives, roughly speaking, mostly positive-parity orbitals below and negative-parity states above the Fermi levels. Knowing this, one would expect a relatively homogeneous mixture of positive and negative parity states in the whole excitation-energy region covered by the calculations. In order to investigate this feature, we utilize the parity asymmetry defined in Ref. [37] by

$$\alpha = \frac{\rho_+ - \rho_-}{\rho_+ + \rho_-}, \tag{12}$$

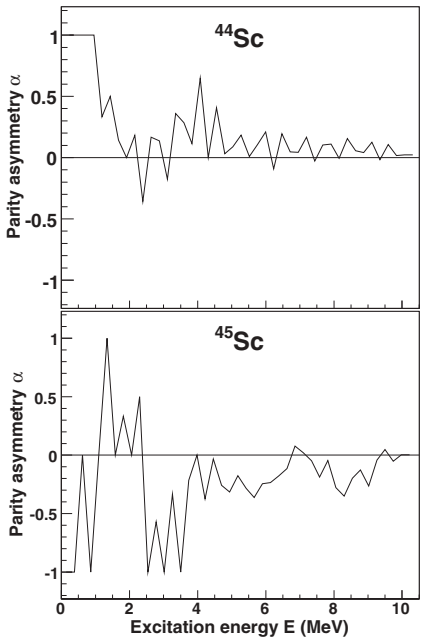

FIG. 10. The parity asymmetry as function of excitation energy for ^{44,45}Sc.

which gives −1 and 1 for only negative and positive parities, respectively, and 0 when both parities are equally represented. In Fig. 10 the parity asymmetry α is shown as a function of excitation energy. On the average, for $E > 4$ MeV, there seems to be a slight excess of positive- and negative-parity states in ^{44}Sc and ^{45}Sc, respectively. However, as the excitation energy increases, the model predicts that the parity asymmetry becomes smaller and smaller for both nuclei. The proton-resonance data in Ref. [37] from the reaction ^{44}Ca+p (compound nucleus ^{45}Sc, with excitation-energy region 9.77–10.53 MeV), gives an asymmetry parameter $\alpha = -0.18^{+0.07}_{-0.06}$ for $J = 1/2$ resonances, and $\alpha = 0.23 \pm 0.07$ for $J = 3/2$ resonances. Given the level densities of $J = 1/2$ and $J = 3/2$ resonances (see Table III in Ref. [37]), the parity asymmetry for $\rho(J = 1/2, J = 3/2)$ can be estimated to $\alpha \sim 0.02$, in good agreement with the model's result in this excitation-energy region.

IV. THE γ-RAY STRENGTH FUNCTIONS

As mentioned in Sec. II, the γ-decay process in the (quasi-)continuum is governed by the level density and the γ-ray transmission coefficient. By using the Oslo method, also the γ-ray transmission coefficient can be extracted from the experimental data.

The slope of the γ-ray transmission coefficient $\mathcal{T}(E_\gamma)$ has already been determined through the normalization of the level densities (Sec. III A). However, the constant B in Eq. (6) remains to be determined. If there was data on the average total radiative width $\langle\Gamma_\gamma\rangle$ for these nuclei, this data could be utilized for the absolute normalization of $\mathcal{T}$ as described in, e.g, Refs. [38,39]. Because such data does not exist for ^{44,45}Sc, other considerations had to be made to obtain the absolute value of the strength function.

The experimental $\mathcal{T}$ contains components from all electromagnetic characters X and multipolarities L. It is closely connected to the total γ-ray strength function through the relation [40]

$$\mathcal{T}(E_\gamma) = 2\pi \sum_{XL} E_\gamma^{2L+1} f_{XL}(E_\gamma), \tag{13}$$

where f_{XL} is the γ-ray strength function for electromagnetic character X and multipolarity L. Assuming that the γ-decay taking place in the continuum is dominated by $E1$ and $M1$ transitions, the total γ-ray strength function can be approximated by

$$f(E_\gamma) \simeq \frac{1}{2\pi}\frac{\mathcal{T}(E_\gamma)}{E_\gamma^3}. \tag{14}$$

The resulting γ-ray strength functions of ^{44,45}Sc are then scaled to agree with data from Ref. [41]. Based on two resonances from the reaction ^{45}Sc(n,γ) and on the observation of 13 $E1$ transitions and 9 $M1$ transitions of average energy 7.0 and 7.2 MeV, respectively, the strength functions are found to be $f_{E1} = 1.61(59) \times 10^{-8}$ MeV^{-3} and $f_{M1} = 1.17(59) \times 10^{-8}$ MeV^{-3} [41]. By adding these values together, the absolute normalization is given at this specific γ energy. The experimental γ-ray strength functions of ^{44,45}Sc are displayed in Fig. 11, together with the data point from Ref. [41] used for the normalization.

Several interesting features can be seen in Fig. 11. In general, for $E_\gamma \geqslant 3.5$ MeV, the data show that the γ-ray strength functions of ^{44,45}Sc are slowly increasing with γ energy. For γ energies below ∼3 MeV, the γ-ray strength functions of both nuclei have an increase of a factor ∼3 relative to their minimum.

To investigate the experimental strength functions further, they are compared to theoretical predictions. For the $E1$ part of the total γ-strength function, the Kadmenskiĭ, Markushev, and Furman (KMF) model [26] described by

$$f_{E1}(E_\gamma) = \frac{1}{3\pi^2\hbar^2c^2}\frac{0.7\sigma_{E1}\Gamma_{E1}^2\left(E_\gamma^2 + 4\pi^2T^2\right)}{E_{E1}\left(E_\gamma^2 - E_{E1}^2\right)^2} \tag{15}$$

is applied. Here, σ_{E1} is the cross section, Γ_{E1} is the width, and E_{E1} is the centroid of the giant electric dipole resonance (GEDR). The Lorentzian parameters are taken from Ref. [42] (see Table III). The nuclear temperature on the final state, introduced to ensure a nonvanishing GEDR for $E_\gamma \to 0$, is given by $T(E_f) = \sqrt{U_f/a}$.

For f_{M1}, which is supposed to be governed by the spin-flip $M1$ resonance [38], the Lorentzian giant magnetic dipole resonance (GMDR)

$$f_{M1}(E_\gamma) = \frac{1}{3\pi^2\hbar^2c^2}\frac{\sigma_{M1}E_\gamma\Gamma_{M1}^2}{\left(E_\gamma^2 - E_{M1}^2\right)^2 + E_\gamma^2\Gamma_{M1}^2} \tag{16}$$

is adopted.

TABLE III. Parameters used for the theoretical γ-ray strength functions.

Nucleus	κ	A	b	E_{E1} (MeV)	σ_{E1} (mb)	Γ_{E1} (MeV)	E_{M1} (MeV)	σ_{M1} (mb)	Γ_{M1} (MeV)	E_{E2} (MeV)	σ_{E2} (mb)	Γ_{E2} (MeV)
^{44}Sc	1.11(3)	0.52(10)	2.57(23)	19.44	39.40	8.0	11.61	1.239	4.0	17.85	1.069	5.58
^{45}Sc	1.20(1)	1.62(9)	2.93(5)	19.44	39.40	8.0	11.53	1.214	4.0	17.71	1.047	5.57

The contribution from $E2$ radiation to the total strength function is assumed to be very small. However, for the sake of completeness, the $E2$ isoscalar reconance described by

$$f_{E2}(E_\gamma) = \frac{1}{5\pi^2\hbar^2c^2E_\gamma^2}\frac{\sigma_{E2}E_\gamma\Gamma_{E2}^2}{\left(E_\gamma^2 - E_{E2}^2\right)^2 + E_\gamma^2\Gamma_{E2}^2} \quad (17)$$

is included in the total, theoretical strength function.

In lack of any established theoretical prediction of the observed increase at low γ energy, this phenomenon is modelled by a simple power law as

$$f_{\text{upbend}}(E_\gamma) = \frac{1}{3\pi^2\hbar^2c^2}AE_\gamma^{-b}, \quad (18)$$

where A and b are fit parameters.

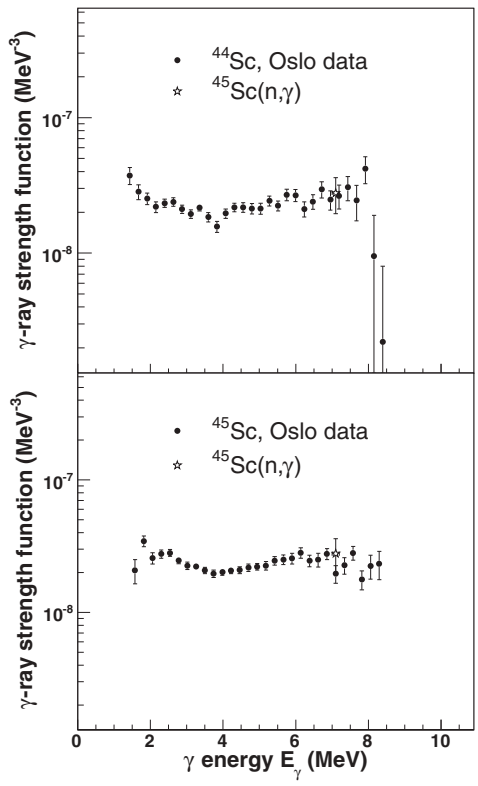

FIG. 11. Normalized γ-strength functions of ^{44,45}Sc (black dots), and $f_{E1} + f_{M1}$ from Ref. [41] (star).

The total, theoretical γ-ray strength function is then given by

$$f_{\text{total}} = \kappa(f_{E1} + f_{M1} + f_{\text{upbend}}) + E_\gamma^2 f_{E2}, \quad (19)$$

where κ is a renormalization factor that should be close to unity. All parameters employed are listed in Table III, and the result for ^{44}Sc is displayed in Fig. 12. It is seen that the theoretical strength function fits the data well. From Fig. 12, one would also conclude that the data points below ~3 MeV are not described by the standard models.

In Fig. 12 also the photoneutron cross-section data from the reaction ^{45}Sc$(\gamma,n)^{44}$Sc [43] and the photoproton cross-section data from the reaction ^{45}Sc$(\gamma,p)^{44}$Ca [44] are shown. The photoabsorbtion cross-section $\sigma(E_\gamma)$ is converted into strength function through the relation

$$f(E_\gamma) = \frac{1}{3\pi^2\hbar^2c^2}\left[\frac{\sigma(E_\gamma)}{E_\gamma}\right]. \quad (20)$$

The (γ,n) and (γ,p) data exhaust ~57% and ~25% of the Thomas-Reiche-Kuhn sum rule, respectively [42]. The summed strength of the two photoabsorption experiments for

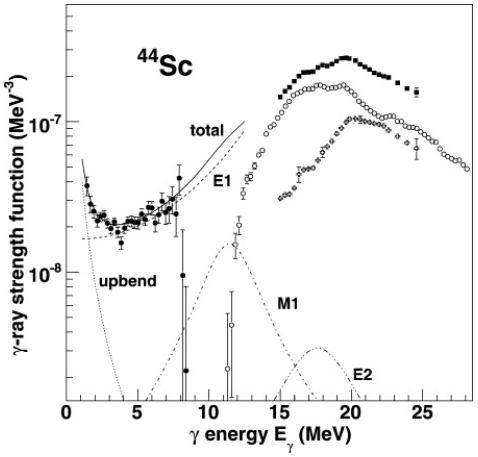

FIG. 12. The γ-strength functions of ^{44,45}Sc from Oslo experiments (black dots) and GDR data from (γ,n) (white dots) and (γ,p) (white crosses) experiments [43,44]. The black squares represent the summed strength from the (γ,n) and (γ,p) experiments for $E_\gamma = 15.0$–24.6 MeV. Also the total, theoretical strength function (solid line), the $E1$ tail from the KMF model (dashed line), the spin-flip $M1$ resonance (dashed-dotted line), the $E2$ isoscalar resonance (dashed-dotted line), and a fit to the upbend structure (dotted line) are shown.

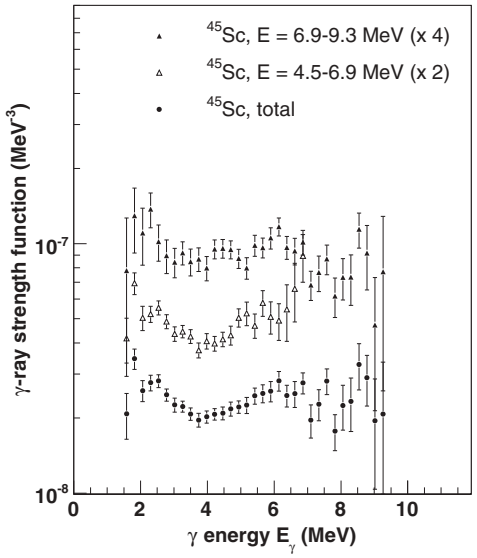

FIG. 13. The γ-strength function of ^{45}Sc extracted from different excitation-energy regions together with the strength function obtained from the total excitation-energy region considered.

$E_\gamma = 15.0$–24.6 MeV is also displayed in Fig. 12, and it seems to fit reasonably well with the theoretical expectation and the Oslo data. Note that the photoabsorption cross sections from the (γ, n) and (γ, p) reactions may have some overlap in strength in the energy region where the (γ, pn) channel is opened.

For γ energies below $\sim$3 MeV, the γ-ray strength functions of ^{44,45}Sc display an increase of a factor $\sim$3 relative to their minimum. This behavior has been observed in several medium-mass nuclei; first in ^{56,57}Fe [45], then recently in $^{93-98}$Mo [39] and ^{50,51}V [12]. For the iron and molybdenum isotopes, the upbend structure has been shown to be independent of excitation energy. This has also been tested for the Sc isotopes, as demonstrated in Fig. 13. Here, the γ-ray strength function of ^{45}Sc has been extracted from two different excitation-energy regions (the intervals 4.5–6.9 MeV and 6.9–9.3 MeV), representing two independent sets of data. As seen in Fig. 13, the result is quite convincing. The general trends are very similar, and the enhancement at low γ energies appears in both data sets.

The physical origin of this low-energy enhancement in strength is not yet understood. To check if the upbend feature could be due to peculiarities of the nuclear reactions or the Oslo method, a two-step cascade $(n, 2\gamma)$ experiment was carried out with ^{56}Fe as a target [45]. This experiment confirmed the large increase in γ-ray strength observed in the Oslo data but was unable to establish the character and multipolarity of the enhancement. To pin down the physical reason behind these observations, it is necessary to design and carry out experiments that have the possibility to determine the electromagnetic nature of this low-energy structure. Also, it would give better confidence to the findings to have independent confirmation of the increase from, e.g, $(n, 2\gamma)$ experiments on the Mo, V, and Sc isotopes as well.

V. SUMMARY AND CONCLUSIONS

The nuclear level densities and the γ-ray strength functions of the scandium isotopes ^{44,45}Sc were measured from primary γ rays using the Oslo method. The level densities display bump structures that cannot be obtained from standard statistical level-density models. A new, microscopic model to calculate the level density has been developed and applied on both nuclei, giving an overall good agreement with the experimental data. From the model, information on the average number of broken pairs and the parity asymmetry can also be extracted.

The γ-ray strength functions are in general found to be increasing functions of γ energy in the energy region examined in this work. The new data sets from the Oslo experiment are compared to theoretical models of the strength function and photoabsorbtion data, and the agreement seems to be good. At low γ energies a substantial enhancement of the total γ-ray strength is observed that is not accounted for in any of the standard theories. As of today, this puzzling feature has no satisfying, physical explanation.

ACKNOWLEDGMENTS

Financial support from the Norwegian Research Council (NFR) is gratefully acknowledged. A. Schiller acknowledges support from the U.S. National Science Foundation, grant number PHY-06-06007.

[1] E. Melby, L. Bergholt, M. Guttormsen, M. Hjorth-Jensen, F. Ingebretsen, S. Messelt, J. Rekstad, A. Schiller, S. Siem, and S. W. Ødegård, Phys. Rev. Lett. **83**, 3150 (1999).
[2] M. Guttormsen, M. Hjorth-Jensen, E. Melby, J. Rekstad, A. Schiller, and S. Siem, Phys. Rev. C **63**, 044301 (2001).
[3] J. M. Blatt and V. F. Weisskopf, *Theoretical Nuclear Physics* (John Wiley & Sons, New York, 1952).
[4] T. von Egidy, H. H. Schmidt, and A. N. Behkami, Nucl. Phys. **A481**, 189 (1988).
[5] W. P. Abfalterer, R. W. Finlay, and S. M. Grimes, Phys. Rev. C **62**, 064312 (2000).
[6] S. Siem, M. Guttormsen, K. Ingeberg, E. Melby, J. Rekstad, A. Schiller, and A. Voinov, Phys. Rev. C **65**, 044318 (2002).
[7] M. Guttormsen, A. Bagheri, R. Chankova, J. Rekstad, S. Siem, A. Schiller, and A. Voinov, Phys. Rev. C **68**, 064306 (2003).
[8] U. Agvaanluvsan *et al.*, Phys. Rev. C **70**, 054611 (2004).
[9] M. Guttormsen, E. Melby, J. Rekstad, A. Schiller, S. Siem, T. Lönnroth, and A. Voinov, J. Phys. G **29**, 263 (2003).
[10] A. Schiller *et al.*, Phys. Rev. C **68**, 054326 (2003).
[11] R. Chankova *et al.*, Phys. Rev. C **73**, 034311 (2006).
[12] A. C. Larsen *et al.*, Phys. Rev. C **73**, 064301 (2006).

[13] F. B. Malik and W. Scholz, Phys. Rev. **150**, 919 (1966).
[14] B. J. Cole, Nucl. Phys. **11**, 953 (1985).
[15] P. Bednarczyk *et al*., Phys. Lett. **B393**, 285 (1997).
[16] E. Caurier, G. Martinez-Pinedo, F. Nowacki, A. Poves, and A. P. Zuker, Rev. Mod. Phys. **77**, 427 (2005).
[17] M. Guttormsen, A. Atac, G. Løvhøiden, S. Messelt, T. Ramsøy, J. Rekstad, T. F. Thorsteinsen, T. S. Tveter, and Z. Zelazny, Phys. Scr. **T32**, 54 (1990).
[18] M. Guttormsen, T. S. Tveter, L. Bergholt, F. Ingebretsen, and J. Rekstad, Nucl. Instrum. Methods Phys. Res., Sect. A **374**, 371 (1996).
[19] M. Guttormsen, T. Ramsøy, and J. Rekstad, Nucl. Instrum. Methods A **255**, 518 (1987).
[20] A. Schiller, L. Bergholt, M. Guttormsen, E. Melby, J. Rekstad, and S. Siem, Nucl. Instrum. Methods Phys. Res., Sect. A **447**, 498 (2000).
[21] A. Bohr and B. Mottelson, *Nuclear Structure* (Benjamin, New York, 1969), Vol. I, p. 169, pp. 184–185.
[22] L. Henden, L. Bergholt, M. Guttormsen, J. Rekstad, and T. S. Tveter, Nucl. Phys. **A589**, 249 (1995).
[23] D. M. Brink, Ph.D. thesis, Oxford University, 1955.
[24] P. Axel, Phys. Rev. **126**, 671 (1962).
[25] G. Gervais, M. Thoennessen, and W. E. Ormand, Phys. Rev. C **58**, R1377 (1998).
[26] S. G. Kadmenskiĭ, V. P. Markushev, and V. I. Furman, Yad. Fiz. **37**, 277 (1983); [Sov. J. Nucl. Phys. **37**, 165 (1983)].
[27] Data extracted using the NNDC On-Line Data Service from the ENSDF database (http://www.nndc.bnl.gov/ensdf/).
[28] C. P. Poirier and J. C. Manthuruthil, *Proceedings from Topical Conference on the Structure of* $1f_{7/2}$ *Nuclei, Legnaro (Padova)*, Editrice Compositori, Bologna (1971).
[29] S. J. Lokitz, G. E. Mitchell, and J. F. Shriner, Jr., Phys. Rev. C **71**, 064315 (2005).
[30] A. Voinov (private communication).
[31] A. Gilbert and A. G. W. Cameron, Can. J. Phys. **43**, 1446 (1965).
[32] T. von Egidy and D. Bucurescu, Phys. Rev. C **72**, 044311 (2005); **73**, 049901(E) (2006).
[33] J. Bardeen, L. N. Cooper, and J. R. Schrieffer, Phys. Rev. **108**, 1175 (1957).
[34] D. C. S. White, W. J. McDonald, D. A. Hutcheon, and G. C. Neilson, Nucl. Phys. **A260**, 189 (1976).
[35] R. Firestone and V. S. Shirley, *Table of Isotopes*, 8th ed. (Wiley, New York, 1996), vol. II.
[36] J. Dobaczewski, P. Magierski, W. Nazarewicz, W. Satuła, and Z. Szymański, Phys. Rev. C **63**, 024308 (2001).
[37] U. Agvaanluvsan, G. E. Mitchell, J. F. Shriner Jr., and M. Pato, Phys. Rev. C **67**, 064608 (2003).
[38] A. Voinov, M. Guttormsen, E. Melby, J. Rekstad, A. Schiller, and S. Siem, Phys. Rev. C **63**, 044313 (2001).
[39] M. Guttormsen, R. Chankova, U. Agvaanluvsan, E. Algin, L. A. Bernstein, F. Ingebretsen, T. Lönnroth, S. Messelt, G. E. Mitchell, J. Rekstad, A. Schiller, S. Siem, A. C. Sunde, A. Voinov, and S. Ødegård, Phys. Rev. C **71**, 044307 (2005).
[40] J. Kopecky and M. Uhl, Phys. Rev. C **41**, 1941 (1990).
[41] J. Kopecky and M. Uhl, *Proceedings of a Specialists' Meeting on Measurement, Calculation and Evaluation of Photon Production Data, Bologna, Italy, 1994,* edited by C. Coceva, A. Mengoni, and A. Ventura [Report No. NEA/NSC/DOC(95)1].
[42] Centre for Photonuclear Experiments Data, http://cdfe.sinp.msu.ru
[43] A. Veyssiere, H. Beil, R. Bergere, P. Carlos, A. Lepretre, and A. de Miniac, Nucl. Phys. **A227**, 513 (1974).
[44] S. Oikawa and K. Shoda, Nucl. Phys. **A277**, 301 (1977).
[45] A. Voinov, E. Algin, U. Agvaanluvsan, T. Belgya, R. Chankova, M. Guttormsen, G. E. Mitchell, J. Rekstad, A. Schiller, and S. Siem, Phys. Rev. Lett. **93**, 142504 (2004).

7.4 Paper 3: Level densities of ^{44}Sc and ^{47}Ti from different experimental techniques

Level densities of ^{44}Sc and ^{47}Ti from different experimental techniques

A. V. Voinov,[1,*] S. M. Grimes,[1] A. C. Larsen,[2] C. R. Brune,[1] M. Guttormsen,[2] T. Massey,[1] A. Schiller,[1] S. Siem,[2] and N. U. H. Syed[2]

[1]*Department of Physics and Astronomy, Ohio University, Athens, Ohio 45701, USA*

[2]*Department of Physics, University of Oslo, N-0316 Oslo, Norway*

(Received 18 December 2007; published 31 March 2008)

The level densities of ^{44}Sc and ^{47}Ti have been determined from measurements of particle evaporation spectra from the compound nuclear reaction ^{3}He + ^{45}Sc with an 11 MeV ^{3}He beam. The level density of ^{44}Sc has been compared to the level density obtained from an independent experimental method based on an analysis of α-γ coincidences from the transfer reaction ^{45}Sc(^{3}He,$\alpha\gamma$)^{44}Sc. The good agreement between the two experiments indicates the reliability of the level density obtained. Some level density systematics have been tested against the experimental data. New Fermi-gas level density parameters have been derived.

DOI: 10.1103/PhysRevC.77.034613 PACS number(s): 21.10.Ma, 24.60.Dr, 27.40.+z

I. INTRODUCTION

The nuclear level density is difficult to measure precisely because of the lack of reliable experimental techniques. The counting of discrete levels is restricted to excitation energies below about 3–5 MeV for medium mass nuclei because above this limit the levels become too close in energy to resolve. Above these energies more sophisticated methods need to be applied (see Ref. [1]). The main approach for estimating the level density above the discrete level region is to use some model-based function with parameters fitted to the density of discrete low-lying levels and the density of neutron resonances. For nuclei for which information about the neutron resonance spacing is not available, parameter systematics must be used. There are several systematics of level density parameters (mainly related to either Fermi-gas or constant temperature models) that modern computer codes utilize to calculate reaction cross sections. However, because neutron resonances are known only for a very narrow spin interval, and because the shape of the level density function is not well established, it is not yet clear how well available systematics reproduce total level densities above the discrete level region.

At this time, two experimental techniques appear to be good candidates for the systematic investigation of the total level density in nuclei above the region of discrete levels. The first one was developed at the Oslo Cyclotron Laboratory (hereafter referred to as the "Oslo method") to extract both level density and γ-strength functions from the particle-γ coincidence matrix measured from inelastic scattering (^{3}He,^{3}He$'\gamma$) and transfer (^{3}He,$\alpha\gamma$) reactions [2]. The second method uses particle evaporation spectra from compound nuclear reactions [3]. The problem is that both methods might contain intrinsic systematic uncertainties, which are difficult to estimate while remaining inside of these methods. Particularly the Oslo method suffers from normalization uncertainties because it produces only a level density function with an uncertainty factor of $A\exp(BE_x)$, where E_x is the excitation energy. The coefficients (A, B) then have to be determined from auxiliary experimental information such as neutron resonance spacing (when available) and the density of discrete levels. The Oslo method is also based on assumptions discussed below, which are possible sources of systematic uncertainties as well. The main problem with the particle evaporation technique is possible contaminations of the evaporation spectra due to multistep and/or direct reaction contributions. It could result in an incorrect slope of the obtained level density function and could cause an absolute normalization problem.

The consistency of these two experimental techniques has been confirmed in Ref. [4], where the level density of ^{56}Fe was investigated with the reaction ^{57}Fe(^{3}He,$\alpha\gamma$)^{56}Fe by the Oslo method and with the neutron evaporation spectrum from the ^{55}Mn(d,n)^{56}Fe reaction. Neutron spectra are most suitable for level density studies because neutron transmission coefficients are better known than proton and α-transmission coefficients. Moreover, the neutron channel is a preferred decay channel for the compound nucleus. This means that it is more likely that compound reactions dominate the neutron spectrum. On the other hand, it would be highly desirable to study different types of reactions for these purposes. In this work we have studied the level density from the evaporation spectra of α particles from the ^{45}Sc(^{3}He,α)^{44}Sc reaction and compared it to the level density obtained recently from the ^{45}Sc(^{3}He,$\alpha\gamma$)^{44}Sc reaction using the Oslo method. The level density of ^{47}Ti populated by the ^{45}Sc(^{3}He,p)^{47}Ti reaction has been obtained as well. Different available level density systematics have been tested.

II. EXPERIMENTS AND METHODS

A. The Oslo method

At the Oslo Cyclotron Laboratory, a measurement of the ^{45}Sc(^{3}He,$\alpha\gamma$)^{44}Sc reaction with a 38 MeV ^{3}He beam was performed. The self-supporting natural target of 99.9% ^{45}Sc had a thickness of 3.4 mg/cm^2. Eight Si ΔE-E telescopes were arranged close to the target at an angle of 45° relative to the beam. The γ-ray detector CACTUS [5], consisting of 28 collimated NaI crystals with a total efficiency of 15%

*voinov@ohio.edu

surrounded the target and particle detectors. The experimental setup enabled particle-γ coincidence measurements of the reaction ^{45}Sc(^{3}He,$\alpha\gamma$)^{44}Sc. The experiment ran for about 5 days, with a typical beam current of $\sim$1 nA.

The essential part of the analysis of particle-γ coincidences is the extraction of first-generation spectra $P(E_x, E_\gamma)$ at each excitation energy bin E_x, which is the initial excitation energy of the γ transitions. The corresponding technique is described in Ref. [6]. The first generation matrix $P(E_x, E_\gamma)$ can be decomposed into a level density $\rho(E_x - E_\gamma)$ and γ-transmission function $T(E_\gamma)$ as

$$P(E_x, E_\gamma) \propto \rho(E_x - E_\gamma) T(E_\gamma). \tag{1}$$

The details of this particular experiment and its analysis are described in Ref. [7]. Here we would like to outline the important assumptions behind this decomposition.

(i) The γ decay from each excitation energy bin and the spin population within the bin are independent of how the levels were populated; whether directly by the reaction or by γ decay from higher-lying states.
(ii) The γ-strength function does not depend on the excitation energies of either initial or final states, it depends only on the γ energy.

It is difficult to estimate how large the possible violations of the assumptions are and how they affect the final results. Special concern is caused by the possible temperature dependence of the γ-strength function suggested in theoretical work [8] which would mean a violation of the second assumption.

B. Level density from evaporation spectra

To obtain an independent result on the level density of ^{44}Sc, we measured the α-particle evaporation spectrum from the ^{45}Sc(^{3}He,α)^{44}Sc reaction. The proton spectrum was also studied, which allowed us to investigate the level density of the residual ^{47}Ti nucleus. The experiment was performed with an 11-MeV ^{3}He beam from the tandem accelerator of the Ohio University Edwards Accelerator Laboratory. Proton and α-particle spectra were measured with a charged-particle spectrometer [1]. Seven 2-m time-of-flight tubes with Si detectors placed at the end were set up at angles ranging from 22.5° up to 157.5°. The masses of the charged particles were determined by measuring both the energy deposited in the Si detectors and the time of flight. The mass resolution was sufficient to resolve protons, deuterons, ^{3}He/^{3}H, and α particles.

The cross section of outgoing particles resulting from compound nucleus decay can be calculated in the framework of the Hauser-Feshbach (HF) model [9], according to which

$$\frac{d\sigma}{d\varepsilon_b}(\varepsilon_a, \varepsilon_b) = \sum_{J\pi^c} \sigma^{\mathrm{CN}}(\varepsilon_a) \frac{\sum_{I\pi^r} \Gamma_b(U, J, \pi^c, E, I, \pi^r) \rho_b(E, I, \pi^r)}{\Gamma(U, J, \pi^c)}, \tag{2}$$

with

$$\Gamma(U, J, \pi^c) = \sum_{b'} \left(\sum_k \Gamma_{b'}(U, J, \pi^c, E_k, I_k, \pi^r_k) + \sum_{I'\pi^{r'}} \int_{E_c}^{U-B_{b'}} dE' \, \Gamma_{b'} \times (U, J, \pi^c, E', I', \pi^{r'}) \, \rho_{b'}(E', I', \pi^{r'}) \right). \tag{3}$$

Here $\sigma^{\mathrm{CN}}(\varepsilon_a)$ is the fusion cross section, ε_a and ε_b are energies of relative motion for incoming and outgoing channels ($\varepsilon_b = U - E_k - B_b$, where B_b is the separation energy of particle b from the compound nucleus), Γ_b is the transmission coefficient of outgoing particles, and the quantities (U, J, π^c) and (E, I, π^r) are the energy, angular momentum, and parity of the compound and residual nuclei, respectively. The energy E_c is the continuum edge, above which levels are modeled using a level density parametrization. For energies below E_c, the known excitation energies, spins, and parities of discrete levels are used. In practice E_c is determined by the available spectroscopic data in the literature. It follows from Eq. (3) that the cross section is determined by both transmission coefficients of outgoing particles and the level density of the residual nucleus $\rho_b(E, I, \pi)$. It is believed that transmission coefficients are known with sufficient accuracy near the line of stability because they can be obtained from optical model potentials, which are usually based on experimental data for elastic scattering and total cross sections in the corresponding outgoing channel. Transmission coefficients obtained from different systematics of optical model parameters do not differ by more that 15–20 % from each other in our region of interest (1–15 MeV of outgoing particles). The uncertainties in level densities are much larger. Therefore, the HF model can be used to improve level densities by comparing experimental and calculated particle evaporation spectra. Details and assumptions of this procedure are described in Refs. [3] and [10]. The code HF2002 [11] was used for calculations of spectra from compound nuclear reactions.

The main uncertainty of this method comes from contributions of noncompound mechanisms of a nuclear reaction including direct, multistep direct, and multistep compound. They correspond to different stages of nucleon-nucleon interactions inside the projectile + target nuclear system until complete equilibrium is achieved. The measurement of the energy distribution of outgoing particles at backward angles reduces considerably the contribution from noncompound reactions, but does not guarantee their complete elimination. Therefore, the systematic uncertainties connected to the presence of noncompound reaction contributions can be estimated only by applying different experimental techniques directed to measure the level density of the same nucleus.

By comparing data obtained from the Oslo method with data extracted from particle evaporation spectra one can estimate possible systematic uncertainties pertaining to these methods.

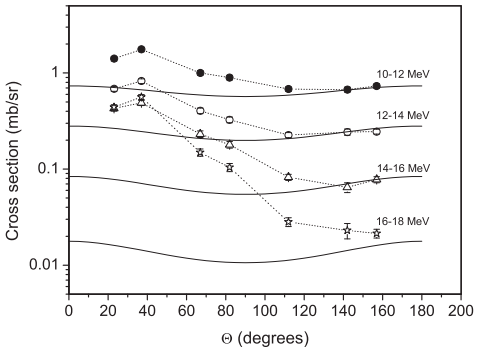

FIG. 1. Angular distributions of α particles in the c.m. system for different energy intervals. The points are experimental data and the solid lines are HF calculations normalized to match the experimental points at backward angles for low energy particles.

III. RESULTS

To investigate the reaction mechanism, the proton and α-particle angular distributions were measured (Figs. 1 and 2). In the figures the particle energies are restricted to ensure that only first stage particles emitted immediately from the compound nucleus ^{48}V can contribute. For compound nuclear reactions the HF calculation predicts a symmetric angular distribution of the cross section with respect to 90° in the center of mass system. The present measurement exhibits forward-peaked distributions for both protons and α particles. However, it is important to note that for lower energy α particles, the angular distribution starts to follow the calculated curve at ≈115° and beyond. For higher energy particles the asymmetry is stronger. For α particles in the energy interval 16–18 MeV, i.e., for those populating the discrete levels of ^{44}Sc, the angular distribution does not agree with calculations even at backward angles. This means that high energy α particles contain contributions from noncompound reactions even at backward angles. From this analysis, it is possible to conclude that the α-particle spectra measured at backward

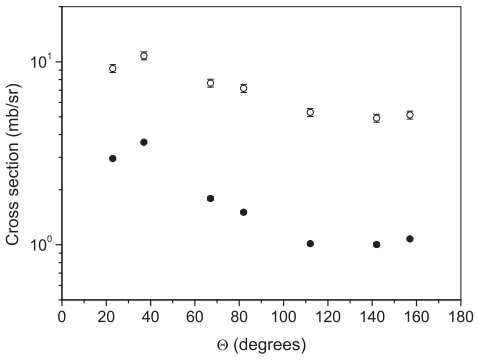

FIG. 2. Angular distributions of protons (open circles) and α particles (solid circles) in the c.m. system.

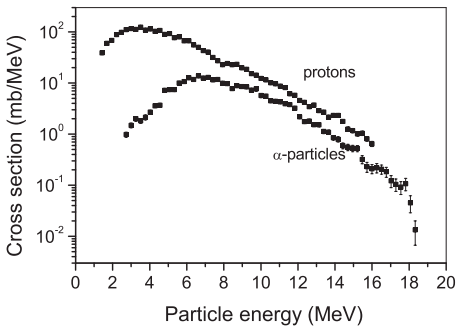

FIG. 3. Experimental energy spectra of protons and α particles measured at 157° with respect to the beam line.

angles can be used for extracting level densities but only in the energy region 10–16 MeV, which corresponds to excitation energies of the residual ^{44}Sc nucleus between 2 and 8 MeV. We could not make a similar analysis for protons because the thickness of our detectors (1000 and 1500 μm) was not sufficient to stop protons with energies greater than 10 and 15 MeV, respectively (note that the maximum proton energy from this reaction is 21 MeV). Therefore, the proton angular distribution is integrated over all energies and is presented in Fig. 2 along with integrated distribution for α particles. The similarity of these distributions indicates that the compound mechanism is the main mechanism determining both proton and α-particle spectra measured at backward angles.

The energy dependence of proton and α-particle cross sections measured at 157° with respect to the beam axis are shown in Fig. 3. The level densities for both ^{44}Sc (populated by α particles) and ^{47}Ti (populated by protons) nuclei were obtained by the method described in Ref. [3] and in our previous article [1]: a level density model is chosen for the calculation of the differential cross section of Eq. (3). The parameters of the model are then adjusted to reproduce the experimental spectra as closely as possible. The input level density is improved by binwise renormalization according to the expression

$$\rho_b(E, I, \pi) = \rho_b(E, I, \pi)_{\text{input}} \frac{(d\sigma/d\varepsilon_b)_{\text{meas}}}{(d\sigma/d\varepsilon_b)_{\text{calc}}}. \qquad (4)$$

To get the absolute normalization, information about the level density of discrete levels is used.

The level densities of ^{47}Ti and ^{44}Sc extracted from proton and α-particle evaporation spectra are shown in Fig. 4. The level density of ^{44}Sc extracted from the Oslo experiment is presented for comparison.

The absolute normalization of the level density for ^{44}Sc has been obtained by matching the Oslo level density to the density of discrete levels in the low energy region and by matching the slope of the Oslo level density to the slope of the level density obtained from the particle evaporation spectrum. One can see the good agreement between the shapes of the level densities from two types of experiments. The absolute normalization of the level density for ^{47}Ti was obtained from the ratio of α/proton cross sections of the ^{3}He + ^{45}Sc reaction.

TABLE I. Ratio of experimental and model level densities at different excitation energies E_x. The bottom line shows the comparison of the experimental and calculated ratios of α-particle and proton cross sections.

Nucleus	E_x (MeV)	$\rho^{\exp}/\rho^{\text{model}}$			
		FG [12]	HFBCS [15]	GC [14]	CT [12]
^{47}Ti	5.5	0.78(16)	0.92(19)	1.52(31)	1.19(24)
	6.5	0.83(17)	1.14(23)	1.73(35)	1.18(24)
	7.5	0.69(14)	1.12(23)	1.53(31)	0.92(19)
	8.5	0.58(12)	1.10(22)	1.34(27)	0.70(14)
	9.5	0.60(12)	1.30(26)	1.40(28)	0.63(12)
	10.5	0.53(10)	1.29(26)	1.20(24)	0.45(9)
	11.5	0.49(10)	1.35(27)	1.06(21)	0.36(7)
^{44}Sc	2.5	1.41(30)	0.67(14)	1.50(31)	1.53(32)
	3.5	1.16(24)	0.61(13)	1.46(30)	1.27(26)
	4.5	1.00(20)	0.56(11)	1.42(29)	1.04(21)
	5.5	0.91(18)	0.56(11)	1.43(29)	0.88(18)
	6.5	0.93(19)	0.60(12)	1.55(31)	0.81(16)
		$\frac{\sigma_\alpha^{\exp}/\sigma_p^{\exp}}{\sigma_\alpha^{\text{cal}}/\sigma_p^{\text{cal}}}$			
		1.6(2)	0.5(2)	1.1(2)	1.2(2)

The experimental level densities have been compared to some level density models widely used in modern HF computer codes. These prescriptions are based on the Fermi gas (FG) model, the constant temperature (CT) model with parameters from the recent compilation of Ref. [12], and the Gilbert-Cameron (GC) formula [13]. Parameter systematics are obtained mainly on the basis of available information about the level density in the region of discrete levels and neutron resonances. For the GC model the Fermi-gas level density parameter a was calculated according to the Ignatyuk systematics [14] while parameters of the constant temperature part of the GC formula were obtained from the fit to discrete levels. We also tested the level density calculations based on the Hartree-Fock-BCS approach (HFBCS) [15] recommended by the RIPL data base [16]. Table I shows the ratio between experimental and model level densities at different excitation energies. It shows also how well HF calculations reproduce the ratio of α and proton cross sections. This is an important issue because this ratio gives an additional constraint on level densities of residual nuclei. The conclusion is that the level density of ^{47}Ti is best reproduced with the HFBCS model but the FG systematics fit better for ^{44}Sc. No single model with parameters from systematics reproduces level densities of both nuclei equally well. However, HF calculations with GC and CT models reproduce well the ratio of α and proton cross sections.

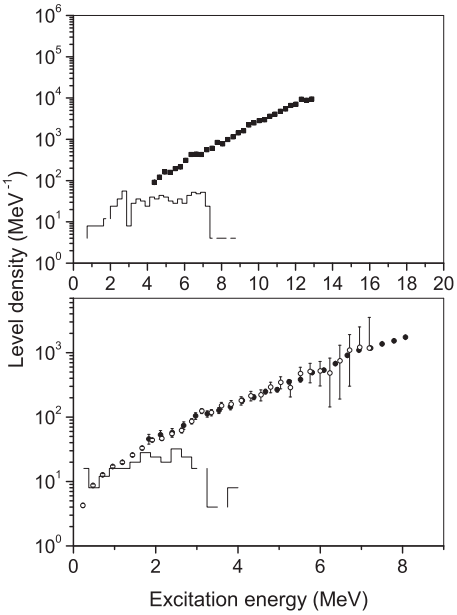

FIG. 4. Level densities of ^{47}Ti (upper panel) and ^{44}Sc (lower panel) nuclei obtained from proton and α-particle energy spectra, respectively. Black points are data from particle evaporation spectra. Open points are data from the Oslo experiment [7]. The histograms represent level densities from the counting of discrete levels.

To improve the level density prescription for these nuclei, we used the FG model with free parameters a and δ to fit the experimental level densities. The rigid-body spin cutoff parameter was adopted for this fit. The parameters we obtained are $a = 5.13$ MeV^{-1} and $\delta = -2.91$ MeV for ^{44}Sc and $a = 5.06$ MeV^{-1} and $\delta = -1.95$ MeV for ^{47}Ti. These parameters can be compared to parameters from systematics [12]: $a = 5.68$ MeV^{-1} and $\delta = -2.064$ MeV for ^{44}Sc and $a = 5.99$ MeV^{-1} and $\delta = -0.738$ MeV for ^{47}Ti. Discrepancies in corresponding level densities are shown in Table I. The systematics of Ref. [12] agree with the experimental level density of the ^{44}Sc nucleus but are off by a factor of 1.3–2 for ^{47}Ti. However, in the case of ^{47}Ti, level density parameters

from our experiment agree better with ones determined in Ref. [12] on the basis of a fit to low-lying discrete levels and neutron resonance spacings ($a = 5.14(30)$ MeV^{-1} and $\delta = -1.35(74)$ MeV).

It should be noted that the drawback of all available level density systematics is that all of them use the neutron resonance spacing as a main source for the experimental level density at the neutron binding energy. The problem is that the neutron resonances are known within a narrow spin interval and the spin cutoff parameter must be used to calculate the total level density, which actually affects the reaction cross section calculations. The lack of experimental information on the spin cutoff parameter above the discrete level region introduces additional uncertainties in the calculation of reaction cross sections and can cause deviations from our experimental data (see Table I). An alternative option would be to establish a level density systematic based on experimental data on total level densities. There was an attempt [17] to establish the systematic based on particle evaporation spectra. About 50 nuclei from the $A = 10$–70 region have been analyzed. However, because of large discrepancies in level density parameters from different experiments, no good systematic regularity has been found.

The consistency between experimental level densities obtained from the Oslo method and particle evaporation spectra supports the underlying assumption of the Oslo method. It shows that the statistical mechanism is the major mechanism of γ decay following α-particle emission in the ^{45}Sc(^{3}He,$\alpha\gamma$) reaction. The spin of levels populated by either α particles or γ transitions does not seem to be much different. Also, the uncertainties due to the possible temperature dependence of the γ-strength function are small enough to not affect the final level density obtained by the Oslo method. All of these results indicate that the Oslo method, within its limitations, is a reliable tool for studying nuclear level densities.

The method based on particle energy spectra may suffer from systematic uncertainties connected to contributions of noncompound reaction mechanisms. These contributions depend on the type of reaction used as well as on the angle at which the spectra are measured. Backward angles allow one to reduce the contribution from noncompound reactions considerably but do not eliminate completely this effect, especially for high energy particles. The measurement of the angular distribution is an important tool in the analysis helping to determine the angle and energy ranges to be used for the level density determination.

IV. CONCLUSION

The level density of ^{44}Sc has been obtained from two independent experiments by using two different methods. These are the Oslo method based on the analysis of particle-γ coincidences from the ^{45}Sc(^{3}He,$\alpha\gamma$) reaction and the method based on the analysis of particle spectra from the compound nuclear reaction ^{45}Sc(^{3}He,α). Both methods produce the level densities that are in good agreement with each other. It has been shown that possible systematic uncertainties of the Oslo method resulting from underlying assumptions are negligible and do not cause any serious problems. The α particles from the ^{45}Sc(^{3}He,α) compound reaction measured at backward angles can be used to extract the level density of the corresponding residual nucleus. The angular distribution is an important factor in determining the range of energies of outgoing particles where the compound reaction mechanism is dominant.

The level density of ^{47}Ti has been obtained from the proton evaporation spectrum of the ^{45}Sc(^{3}He,p) reaction. Both ^{44}Sc and ^{47}Ti experimental level densities have been compared to several level density models. Despite the fact that some of these models reproduce experimental data well for one of these nuclei, none of the models seem to fit experimental data for both of them. The deviation from the best fit can be as large as 50%. New Fermi-gas level density parameters have been obtained.

ACKNOWLEDGMENTS

We are grateful to J. E. O'Donnell and D. Carter for computer and electronic support during the experiment and to A. Adekola, C. Matei, B. Oginni, and Z. Heinen for taking shifts. We also acknowledge financial support from the Department of Energy, Grant N DE-FG52-06NA26187/A000.

[1] A. V. Voinov, S. M. Grimes, C. R. Brune, M. J. Hornish, T. N. Massey, and A. Salas, Phys. Rev. C **76**, 044602 (2007).
[2] A. Schiller, L. Bergholt, M. Guttormsen, E. Melby, J. Rekstad, and S. Siem, Nucl. Instrum. Methods Phys. Res. A **447**, 498 (2000).
[3] H. Vonach, in *Proceedings of the IAEA Advisory Group Meeting on Basic and Applied Problems of Nuclear Level Densities, Upton, NY, 1983, BNL Report No. BNL-NCS-51694, 1983*, edited by M. R. Bhat (Brookhaven National Laboratory, New York, 1983) p. 247.
[4] A. V. Voinov, S. M. Grimes, U. Agvaanluvsan, E. Algin, T. Belgya, C. R. Brune, M. Guttormsen, M. J. Hornish, T. Massey, G. E. Mitchell, J. Rekstad, A. Schiller, and S. Siem, Phys. Rev. C **74**, 014314 (2006).
[5] M. Guttormsen, A. Atac, G. Løvhøiden, S. Messelt, T. Ramsøy, J. Rekstad, T. F. Thorsteinsen, T. S. Tveter, and Z. Zelazny, Phys. Scr., T **32**, 54 (1990).
[6] M. Guttormsen, T. Ramsøy, and J. Rekstad, Nucl. Instrum. Methods Phys. Res. A **255**, 518 (1987).
[7] A. C. Larsen, M. Guttormsen, R. Chankova, T. L Lönnroth, S. Messelt, F. Ingebretsen, J. Reckstad, A. Schiller, S. Siem, N. U. H. Syed, and A. Voinov, Phys. Rev. C **76**, 044303 (2007).
[8] S. G. Kadmenski, V. P. Markushev, and V. I. Furman, Yad. Fiz. **37**, 277 (1983) [Sov. J. Nucl. Phys. **37**, 165 (1983)].
[9] W. Hauser and H. Feshbach, Phys. Rev. **87**, 366 (1952).
[10] A. Wallner, B. Strohmaier, and H. Vonach, Phys. Rev. C **51**, 614 (1995).
[11] S. M. Grimes, Ohio University Report INPP-04-03, 2004 (unpublished).
[12] T. von Egidy and D. Bucurescu, Phys. Rev. C **72**, 044311 (2005); **73**, 049901(E) (2006).
[13] A. Gilbert and A. G. W. Cameron, Can. J. Phys. **43**, 1446 (1965).

[14] A. V. Ignatyuk, G. N. Smirenkin, and A. S. Tishin, Sov. J. Nucl. Phys. **21**, 255 (1975).
[15] P. Demetriou and S. Goriely, Nucl. Phys. **A695**, 95 (2001).
[16] T. Belgya, O. Bersillon, R. Capote, T. Fukahori, G. Zhigang, S. Goriely, M. Herman, A. V. Ignatyuk, S. Kailas, A. Koning, P. Oblozinsky, V. Plujko, and P. Young, Handbook for Calculations of Nuclear Reaction Data: Reference Input Parameter Library. Available online at http://www-nds.iaea.org/RIPL-2/, IAEA, Vienna, 2005.
[17] E. Gadioli and L. Zetta, Phys. Rev. **167**, 1016 (1968).

7.5 Paper 4: Level density and γ-decay properties of closed shell Pb nuclei

Level density and γ-decay properties of closed shell Pb nuclei

N.U.H. Syed[1*], M. Guttormsen[1], F. Ingebretsen[1], A.C. Larsen[1],
T. Lönnroth[2], J. Rekstad[1], A. Schiller[3], S. Siem[1], and A. Voinov[3]
[1]*Department of Physics, University of Oslo,*
P.O.Box 1048 Blindern, N-0316 Oslo, Norway
[2]*Department of Physics, Åbo Akademi, FIN-20500 Åbo, Finland*
[3]*Department of Physics and Astronomy,*
Ohio University, Athens, OH-45701, USA

(Dated: January 23, 2009)

The level densities and γ-ray strength functions of $^{205-208}$Pb have been measured with the Oslo method, utilizing the (^{3}He, ^{3}He$'\gamma$) and (^{3}He, $\alpha\gamma$) reactions on the target nuclei ^{206}Pb and ^{208}Pb. The extracted level densities are consistent with known discrete levels at low excitation energies. The entropies and temperatures in the micro-canonical ensemble have been deduced from the experimental level density. An average entropy difference of $\Delta S \sim 0.9 k_B$ has been observed between ^{205}Pb and ^{206}Pb. The γ-ray strength functions in $^{205-208}$Pb have been extracted and compared with two models; however, none of them describe the data adequately. Intermediate structures have been observed in the γ-ray strength functions for γ-ray energies below neutron threshold in all the analyzed Pb nuclei. These structures become less pronounced while moving from the doubly-magic nucleus ^{208}Pb to ^{205}Pb.

PACS numbers: 21.10.Ma, 21.10.Pc, 25.55.Hp, 27.80.+w

I. INTRODUCTION

Tracing average nuclear properties such as nuclear level density and γ-ray strength function in the quasi-continuum region are of particular importance. Both level density and γ-ray strength function are inputs in statistical model calculations of compound nuclear reactions and the subsequent decay of the compound system. These calculations are important for many aspects of nuclear structure studies, e.g., fission hindrance in heavy nuclei, giant resonances built on excited states, yields of evaporation residues to populate certain exotic nuclei and production of heavy elements in stellar processes. The level density is also an essential quantity for determining thermodynamic properties of nuclei, such as entropy and temperature – quantities that describe the many-particle behavior of the system.

The level density is defined as the number of levels per unit of excitation energy. It can be obtained experimentally from different methods such as counting of resonances following neutron capture [1] and modeling of particle evaporation spectra from compound nucleus reactions [2]. The γ-ray strength function characterizes the nuclear electromagnetic response. The concept of γ-ray strength function was introduced in the work of Blatt and Weisskopf [3]. Most of the experimental information on the γ-ray strength function has been obtained from the study of photonuclear cross-sections for high energy γ transitions ($E_\gamma \sim 10-20$ MeV) [4]; however, at low γ energies experimental data are scarce.

The Oslo cyclotron group has developed a method [5] to isolate the first γ-rays emitted in all decay cascades at various initial excitation energies. The energy distribution of these primary (or first-generation) γ-rays provides information on the level density and the γ-ray strength function. The Oslo method has previously been applied for rare earth nuclei, obtaining information on the level density and average γ-decay properties in this mass region [6, 7]. Recently, the method has been extended to other mass regions like Fe, Mo, V and Sc [8–12]. In order to check the validity of the method in cases where nuclei have low level density and strong Porter-Thomas fluctuations [13], the ^{27,28}Si nuclei were studied with gratifying results [14]. These achievements have encouraged us to apply the method on closed shell $^{205-208}$Pb nuclei, where the decay properties are less statistical due to shell effects and more dominated by single-particle selection rules.

Based on the shell model, the nucleon configuration of lead isotopes is such that the protons fill the $h_{11/2}$ shell, and the valence neutrons reside in the $i_{13/2}$ shell. The chain of $A = 205-208$ lead isotopes in general, and the doubly-magic ^{208}Pb nucleus with $Z = 82$ and $N = 126$ in particular, are interesting nuclei for studying the nuclear structure and γ-decay properties at and in the vicinity of a two major shell closures.

In the following sections a brief outline of the experimental method and data analysis are given. The level densities, thermodynamic properties and the γ-ray strength functions will be discussed. Finally, a summary and conclusions are drawn.

II. EXPERIMENTAL METHOD AND DATA ANALYSIS

The experiments were conducted at the Oslo Cyclotron Laboratory (OCL) using a 38-MeV ^{3}He ion beam. Self-supporting targets of ^{206}Pb and ^{208}Pb metallic foils, enriched to 99.8% and 99.9% and with thicknesses of 4.7 mg/cm^2 and 1.4 mg/cm^2, respectively, were used. The experiments ran for twelve days with a beam current of $\approx$0.6 nA.

*Electronic address: n.u.h.syed@fys.uio.no

The bombardment of ^{3}He ions on the Pb targets opens a number of reaction channels, such as (^{3}He, ^{3}He$'\gamma$), (^{3}He, $\alpha\gamma$), (^{3}He, $xn\alpha\gamma$) and (^{3}He, ^{3}He$'xn\gamma$). The following reactions are analyzed in the present study:

1. ^{208}Pb(^{3}He,^{3}He$'\gamma$)^{208}Pb
2. ^{208}Pb(^{3}He, $\alpha\gamma$)^{207}Pb
3. ^{206}Pb(^{3}He, ^{3}He$'\gamma$)^{206}Pb
4. ^{206}Pb(^{3}He, $\alpha\gamma$)^{205}Pb

Particle-γ coincidences were measured for $^{205-208}$Pb using the CACTUS multidetector array [15]. The charged particles were detected by eight collimated ΔE$-$E type Si particle telescopes, placed at a distance of 5 cm from the target and making an angle of 45° with the beam line. The thicknesses of the ΔE and E detectors are $\approx$145 μm and $\approx$1500 μm, respectively. For the detection of γ-rays, 28 5″$\times$5″ NaI detectors were used, surrounding the particle telescopes and the target. The total efficiency of the NaI detectors is $\sim$ 15% of 4π.

The data analysis consists of four main steps: (i) making the particle-γ coincidence matrix, (ii) unfolding the total γ-ray spectra, (iii) extracting the first generation γ-ray spectra and (iv) the factorization of the first generation γ-ray matrix into level density and γ-ray transmission coefficient. From the known Q values and reaction kinematics the ejectile energy can be transformed into initial excitation energy of the residual nuclei. Using the particle-γ coincidence technique, each γ-ray can be assigned to a cascade depopulating an excitation energy region in the residual nucleus. Thus, the particle-γ coincidence measurements give a total γ-ray spectrum for each excitation energy bin. Each row of the coincidence matrix corresponds to a certain excitation energy (E) while each column corresponds to a certain γ-ray energy (E_γ). In ^{205,206}Pb and ^{207,208}Pb the excitation energy bins are chosen to be 240 keV/channel and 220 keV/channel, respectively.

The γ-ray spectra are corrected for the NaI response function. The unfolding procedure of Ref. [16] is employed for this purpose, which is based on the Compton-subtracting technique that prevents additional spurious fluctuations in the unfolded spectrum. The reliability of the unfolding technique is tested for ^{207}Pb γ-ray spectra, see Fig. 1. Here, the raw γ-ray spectrum from the excitation energy region $E = 4.5 - 6.7$ MeV is compared with the spectrum that has been folded after unfolding. The good agreement with the raw γ-ray spectrum and the folded spectrum gives confidence in the employed unfolding technique. The set of unfolded γ-ray spectra are organized in a (E,E_γ) matrix, which comprises the energy distribution of all γ-rays from all decay cascades as a function of excitation energy. This matrix of total, unfolded γ-ray spectra is the basis for the next step of the Oslo method.

The first generation (primary) γ-ray energy distribution is extracted by an iterative subtraction technique described in Ref. [17]. The basic assumption of the subtraction method is that the γ-decay pattern from any excitation energy bin is independent of whether the state is populated directly via scattering or neutron pick-up, or through γ-decay from a higher-lying excited state.

The basic assumption may not be fulfilled if the direct reaction at lower excitation bins, whose γ-spectra are utilized to subtract higher-generation γ-rays from total spectra at higher excitation energies, do not favor some levels within the excitation bin that are populated by γ-rays from above. Such situations may cause that some γ-rays are not fully subtracted from the total spectrum.

The influence of a possible different selectivity of levels at one excitation energy in the direct reaction compared to γ-decay from higher lying levels, is expected to be most pronounced when only a few levels are present in the excitation bin. Thus, these considerations are increasingly important for nuclei in the vicinity of closed shells having low level density. It is therefore necessary to be cautious when applying the Oslo method to the Pb nuclei, and to carefully check that the method gives reasonable results compared to other data.

In Fig. 2 the application of the first generation γ-rays extraction technique is shown for ^{207}Pb. The first generation γ-rays are extracted by subtracting the weighted sum of higher generation γ-rays from the total unfolded γ-ray spectrum. Figure 2 shows the total unfolded γ-ray spectrum, the first generation γ-ray spectrum, and the second and higher generation γ-spectrum from $E = 4.5 - 6.7$ MeV for ^{207}Pb. It is seen how the higher generation γ-rays are well separated from the total γ-ray spectrum in the specified excitation energy region.

III. NUCLEAR LEVEL DENSITIES

A. Application of the Axel-Brink hypothesis

The energy distribution of primary γ-rays emitted from a well-defined initial excitation energy provides information on the level density and the γ-strength function. First, the experimental primary γ-ray matrix $P(E,E_\gamma)$ is normalized for the various excitation energy bins E. This is done by summing $P(E,E_\gamma)$ over all γ-ray energies E_γ, for each excitation energy bin E such that

$$\sum_{E_\gamma=E_\gamma^{\min}}^{E} P(E,E_\gamma) = 1. \quad (1)$$

The entries of the first generation matrix are the probabilities $P(E,E_\gamma)$ that a γ-ray of energy E_γ is emitted from excitation energy E. In accordance with Fermi's golden rule, the decay rate is proportional to the level density of final states and the square of the transition matrix element. Thus, entries of the primary γ-ray matrix $P(E,E_\gamma)$ in the statistical region are proportional to the level density $\rho(E-E_\gamma)$ and the γ-ray transmission coefficient $\mathcal{T}(E_\gamma)$:

$$P(E,E_\gamma) \propto \rho(E-E_\gamma)\mathcal{T}(E_\gamma). \quad (2)$$

In the factorization procedure of the two-dimensional primary γ-ray matrix, a lower limit of the excitation energy region $E \sim 3.0$ MeV was used for all the analyzed nuclei in order to exclude the main part of non-statistical transitions from our data. The normalized experimental primary γ-ray matrix

$P(E,E_\gamma)$ can be approximated by

$$P_{\rm th}(E,E_\gamma) = \frac{\rho(E-E_\gamma)\mathscr{T}(E_\gamma)}{\sum_{E_\gamma=E_\gamma^{\rm min}}^{E}\rho(E-E_\gamma)\mathscr{T}(E_\gamma)}. \quad (3)$$

The first trial function for ρ is assumed to be unity i.e., $\rho = 1$ and the corresponding $\mathscr{T}$ can be determined by Eq. (3). Then, a χ^2 minimum is calculated for each data point of ρ and $\mathscr{T}$ simultaneously. This procedure is repeated until a global least-square fit is achieved for all the data points of $P(E,E_\gamma)$.

In Fig. 3 such a least χ^2 fit is compared with the experimental primary γ-ray matrix for the ^{208}Pb(^{3}He,$\alpha\gamma$)^{207}Pb reaction at different initial excitation energies between $E = 3.8 - 6.7$ MeV with energy bins of 220 keV. The calculated primary γ-ray spectra (solid lines) are obtained by multiplying the extracted ρ and $\mathscr{T}$, as defined in Eq. (3).

The γ-ray transmission coefficient $\mathscr{T}(E_\gamma)$ in Eqs. (2) and (3) is independent of excitation energy according to the generalized Axel-Brink hypothesis [18, 19], stating that collective excitations built on excited states have the same properties as those built on the ground state. The average temperature in the excitation energy region studied is below 1.0 MeV for the final levels. The temperature is believed to depend on the final excitation energy by $T \propto \sqrt{E_f}$, which is a slowly varying function. Thus, we assume that using a constant temperature for the factorization of Eq. (2) is approximately valid in our excitation region. The error bars of the data points take into account only the statistical errors, see Ref. [5]. This means that neither possible shortcomings of the first-generation procedure nor a weak dependence on the excitation energy in the transmission coefficient, which means that the Axel-Brink hypothesis is not fully valid, are included in the error bars. Keeping this in mind, the comparison shown in Fig. 3 indicates that the analyzing method works satisfactorily for the ^{207}Pb nucleus.

The multiplicative functions of Eq. (2) give an infinite number of solutions. It has been shown in Ref. [5] that if one solution is known for Eq. (2), then the product $\rho\cdot\mathscr{T}$ is invariant under the transformation

$$\tilde{\rho}(E-E_\gamma) = A\exp[\alpha(E-E_\gamma)]\rho(E-E_\gamma), \quad (4)$$

$$\tilde{\mathscr{T}}(E_\gamma) = B\exp(\alpha\ E_\gamma)\ \mathscr{T}(E_\gamma). \quad (5)$$

Therefore, neither the slope nor the absolute value of ρ and $\mathscr{T}$ can be determined directly from the iteration procedure. The free parameters A, B and α must be determined by experimental data in order to normalize ρ and $\mathscr{T}$.

B. Normalization of nuclear level density

The parameters A and α in Eqs. (4) and (5) are obtained by fitting the inferred data points to the known discrete levels [20] at low excitation energies and to the level density at the neutron separation energy S_n. The level density at S_n can be deduced from the Fermi-gas expression [21] using the available proton or neutron-resonance spacing data [22] and assuming that positive and negative parities contribute equally to the level density at S_n. For $\ell = 0$ capture (s-waves), the level density ρ_0 becomes:

$$\rho_0(S_n) = \frac{2\sigma^2}{D_0}[(I_t+1)\exp(-(I_t+1)^2/2\sigma^2) + I_t\exp(-I_t^2/2\sigma^2)]^{-1}. \quad (6)$$

For $\ell = 1$ capture (p-waves), the above equation becomes:

$$\rho_1(S_n) = \frac{2\sigma^2}{D_1}[(I_t-1)\exp(-(I_t-1)^2/2\sigma^2) + I_t\exp(-I_t^2/2\sigma^2) + (I_t+1)\exp(-(I_t+1)^2/2\sigma^2) + (I_t+2)\exp(-(I_t+2)^2/2\sigma^2)]^{-1}, \quad (7)$$

where D_0 and D_1 are the average s- and p-wave resonance spacings. The parameter I_t is the spin of the target nucleus. For spin $I_t = 0$, the first two terms inside the bracket $[\cdots]$ of Eq. (7) should be omitted and for spin $I_t = 1/2$ and 1 only the first term should be omitted. The spin-cut off parameter σ is defined in Ref. [21] by

$$\sigma^2 = 0.0888A^{2/3}\sqrt{a(E-E_{\rm pair})}. \quad (8)$$

where A is the mass number, a is the level density parameter and E_{pair} is the pairing correction parameter. The pairing correction parameter is estimated following the description of Ref. [23]. The spin distribution of levels at one excitation energy is given by [21]:

$$g(E,I) = \frac{2I+1}{2\sigma^2}\exp[-(I+1/2)^2/2\sigma^2], \quad (9)$$

which is normalized to $\Sigma_I g(E,I) \sim 1$. The spin assignments of ^{206,208}Pb in the excitation region $E \sim 4 - 5$ MeV are taken from Ref. [20]. The average spin distribution of these data points are compared with the relative spin distribution determined from Eq. (9), as shown in Fig. 4. Within the statistical uncertainty of the data points the agreement of the experimental and theoretical spin distributions is very good and supports our adopted σ in Eq. (8).

In Ref. [22] both s-wave and p-wave resonance spacings D_0 and D_1 for the target ^{204,206,207}Pb nuclei are given at S_n. The deduced level densities ρ_0 and ρ_1 at S_n are listed in Table I. Since the s-wave resonances in ^{207,208}Pb are more weakly populated than the p-wave resonances, the level densities determined using D_0 are less reliable than those determined using D_1. Therefore, the ρ_1 level density has been used for normalizing our data.

The parameters used in the analysis of $^{205-208}$Pb are summarized in Table I. The level density parameter a of the Pb nuclei is taken from Ref. [24] using the Gilbert and Cameron approach [21]. Since the proton/neutron resonance spacing information for ^{206}Pb is unavailable, we estimate the level density at the neutron separation energy using the systematics of Ref. [21]. Figure 5 demonstrates the estimation procedure, where the level densities of odd and even Pb nuclei are

shown. In ^{208}Pb and ^{209}Pb the Fermi gas level densities at S_n are comparable with those deduced from the neutron resonance data [22]. However, in ^{205}Pb and ^{207}Pb the large discrepancy between the two level densities is obvious. In view of this discrepancy we have estimated an uncertainity of 80% for the adopted Fermi gas level density in ^{206}Pb.

The experimental level density is extracted up to ~ 2 MeV below S_n since the γ-rays below 2 MeV are omitted in the extraction procedure. In order to fill the gap between the data points and the level density at S_n deduced from resonance data, an interpolation is required. The Fermi gas level density formula for all spins and parities

$$\rho_{\mathrm{FG}}(U) = \eta \frac{\exp(2\sqrt{aU})}{12\sqrt{2}a^{1/4}U^{5/4}\sigma} \tag{10}$$

is employed for the interpolation. Here, $U = E - E_{pair}$ is the intrinsic excitation energy and η is a constant used to adjust ρ_{FG} to the experimental level density at S_n (values are given in Table I).

Figures 6 and 7 show the normalized level densities extracted for ^{205,206}Pb and ^{207,208}Pb, respectively, up to $\sim 5-6$ MeV of excitation energy. The exponential increase of level density with excitation energy is evident from these figures, where the Oslo data points are shown as filled squares. The Fermi gas level densities (dashed lines) that are used for normalization at the highest energy points, are seen to describe the data points only to some extent. This feature is expected for nuclei near closed shells, having few nuclear levels. For the lead region, it is clear that the Fermi gas gives a poor description below 4–5 MeV of excitation energies.

By comparing our data with the discrete levels from spectroscopic experiments [20], a very good resemblance is seen at lower excitation energies in all the nuclei. Local differences might be due to violation of the assumptions behind Eq. (2) for nuclei where level densities are low and large fluctuations of the γ-ray intensity are observed. In the doubly magic ^{208}Pb the level density is low and the Oslo data agree nicely with the spectroscopic measurements [20] up to 5 MeV of excitation energy. The presence of a single unpaired neutron in ^{207}Pb increases the level density compared to ^{208}Pb at a given excitation energy. The Oslo data of ^{207}Pb provide new information on level density above $E = 4$ MeV. Similarly, in ^{205,206}Pb new information on the level densities are determined at higher excitation energies where spectroscopic methods fail to find levels.

Figure 6 shows that the level densities of ^{205,206}Pb are smoother functions of excitation energy with an overall higher absolute value than of ^{207,208}Pb, where characteristic structures are prominent. This feature is expected due to the presence of two and three neutron vacancies, which provide extra degrees of freedom for the nucleons to arrange themselves for a given excitation energy.

The drop of the total level density for $E \leq 4$ MeV while going from ^{205}Pb to ^{208}Pb, is interpreted as a shell closure effect. The extraction of level density in ^{208}Pb does not provide any new information above the known levels. However, these results give further confidence in the Oslo method and its applicability in this mass region, as our data show good agreement with the data found in literature. In summary, these results are gratifying and support the applicability of the Oslo method in closed-shell nuclei where the level densities are low.

IV. THERMODYNAMICS

The nuclear level density is closely related to the entropy S of the system at a given excitation energy E. In fact, the level density $\rho(E)$ is directly proportional to the number of accessible levels at excitation energy E. In order to derive thermodynamic quantities for mesoscopic systems, it is common to use the micro-canonical or canonical ensemble. The micro-canonical ensemble is the most appropriate ensemble according to Ref. [25], since the nucleus is considered as an isolated system with well-defined energy. The micro-canonical ensemble theory will therefore be utilized for $^{205-208}$Pb, although temperature and heat capacity may become negative due to fluctuations in the entropy.

In the micro-canonical ensemble, the entropy $S(E)$ is identical to the partition function determined by the multiplicity of states $\Omega(E)$ at excitation energy E which corresponds to the level density $\rho(E)$. The entropy in the micro-canonical ensemble can be derived as

$$\begin{aligned} S(E) &= k_B \ln \Omega(E) \\ &= k_B \ln \frac{\rho(E)}{\rho_0} \\ &= k_B \ln \rho(E) + S_0, \end{aligned} \tag{11}$$

where Boltzmann's constant k_B is set to unity for the sake of simplicity. The value of the normalization factor S_0 is adjusted such that the third law of thermodynamics is fulfilled: $S \to 0$ for $T \to 0$. Since the ground-state band of the even-even ^{206}Pb and ^{208}Pb nuclei has $T = 0$, the parameter S_0 used for $^{205-208}$Pb is 0.34. From the entropy, one can derive the temperature by

$$\frac{1}{T(E)} = \frac{\partial S}{\partial E}. \tag{12}$$

In Figs. 8 and 9 the micro-canonical entropies of ^{205,206}Pb and ^{207,208}Pb are shown, respectively. The entropies of ^{207,208}Pb are seen to vary strongly with excitation energy. For ^{208}Pb, the first vibrational 3^- state appears at 2.6 MeV, before the two quasi-particle regime which is seen to enter at $E > 3.5$ MeV. Figure 10 shows that the difference in entropy between ^{207}Pb and ^{208}Pb, $\Delta S = S(^{207}\mathrm{Pb}) - S(^{208}\mathrm{Pb})$, is fluctuating between $0.3-2.0$ in the excitation energy region of $E = 3.0-5.7$ MeV. This strong variation in entropy is due to the few available single-particle orbitals for the unpaired neutrons below the closed shell. The strong fluctuation of entropy in ^{207,208}Pb with excitation energy makes it difficult to determine other thermodynamic quantities such as temperature.

In Fig. 10 the average difference in entropy between ^{205}Pb and ^{206}Pb is shown to lie around 0.9 for the excitation energy region between $E = 2-5$ MeV. The entropy difference

of ^{205}Pb and ^{206}Pb is less fluctuating than that observed between ^{207}Pb and ^{208}Pb, thus indicating the departure of shell closure effects in ^{205,206}Pb. The entropy difference between ^{205}Pb and ^{206}Pb is about one half of the value observed in rare earth nuclei ($\Delta S \sim 2$) [26].

The micro-canonical temperature can be extracted from the entropy as given by Eq. (12). Since the level densities in ^{207,208}Pb are low and show large fluctuations, the temperature extraction for these nuclei is probably not reliable. The micro-canonical temperatures of ^{205}Pb and ^{206}Pb are shown in Figs. 11 and 12, respectively. For ^{206}Pb, the temperature extraction gives rise to large bump structures. These structures in the temperature arise from the differentiation of the entropy (see Eq. (12)), and can be interpreted as the breaking of nucleon pairs. When nucleon pairs are broken, new degrees of freedom open up leading to an increase of $\rho(E)$ and decrease in the temperature $T(E)$.

For ^{205}Pb, the situation is not so clear since this nucleus has an unpaired neutron which gives a smoother entropy and thus less structures in the temperature. Bumps indicating the pair-breaking process might also be seen here, but one can also fit a constant temperature to the data points in Fig. 11. By doing so, we get an average temperature of 0.9(1) MeV for $0.4 \leq E \leq 5.0$ MeV, which is in agreement with an average temperature of $T = 0.81(4)$ MeV [27].

In ^{205}Pb and ^{206}Pb one can observe the first drop in temperature at $E \approx 2.0$ MeV and $E \approx 2.5$ MeV, respectively. These excitation energies can be compared with the energy amount necessary to break a neutron Cooper pair, namely $2\Delta_n$, where Δ_n is the neutron pair gap parameter. The description of Ref. [21] gives $2\Delta_n = 1.8$ MeV for ^{205,206}Pb. The observed locations of pair-breaking lie at energies somewhat higher than $2\Delta_n$. This difference could be due to the large energy spacing between the single-particle orbitals. However, the second peak in ^{205}Pb and ^{206}Pb is observed at $E \approx 3.8$ and 3.7 MeV, respectively. These peaks may be due to proton-pair breaking, neutron-pair breaking, or because the proton (or neutron) passes the energy gap between major shell gaps.

V. GAMMA-RAY STRENGTH FUNCTIONS

The γ-ray transmission coefficient $\mathscr{T}$ in Eq. (2) is connected to the electromagnetic decay properties of the nucleus and is expressed as the sum of all the γ-ray strength functions f_{XL} for transitions with electromagnetic character X and multipolarity L, given by:

$$\mathscr{T}(E_\gamma) = 2\pi \sum_{XL} E_\gamma^{2L+1} f_{XL}(E_\gamma), \tag{13}$$

where E_γ is the transition energy, and the slope correction $\exp(\alpha E_\gamma)$ from Eq. (4) has already been included in $\mathscr{T}$. In Fig. 13, $\mathscr{T}$ for ^{206}Pb is shown, where the absolute normalization B remains to be determined. This normalization will be discussed in the following.

As already mentioned in sect. III, the methodological difficulties in the primary γ-ray extraction prevent the determination of ρ for $E > S_n - 2$ MeV and $\mathscr{T}$ for $E_\gamma < 2$ MeV. The level densities were extrapolated with the Fermi gas level density using Eq. (10). However, the transmission coefficients are extrapolated using an exponential form, as shown in Fig. 13.

It is assumed that the main contributions to the function $\mathscr{T}(E_\gamma)$ are $E1$ and $M1$ γ-ray transitions in the statistical region. Further, if one assumes that the number of accessible levels of positive and negative parity are equal for any energy and spin, one finds

$$\rho(E - E_\gamma, I_f, \pm\pi_f) = \frac{1}{2}\rho(E - E_\gamma, I_f). \tag{14}$$

Clearly, this assumption does not hold true for all excitation energy regions in the Pb nuclei considered here. However, by applying these assumptions, the experimental γ-ray transmission coefficient of Eq. (13) yields

$$B\mathscr{T}(E_\gamma) = 2\pi[f_{E1}(E_\gamma) + f_{M1}(E_\gamma)]E_\gamma^3, \tag{15}$$

where B is an unknown factor that gives the absolute normalization of the γ-ray strength function. We might expect a potential error in the absolute normalization of the γ-ray strength functions in the Pb region due to equal-parity assumption used above.

The average total radiative width $\langle\Gamma_\gamma\rangle$ of levels with energy E, spin I and parity π is given by [28]:

$$\langle\Gamma_\gamma(E, I, \pi)\rangle = \frac{1}{2\pi\rho(E, I, \pi)} \sum_{XL} \sum_{I_f, \pi_f} \int_0^E \mathrm{d}E_\gamma \mathscr{T}_{XL}(E_\gamma) \times \rho(E - E_\gamma, I_f, \pi_f), \tag{16}$$

where the summation goes over spins of final levels I_f with parities π_f. Using the assumptions discussed above, one can determine the average total radiative width $\langle\Gamma_\gamma\rangle$ for neutron resonances. For $\ell = 0$ capture (s-waves), the populated spins are $I = |I_t \pm 1/2|$, where I_t represents the spin of the target nucleus in the (n,γ) reaction. For $\ell = 1$ capture (p-waves), the populated spins are $I = |I_t \pm 1/2 \pm 1|$. The parity is determined by the target parity π_t and ℓ by $\pi = \pi_t(-1)^\ell$. The average total radiative width is described at $E = S_n$ by

$$\langle\Gamma_\gamma(S_n, I)\rangle = \frac{1}{4\pi\rho(S_n, I, \pi)} \int_0^{S_n} \mathrm{d}E_\gamma \times B\mathscr{T}(E_\gamma)\rho(S_n - E_\gamma) \times \sum_{J=-1}^{1} g(S_n - E_\gamma, I + J). \tag{17}$$

The factor B can thus be determined from the average total radiative width $\langle\Gamma_\gamma\rangle$ of the compound states. Ref. [22] provides the experimental $\langle\Gamma_\gamma\rangle$ for ^{205}Pb, while the $\langle\Gamma_\gamma\rangle$ in ^{207}Pb is taken from Ref. [1].

In order to normalize the γ-ray strength function of ^{208}Pb the above mentioned method is difficult to apply since the average total radiative width at S_n cannot be found in the literature. However, there are discrete neutron resonance data [29] for ^{208}Pb on the $E1$ and $M1$ γ-ray strength functions at E_γ = 7.5 MeV. The Oslo data for ^{208}Pb is thus normalized with the

data of Ref. [29]. In addition, the (γ,n) photonuclear cross-section data of Ref. [30] has been used to confirm the normalization of the γ-ray strength function of ^{208}Pb. The following relation [22] can be used to deduce the strength function from the cross-section, asumming that dipole radiation is dominant:

$$f(E_\gamma) = \frac{1}{3\pi^2\hbar^2c^2}\frac{\sigma(E_\gamma)}{E_\gamma}. \quad (18)$$

Since ^{205}Pb is unstable, the resonance spacings and $\langle\Gamma_\gamma\rangle$ have not been measured for ^{206}Pb. Therefore, we utilized the (γ,n) cross-section data [30] to normalize the γ-ray strength function of ^{206}Pb. The Oslo data are scaled to match the data of Ref. [30], giving the absolute normalization of the γ-ray strength function of ^{206}Pb. The normalized γ-ray strength functions of ^{205,206}Pb and ^{207,208}Pb are shown in Figs. 14 and 15, respectively.

For ^{207}Pb, the resonance data [29] for electric and magnetic dipole radiation at E_γ = 7.1 MeV have been used to make a consistency check for the normalized γ-ray strength function. Moreover, the (γ,n) data of Ref. [30] for ^{207}Pb at $E_\gamma > S_n$ are also drawn in Fig. 15 for comparison. The agreement of these strength functions with our extracted data is gratifying, and indicates that the normalization procedure works well in this case, in spite of the questionable assumption of equal parity distribution described in Eq. (14).

The (γ,n) data for $^{206-208}$Pb in Ref. [30] display bumps and structures that increase in magnitude when approaching S_n. Similar structures are present in our data below S_n. These intermediate structures are observed in the Oslo data at γ-ray energies 5.6, 6.3 and 7.1 MeV in ^{208}Pb. Similarly, in ^{207}Pb these intermediate structures have been seen at 4.3, 5.0, 5.6 and 6.3 MeV. For ^{205}Pb and ^{206}Pb these structures are observed at γ-ray energies of 4.3, 6.0 and 6.3 MeV. It is hard to interpret these structures without knowing the electromagnetic character and the multipolarity of transitions in this region. However, it is likely that the bumps are due to enhanced single-particle transitions at certain γ-ray energies, reflecting the shell structure below S_n. The Oslo method does not provide any information on the multipolarity of these structures, so to investigate it further, it would be necessary to perform complementary experiments such as (n,$\gamma\gamma$) measurements analyzed with the two-step cascade method [31].

The above extracted γ-ray strength functions depend on the normalization procedure chosen. The slope of the strength function is sensitive to the resonance data at S_n, which have been taken from the literature. In ^{206}Pb the uncertainty of this data play a central role in the normalization of our data. The adopted values influence both the slope of the level density as well as the slope of the strength function. In ^{206}Pb, the uncertainty in the value of α (see Eq. (13)) could be more than 80% due to this uncertainty. In addition, the absolute strength (B of Eq. (15)) is uncertain by a factor of 2 – 3. In the case of ^{208}Pb, the oscillating shape of the strength function makes the absolute normalization between our data and (γ,n) data [29, 30] very difficult, as seen in Fig. 15.

VI. MODELS FOR E1 AND M1 TRANSITIONS

A number of models describing the electric dipole γ-ray strength function have been described in [22]. The simplest of these is the Standard Lorentzian model (SLO), which describes the $E1$ strength as a Lorentzian shape. The model is temperature independent and is given by:

$$f_{\rm SLO}(E_\gamma) = \frac{1}{3\pi^2\hbar^2c^2}\sigma_{E1}\Gamma_{E1}\frac{E_\gamma\Gamma_{E1}}{(E_\gamma^2-E_{E1}^2)^2+(\Gamma_{E1}E_\gamma)^2}, \quad (19)$$

where the Lorentzian parameters σ_{E1}, E_{E1} and Γ_{E1} are the peak cross section, energy and width of the giant dipole resonance, respectively, and are usually derived from photonuclear experiments. However, it has been shown [28, 29, 32–34] that the SLO model overestimates the photonuclear data away from the giant dipole resonance (GDR) centroid in many nuclei.

One model that incorporates the temperature dependency of the γ-ray dipole strength is the Enhanced Generalized Lorentzian model (EGLO) [22]. Considering spherical nuclei, EGLO is defined as

$$f_{\rm EGLO}(E_\gamma) = \frac{1}{3\pi^2\hbar^2c^2}\sigma_{E1}\Gamma_{E1} \left\{\frac{E_\gamma\Gamma_k(E_\gamma,T)}{(E_\gamma^2-E_{E1}^2)^2+(E_\gamma\Gamma_k(E_\gamma,T))^2} + 0.7\frac{\Gamma_k(E_\gamma=0,T)}{E_{E1}^3}\right\}, \quad (20)$$

where T is the temperature of the final states determined by $T=\sqrt{(U/a)}$. The energy and temperature dependent width $\Gamma_k(E_\gamma,T)$ is defined analytically as

$$\Gamma_k(E_\gamma,T) = K(E_\gamma)\frac{\Gamma_{E1}}{E_{E1}^2}[E_\gamma^2+(2\pi T)^2], \quad (21)$$

where

$$K(E_\gamma) = \kappa + (1-\kappa)\frac{E_\gamma-E_0}{E_{E1}-E_0}. \quad (22)$$

is an empirical function. Here we use $E_0 = 4.5$ MeV and the enhancement factor κ, given by [35],

$$\kappa = \begin{cases} 1 & \text{if } A < 148, \\ 1+0.09(A-148)^2\exp(-0.18(A-148)) & \text{if } A \geq 148, \end{cases} \quad (23)$$

for the Fermi gas model. These expressions are developed in the framework of the collisional damping model for $E_\gamma < E_{E1}$ and hold for $T < 2$ MeV.

The magnetic dipole $M1$ radiation is described by a Lorentzian based on the existence of a giant magnetic dipole resonance (GMDR) [36],

$$f_{M1}(E_\gamma) = \frac{1}{3\pi^2h^2c^2}\frac{\sigma_{M1}E_\gamma\Gamma_{M1}^2}{(E_\gamma^2-E_{M1}^2)^2+E_\gamma^2\Gamma_{M1}^2}. \quad (24)$$

where σ_{M1}, Γ_{M1}, and E_{M1} are the GMDR parameters deduced from the systematics given in [22].

The contribution from isoscalar $E2$ transition strength is also included in the total γ-ray strength function and is described by [22]

$$f_{E2}(E_\gamma) = \frac{1}{5\pi^2\hbar^2c^2E_\gamma^2}\frac{\sigma_{E2}E_\gamma\Gamma_{E2}^2}{(E_\gamma^2-E_{E2}^2)^2+E_\gamma^2\Gamma_{E2}^2}. \quad (25)$$

The total model γ-ray strength functions, shown by solid lines in Figs. 16 and 17, are the sum of the EGLO $E1$, Lorentzian $M1$ and $E2$ contributions, i.e.,

$$f_{\rm tot} = f_{\rm EGLO} + f_{M1} + E_\gamma^2 f_{E2}. \quad (26)$$

The GEDR and GMDR parameters for $^{205-208}$Pb are taken from [22] and are listed in Table II. The extracted normalized γ-ray strength functions of $^{205-208}$Pb are plotted together with the models discussed above in Figs. 16 and 17. The photonuclear cross-section data of Ref. [30] have also been drawn for comparison.

The intermediate structures at the tail of GEDR in the Oslo data are observed at different γ-ray energies in the analyzed Pb nuclei. These intermediate structures present in our data oscillate between the above-mentioned models; however, none of them describe our data adequately for the whole energy region. In Figs. 16 and 17 our extracted data points (filled squares) of ^{205,206}Pb and ^{207,208}Pb tend to follow the EGLO model for γ-ray energies $\geq$ 4 MeV. For lower γ-energies the deviation between the theory and data points is obvious. This is not surprising, since one expects that the closed shell(s) will strongly influence the γ-decay, and thus preventing a good description of the γ-strength with smooth functions such as given by the EGLO model.

The strength functions in $^{206-208}$Pb show an increase at γ-ray energies lower than $\sim$3 MeV. This may be due to the possible presence of strong non-statistical transitions, which are not correctly subtracted in the primary γ-ray extraction procedure and thus affecting the strength function at these γ-energies. Therefore, the enhanced γ-ray strength functions at low γ-ray energies are not conclusive.

VII. SUMMARY AND CONCLUSIONS

The primary motivation of this work was to determine the level density and the γ-ray strength function in Pb isotopes near and at shell closure. The applicability of the Oslo method has also been investigated in the doubly magic ^{208}Pb nucleus and its neighboring $^{205-207}$Pb nuclei. In contrast to the rare earth and mid-shell nuclei, these isotopes have low level density so that one can expect strong non-statistical fluctuations of level density and γ-ray strength function.

The level densities and γ-ray strength functions of $^{205-208}$Pb have been extracted simultaneously from the primary γ-ray spectra. The comparison of our extracted level densities with spectroscopic measurements at low excitation energies gives good agreement within the experimental uncertainty. In ^{208}Pb, the Oslo method could not give more information on level density than previously known from discrete spectroscopy. However, the good agreement between our data and known levels in ^{208}Pb indicates the robustness of the method for its use in closed shell nuclei.

The level densities of ^{207,208}Pb show significant step structures, which is an interesting finding of this work. Such structures are expected, partly due to strong shell effects at the $Z = 82$ and $N = 126$ shell closures, and partly due to the breaking of Cooper pairs. In ^{205,206}Pb, these step structures are smoothed out as neutron valence holes come into play.

From the extracted level densities the micro-canonical entropies of the respective nuclei are deduced. The average entropy difference ΔS between ^{205}Pb and ^{206}Pb is found to be 0.9; however, the entropy difference between ^{207}Pb and ^{208}Pb varies violently with excitation energy and thus is difficult to use for finding other thermodynamic properties. The fluctuations in the entropy spectra are strongly enhanced in the temperature spectra. The average temperatures of the ^{205,206}Pb nuclei are found to be $T \approx 1.0$ MeV. This is twice the temperature measured in rare earth nuclei.

The γ-ray strength functions of $^{205-208}$Pb show pronounced structures at energies below the neutron separation energy. However, the γ-ray strength function becomes smoother by the gradual opening of the neutron shell closure at $N = 126$. Such structures have also been observed above the neutron threshold for (γ,n) reactions in $^{206-208}$Pb nuclei. The multipolarities of these intermediate resonances are unknown. The measured γ-ray strength functions of $^{205-208}$Pb are poorly described by the SLO and EGLO models in the energy region considered here. This indicates that there is more interesting physics connected to the shell closure(s), which is revealed in the γ-ray strength functions of the Pb isotopes.

Acknowledgments

Financial support from the Norwegian Research Council (NFR) is gratefully acknowledged.

[1] S.F. Mughabghab, Atlas of Neutron Resonances (Elseveier, 2006).
[2] A.V. Voinov, S.M. Grimes, U. Agvaanluvsan, E. Algin, T. Belgya, C.R. Brune, M. Guttormsen, M.J. Hornish, T. Massey, G.E. Mitchell, J. Rekstad, A. Schiller, and S. Siem, Phys. Rev. C **74** , 014314 (2006).
[3] J.M. Blatt, V.F. Weisskopf, Theoretical Nuclear Physics (Wiley, New York, 1952).
[4] S.S. Dietrich and B.L. Berman, "Atlas of Photoneutron Cross Sections Obtained with Monoenergetic Photons," Atomic Data and Nuclear Data Tables **38** , 199-338 (1988).
[5] A. Schiller, L. Bergholt, M. Guttormsen, E. Melby, J. Rekstad,

TABLE I: Parameters used for the Fermi gas level density

Nucleus	S_n (MeV)	a (MeV^{-}1)	E_{pair} (MeV)	D_0 (keV)	$\rho_0(S_n)$ (10^3 MeV^{-1})	D_1 (keV)	$\rho_1(S_n)$ (10^3 MeV^{-1})	η
^{205}Pb	6.732	15.03	0.878	2.0(5)	29.4(78)	0.8(2)	25.4(68)	0.30
^{206}Pb	8.087	12.40[a]	1.811	-	-	-	28(22)[b]	-
^{207}Pb	6.738	11.15	1.005	32(6)	1.58(34)	5.9(9)	2.98(55)	0.46
^{208}Pb	7.368	10.33	2.226	38(8)	0.66(15)	5(1)	2.21(50)	1.15

[a] Determined using the empirical formula of the Gilbert and Cameron approach given in Ref. [22] and references within.
[b] Estimated from systematics (see text of Fig. 5).

and S. Siem, Nucl. Instrum. Methods Phys. Res. A **447**, 498 (2000).

[6] E. Melby, L. Bergholt, M. Guttormsen, M. Hjorth-Jensen, F. Ingebretsen, S. Messelt, J. Rekstad, A. Schiller, S. Siem, and S. W. Ødegård Phys. Rev. Lett. **83** , 3150(1999).

[7] M. Guttormsen, A.C. Larsen, J. Rekstad, S. Siem, N.U.H. Syed, A. Schiller, A. Voinov, Proc. Workshop on Photon Strength Functions and Related Topics, June 17-20, 2007, Prague, Czech Republic, (http://pos.sissa.it//archive/conferences/044/003/PSF07_003.pdf).

[8] A. Schiller, E. Algin, L.A. Bernstein, P.E. Garrett, M. Guttormsen, M. Hjorth-Jensen, C.W. Johnson, G.E. Mitchell, J. Rekstad, S. Siem, A. Voinov, and W. Younes, Phys. Rev. C **68** 054326 (2003).

[9] R. Chankova, A. Schiller, U. Agvaanluvsan, E. Algin, L.A. Bernstein, M. Guttormsen, F. Ingebretsen, T. Lönnroth, S. Messelt, G.E. Mitchell, J. Rekstad, S. Siem, A.C. Larsen, A. Voinov, and S.W. Ødegård, Phys. Rev. C **73** 034311 (2006).

[10] M. Guttormsen, R. Chankova, U. Agvaanluvsan, E. Algin, L.A. Bernstein, F. Ingebretsen, T. Lönnroth, S. Messelt, G.E. Mitchell, A. Schiller, J. Rekstad, S. Siem, A.C. Sunde, A. Voinov, and S.W. Ødegård, Phys. Rev. C **71** 044307 (2005).

[11] A.C. Larsen, R. Chankova, M. Guttormsen, F. Ingebretsen, S. Messelt, J. Rekstad, S. Siem, N.U.H. Syed, S.W. Ødegård, T. Lönnroth, A. Schiller and A. Voinov, Phys. Rev. C **73**, 064301 (2006).

[12] A.C. Larsen, M. Guttormsen, R. Chankova, F. Ingebretsen, T. Lönnroth, S. Messelt, J. Rekstad, A. Schiller, S. Siem, N.U.H. Syed, and A. Voinov, Phys. Rev. C **76**, 044303 (2007).

[13] C.E. Porter and R.G. Thomas, Phys. Rev. **104**, 483 (1956).

[14] M. Guttormsen, E. Melby, J. Rekstad, A. Schiller, S. Siem, T. Lönnroth, and A. Voinov, J. Phys. G **29**, 263 (2003).

[15] M. Guttormsen, A. Atac, G. Løvhøiden, S. Messelt, T. Ramsøy, J. Rekstad, T.F. Thorsteinsen, T.S. Tveter, and Z. Zelazny, Phys. Scr. **T 32**, 54 (1990).

[16] M. Guttormsen, T.S. Tveter, L. Bergholt, F. Ingebretsen, and J. Rekstad, Nucl. Instrum. Methods Phys. Res. A **374**, 371 (1996).

[17] M. Guttormsen, T. Ramsøy, and J. Rekstad, Nucl. Instrum. Methods Phys. Res. A **255**, 518 (1987).

[18] D.M. Brink, Ph.D. thesis, Oxford University, 1955.

[19] P. Axel, Phys. Rev. **126**, 671 (1962).

[20] Data extracted using the NNDC On-Line Data Service from the ENSDF database (http://www.nndc.bnl.gov/ensdf/).

[21] A. Gilbert, A.G.W. Cameron, Can. J. Phys. **43**, 1446 (1965).

[22] T. Belgya, O. Bersillon, R. Capote, T. Fukahori, G. Zhigang, S. Goriely, M. Herman, A.V. Ignatyuk, S. Kailas, A. Koning, P. Oblozinsky, V. Plujko and P. Young. Handbook for calculations of nuclear reaction data, RIPL-2 (IAEA, Vienna, 2006).

[23] A. Bohr and B.R. Mottelson, Nuclear Structure, Vol. I (Benjamin, New York, 1969) 169.

[24] Data provided by A.V. Ignatyuk, Handbook for calculations of nuclear reaction data, RIPL2 (IAEA, Vienna, 2006), http://www-nds.iaea.org/RIPL-2/

[25] D.J. Morrissey, Annu. Rev. Nucl. Part. Sci. **44**, 27 (1994).

[26] M. Guttormsen, A. Bagheri, R. Chankova, J. Rekstad, S. Siem, Phys. Rev. C **68** , 064306 (2003).

[27] T. von Egidy and D. Bucurescu, Phys. Rev. C **72**, 044311 (2005).

[28] J. Kopecky and M. Uhl, Phys. Rev. C **41**, 1941 (1990).

[29] C.M. McCullagh, M. Stelts and R.E. Chrien, Phys. Rev. C **23** 1394 (1981).

[30] S.N. Belyaev, A.B. Kozin, A.A. Nechkin, V.A. Semenov and S.F. Semenko, Yad. Fiz.**42** , 1050 (1985).

[31] F. Bečvář, J. Honzátko, M. Krtička, S. Pašić, G.Rusev, I. Tomandl, Nucl. Instrum. Methods Phys. Res. B **261**, 930 (2007).

[32] M.A. Lone, Proc. 4th Int. Symp., Smolenice, Czechoslovakia, 1985.

[33] F. Bečvář, P. Cejnar, R.E. Chrien, and J. Kopecky Phys. Rev. C **46**, 1276 (1992).

[34] C. Coceva, Nuovo Cim. **107** A 85 (1994).

[35] M. Uhl and J. Kopecky, Proc. Int. Conf. Nuclear Data for Science and Technology, Gatlinburg, 1994. p. 438.

[36] A. Bohr and B.R. Mottelson, Nuclear Structure (Benjamin, New York, 1975), Vol II, p.636.

TABLE II: GEDR and GMDR parameters, used for the EGLO and SLO model calculations.

Nucleus	E_{E1} (MeV)	Γ_{E1} (MeV)	σ_{E1} (mb)	E_{M1} (MeV)	Γ_{M1} (MeV)	σ_{M1} (mb)	$\langle\Gamma_\gamma\rangle$ (meV)
^{205}Pb†	13.59	3.85	514	6.95	4.0	1.16	330
^{206}Pb	13.59	3.85	514	6.94	4.0	1.16	-
^{207}Pb	13.56	3.96	481	6.93	4.0	1.16	455(50)
^{208}Pb	13.43	4.07	639	6.92	4.0	1.72	-

† GEDR parameters taken from ^{206}Pb.

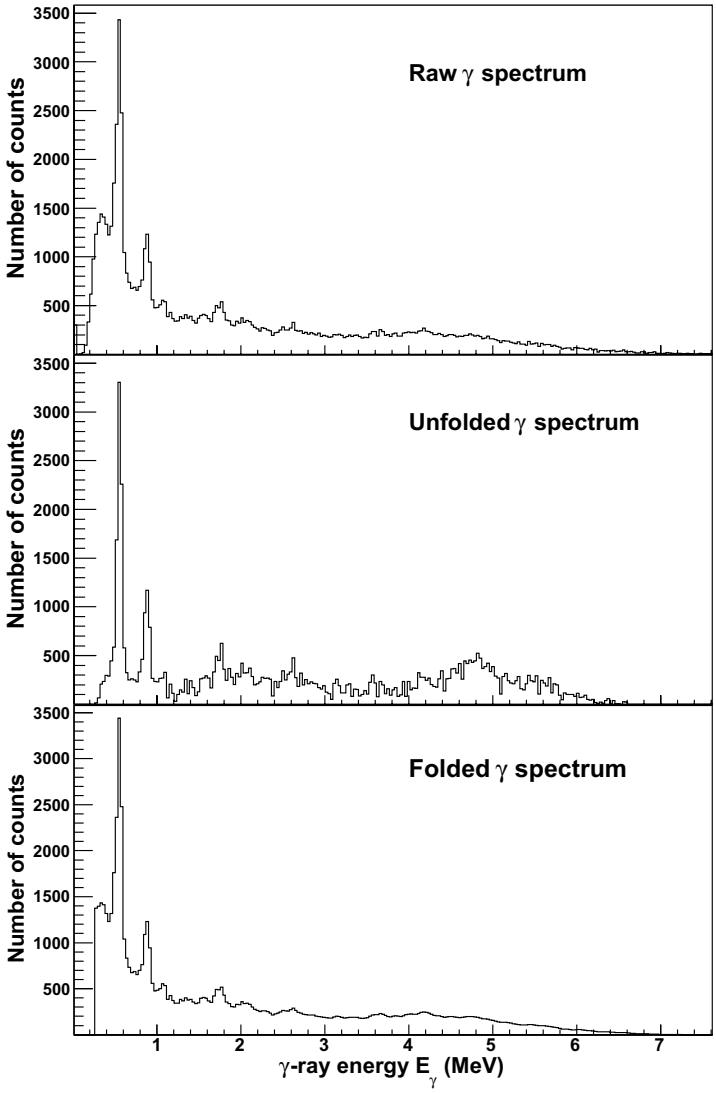

FIG. 1: Unfolding of the γ-ray spectrum of ^{207}Pb measured for the excitation energy region $E = 4.5 - 6.7$ MeV. Note the similarity of the raw and folded spectrum.

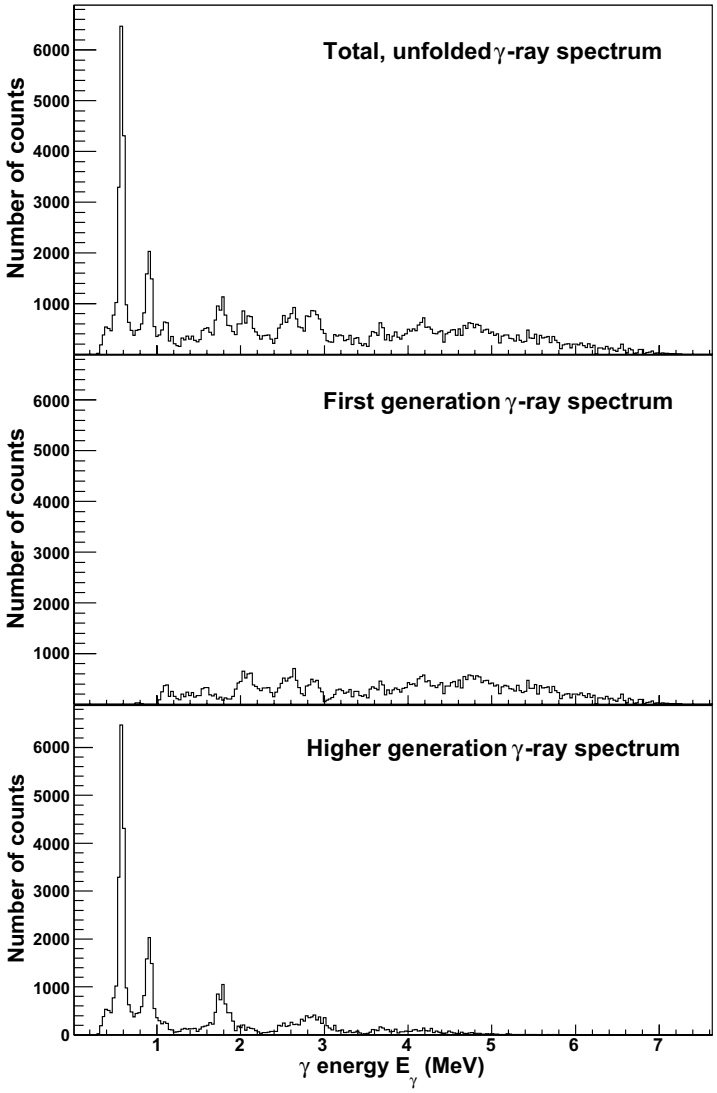

FIG. 2: Extraction of first generation γ-rays (middle panel) from the total, unfolded γ-ray spectrum (top panel) by subtracting the second and higher generation γ-rays (bottom panel) in ^{207}Pb between excitation energies of 4.5 and 6.7 MeV.

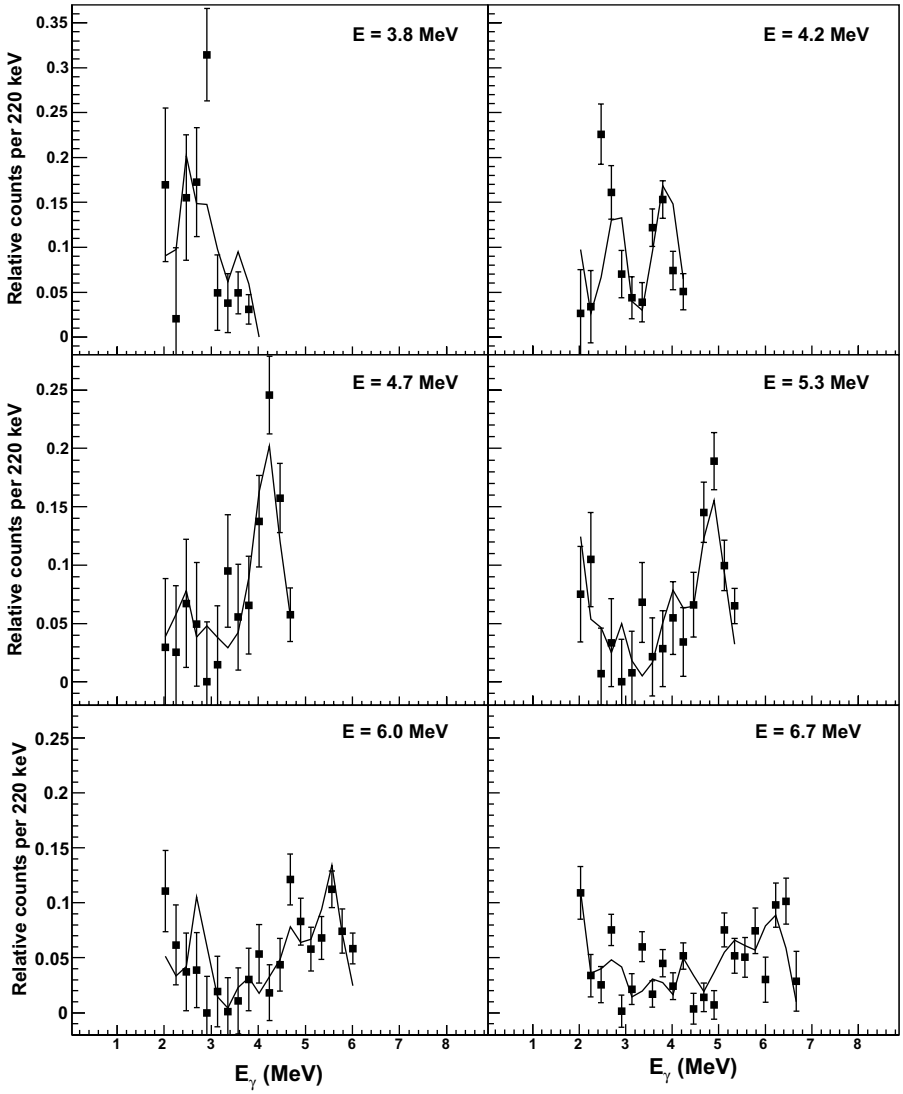

FIG. 3: Comparison of the normalized experimental primary γ-ray spectra for the ^{208}Pb(^{3}He,α)^{207}Pb reaction (data points) at various excitation energies and the fit (solid lines) using the factorization of Eq. (2). The excitation energy widths are 220 keV.

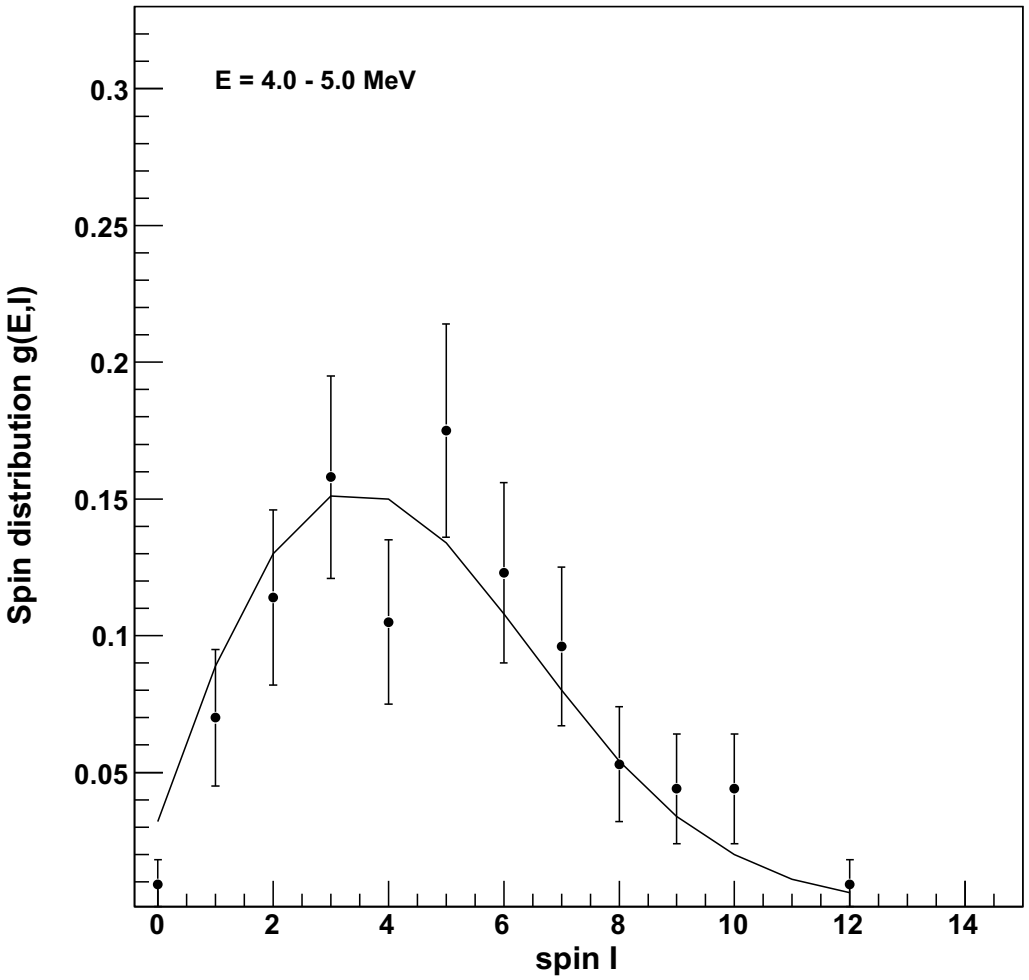

FIG. 4: Average experimental spin distribution (data points with error bars) of ^{206,208}Pb compared to the spin distribution determined using Eq. (9). The error bars include only statistical errors.

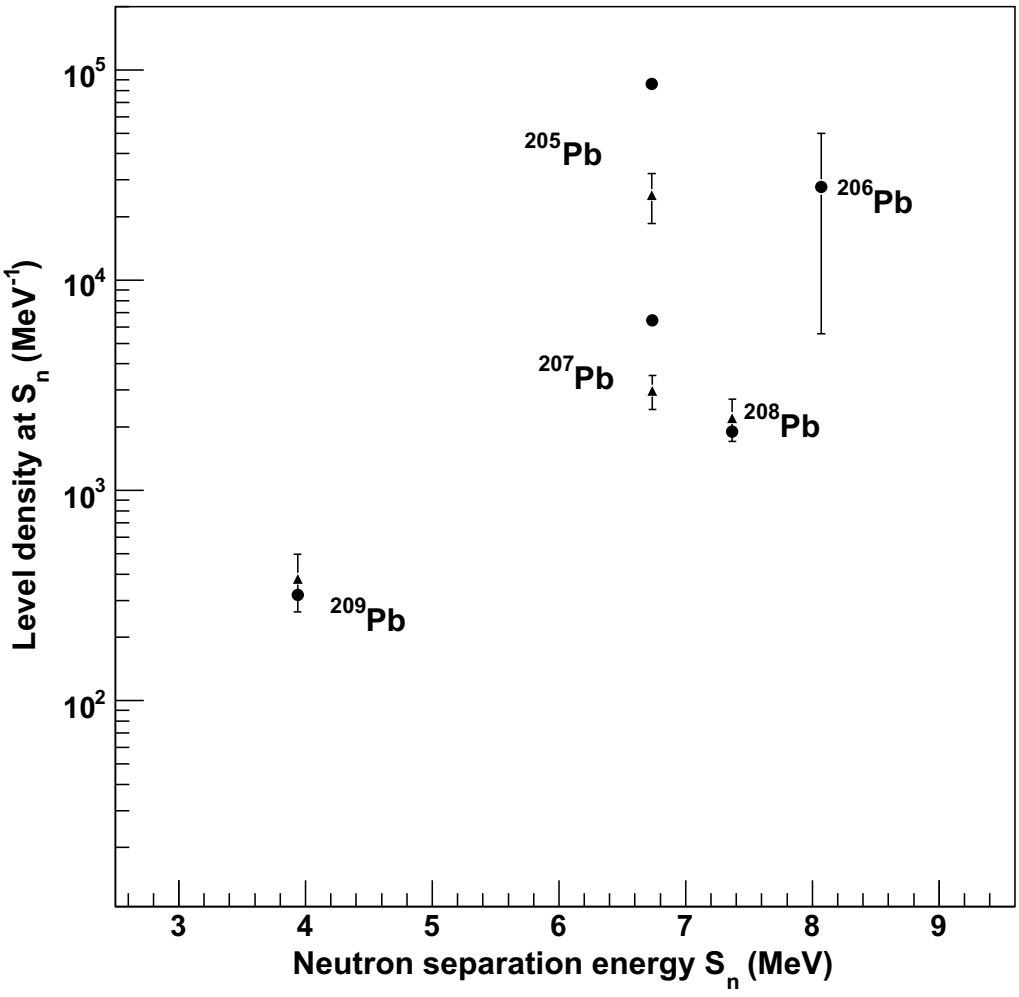

FIG. 5: Estimation of the level density at neutron separation energy $\rho(S_n)$ for ^{206}Pb. The filled triangles represent the deduced $\rho(S_n)$ for $^{205,207-209}$Pb using $\ell = 1$ neutron resonance spacings [22]. The filled circles are the level densities determined by Eq. (10) using parameters of Table I.

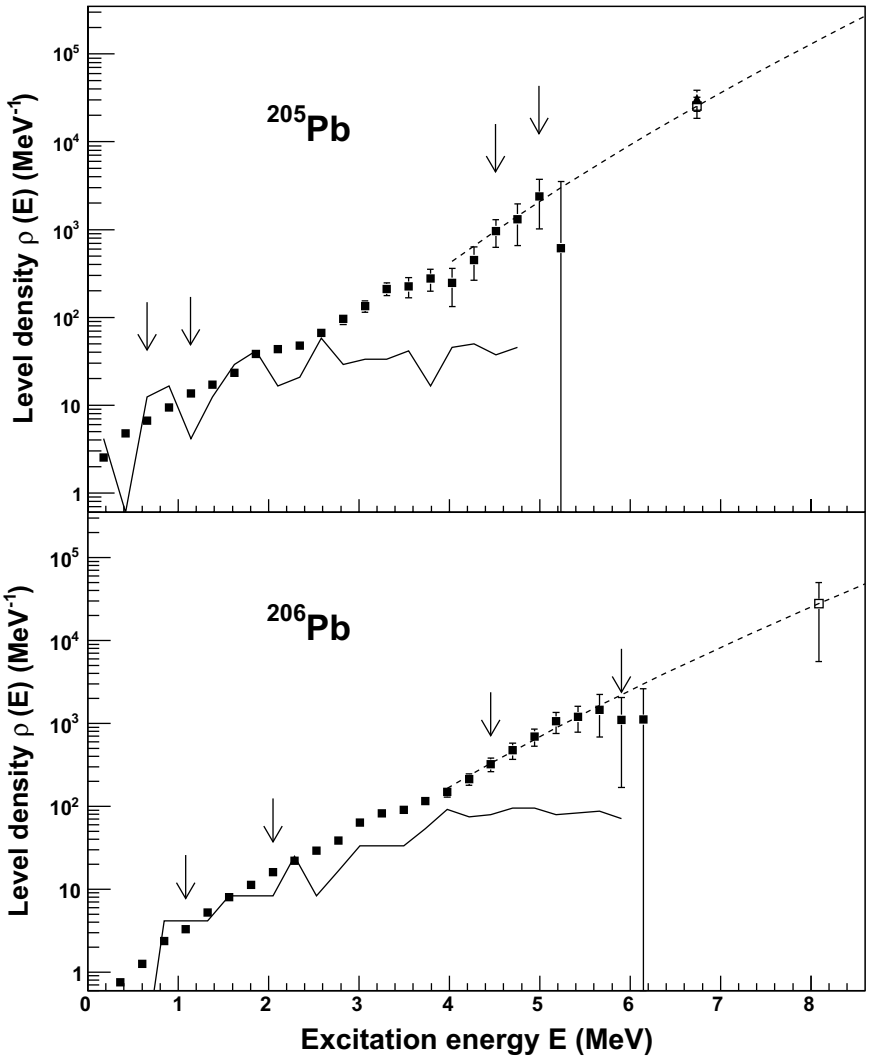

FIG. 6: Normalization of experimental nuclear densities (filled squares) for ^{205}Pb and ^{206}Pb. The arrows indicate the fitting region of data points at low excitation energies with known levels (solid line). To bridge the gap between the level density at S_n (open square) and the data points, the Fermi gas level density (dashed line) is used. The filled triangle and the open square symbols at S_n are based on $\ell = 0$ and 1 neutron resonance spacing data, respectively.

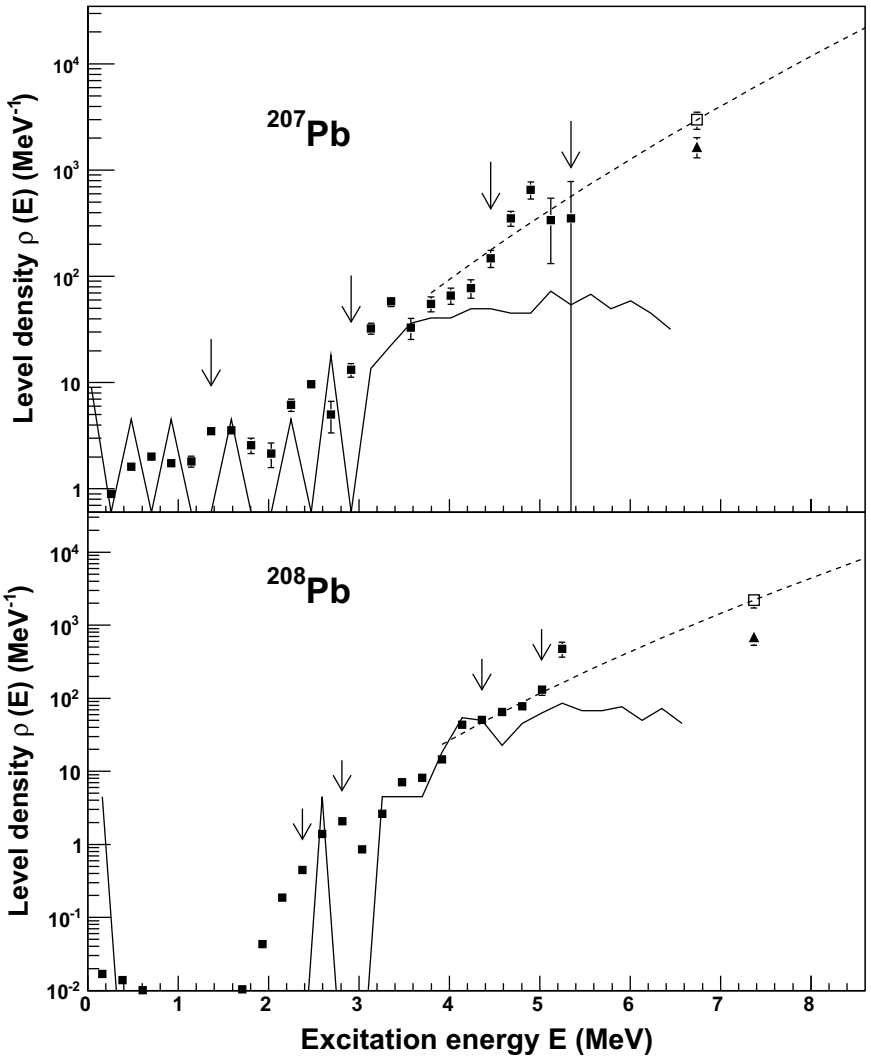

FIG. 7: Normalized nuclear densities (filled squares) of ^{207,208}Pb (see caption of Fig. 6).

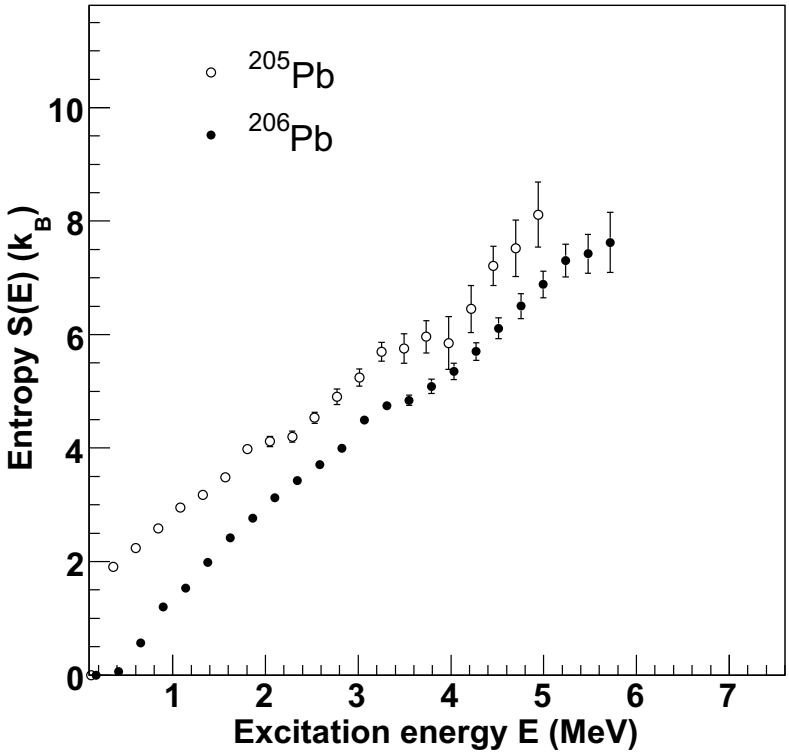

FIG. 8: Micro-canonical entropy for ^{205,206}Pb.

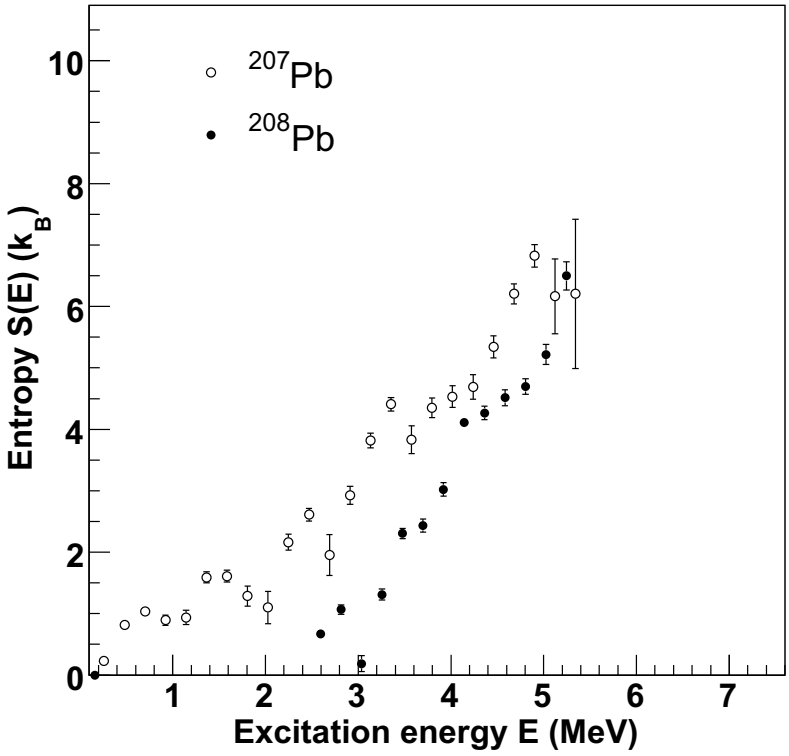

FIG. 9: Micro-canonical entropy for ^{207,208}Pb.

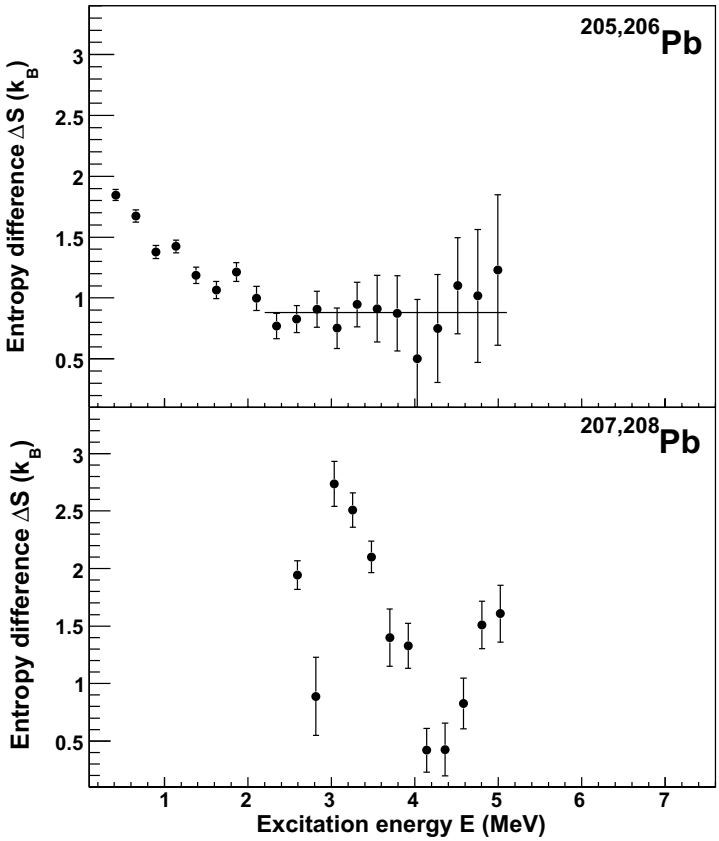

FIG. 10: Difference in entropy between ^{205}Pb and ^{206}Pb (upper panel) and between ^{207}Pb and ^{208}Pb (lower panel). The entropy difference is given by $\Delta S = S_{\rm eo} - S_{\rm ee}$, where $S_{\rm eo}$ and $S_{\rm ee}$ is the entropy of the even-odd and even-even nucleus, respectively.

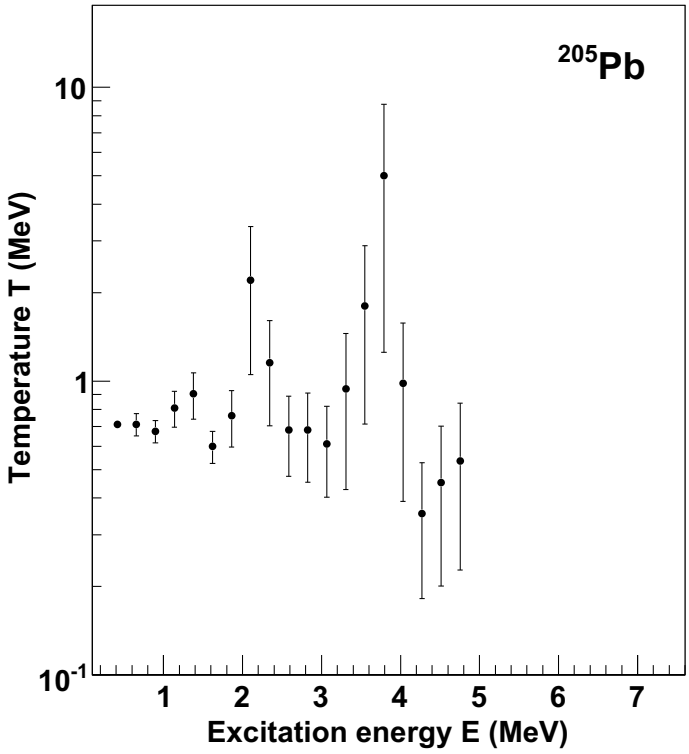

FIG. 11: Temperature as a function of excitation energy in ^{205}Pb.

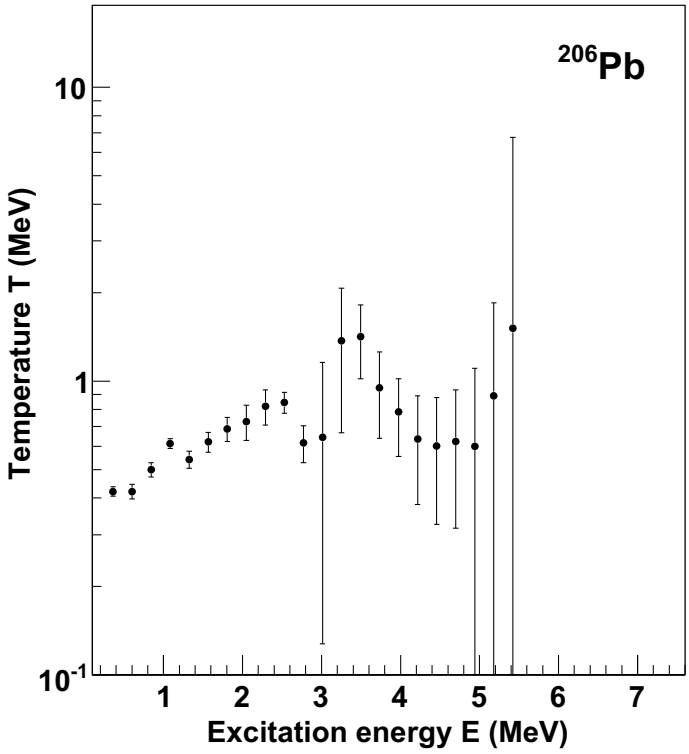

FIG. 12: Temperature as a function of excitation energy in ^{206}Pb.

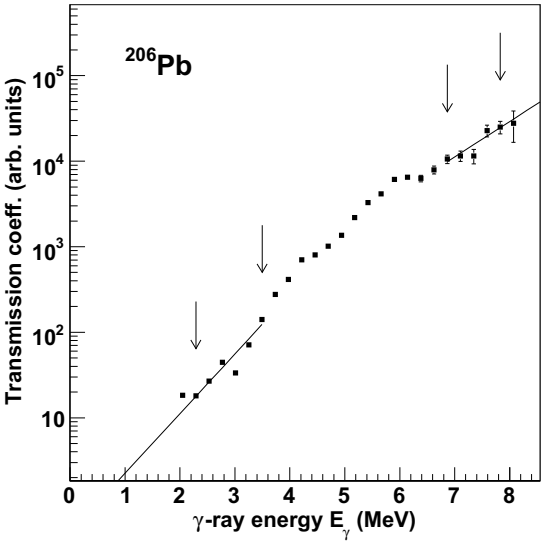

FIG. 13: Transmission coefficient $\mathscr{T}$ in arbitrary units for ^{206}Pb. An exponential function (solid line) is fitted to the data points between the arrows at low and high γ-ray energies.

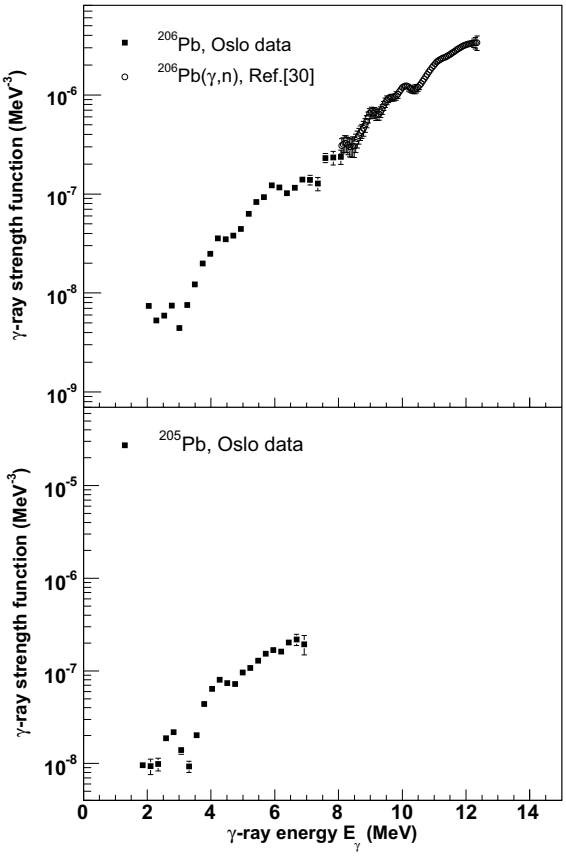

FIG. 14: Normalized γ-ray strength functions for ^{205,206}Pb as a function of γ-ray energy. The Oslo data (filled squares) of ^{206}Pb are normalized to photonuclear data (open circles) taken from Ref. [30].

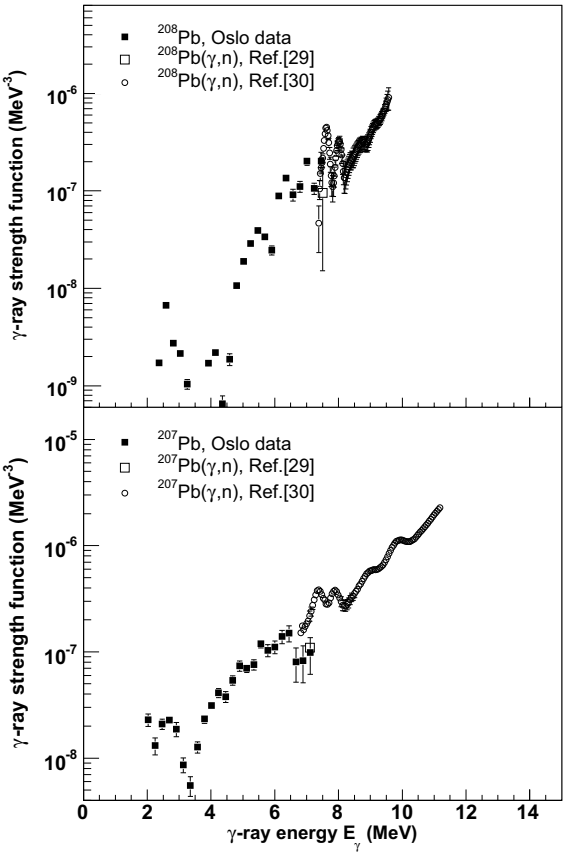

FIG. 15: Normalized γ-ray strength functions for ^{207,208}Pb. The Oslo data (filled squares) of ^{207}Pb is normalized using the data of Ref. [1]. The ^{208}Pb nucleus is normalized by scaling the Oslo data with the sum of $f_{E1} + f_{M1}$ (open square) taken from Ref. [29] and the photonuclear data (open circles) of Ref. [30].

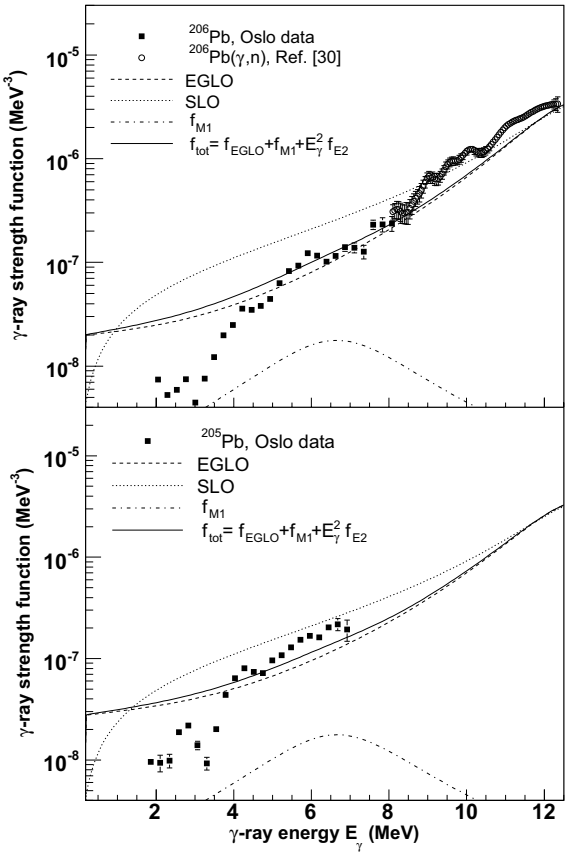

FIG. 16: Normalized γ-ray strength functions for ^{206}Pb and ^{205}Pb. The Oslo data (filled squares) are compared with the SLO (dotted line) and EGLO (dashed line) model predictions. The *M*1 strength function is shown by the dashed-dotted line. The solid line is the total strength function which is the sum of the EGLO model, *E*2 and *M*1. The photonuclear cross-section data from Ref. [30] are shown as open circles.

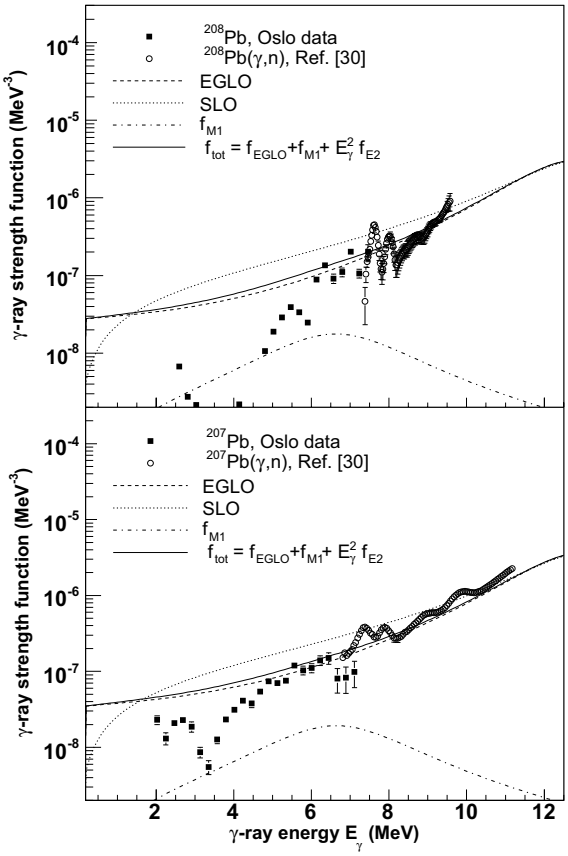

FIG. 17: Normalized γ-ray strength functions for ^{207,208}Pb as a function of γ-ray energy (see caption of Fig. 16).

7.6 Paper 5: Extraction of thermal and electromagnetic properties in ^{45}Ti

Extraction of thermal and electromagnetic properties in ^{45}Ti

N.U.H. Syed*, to be submitted to the Oslo Collaboration
Department of Physics, University of Oslo,
P.O.Box 1048 Blindern, N-0316 Oslo, Norway.

(Dated: December 18, 2008)

The level density and γ-ray strength function of ^{45}Ti have been determined by use of the Oslo method. The coincidences from the $(p,d\gamma)$ pick-up reaction with 32 MeV protons are utilized to obtain γ-ray spectra as function of excitation energy. The extracted level density and strength function are compared with models, which are found to describe these quantities satisfactory. The data do not reveal any single-particle energy gaps of the underlying double magic ^{40}Ca core, probably due to the strong quadrupole deformation.

PACS numbers: 21.10.Ma, 21.10.Pc, 27.40.+z
Keywords: Level density, entropy, γ-ray strength function

I. INTRODUCTION

The density of nuclear levels in quasi-continuum provides information on the gross structure of excited nuclei and is a basic quantity in nuclear reaction theories. Also the γ-ray strength function is important for describing the γ-decay process at high excitation energies. Experimentally, the nuclear level density can be determined reliably up to a few MeV of excitation energy from the counting of low-lying discrete known levels [1]. Previously, the experimental information on the γ-ray strength function has been mainly obtained from the study of photonuclear cross-sections [2].

The Oslo nuclear physics group has developed a tool to determine simultaneously level densities and γ-ray strength function from particle-γ coincidences. The Oslo method, which is applicable for excitation energies below the particle separation threshold, is described in detail in Ref. [3]. In this work, we report for the first time on results using the (p,d) reaction as inputs for the Oslo method. The advantage with this reaction compared to the commonly used (^{3}He,^{3}He') and (^{3}He,^{4}He) reactions, are higher cross-sections and better particle resolution.

The subject of the this paper is to determine the level density and electromagnetic properties of the ^{45}Ti nucleus. The system has only two protons and three neutrons outside the double-magic ^{40}Ca core. It is therefore of great interest to see if the number of levels per MeV are quenched due to the low number of interplaying valence nucleons. Also the decay pattern may be influenced by the expected overrepresentation of negative parity states, originating from the $\pi f_{7/2}$ and $\nu f_{7/2}$ single-particle states.

In Sect. II the experimental set-up and data analysis are described. Nuclear level densities and thermodynamics are discussed in Sect. III, and in Sect. IV the γ-ray strength functions are compared with models. Summary and conclusions are given in Sect. V.

*Electronic address: n.u.h.syed@fys.uio.no

II. EXPERIMENTAL SETUP AND DATA ANALYSIS

The experiment was conducted at Oslo Cyclotron Laboratory (OCL) using a 32-MeV proton beam bombarded on a self-supporting target of ^{46}Ti, enriched to 86% (10.6% ^{48}Ti, 1.6% ^{47}Ti, 1.0% ^{50}Ti, and 0.8% ^{44}Ti). The thickness of the target was 1.8 mg/cm^2. The transfer reaction, ^{46}Ti(p,d)^{45}Ti, is analyzed in the present study. The charged ejectile of deuterium is used to tag the excitation energies for each γ-ray spectrum from the ground state and up to the neutron separation energy.

The particle-γ coincidences are measured with the efficient CACTUS multi-detector array [4]. The coincidence set-up consists of eight collimated ΔE – E type Si particle telescopes, placed at a distance of 5 cm from the target and making an angle of $\theta = 45^\circ$ with the beam line. The particle telescopes are surrounded by 28 $5" \times 5"$ NaI γ-ray detectors, which have a total efficiency of $\sim 15\%$ of 4π.

The experimental extraction procedure and assumptions made are described in Ref. [3]. The registered ejectil energy is transformed into excitation energy of the residual nucleus through reaction kinematics and the known reaction Q-value. The excited residual nucleus produced in the reaction will subsequently decay by one or several γ-rays. Thus, a γ-ray spectrum can be recorded for each initial excitation energy bin E. Furthermore, the γ-ray spectra are corrected for the NaI detector response function by applying the unfolding technique of Ref. [5]. The unfolding is based on the Compton-subtracting technique, which prevents additional count fluctuations to appear in the unfolded spectrum.

The set of these unfolded γ-ray spectra forms the basis of extracting the first-generation γ-ray spectra, which are organized into an (E,E_γ) matrix. Here, the energy distribution of the first (primary) emitted γ-rays in the γ-cascades at various excitation energies is isolated by an iterative subtraction technique [6]. The main assumption of the first-generation method is that the γ-ray spectrum from a bin of excited states are independent of the population mechanism of these states. In the present setting, this means that the γ-spectrum obtained from a direct (p,d) reaction into states at excitation energy bin E is similar to the one obtained if the states at E are populated from the γ-decay of higher-lying states.

The generalized Fermi's golden rule states that the decay probability can be factorized into a factor depending on the transition matrix-element between the initial and final state, and the state density at the final states. Following this factorization, we express the decay probability from the initial excitation energy E to depend on the γ-ray transmission coefficient $\mathscr{T}(E_\gamma)$ and the level density $\rho(E-E_\gamma)$ by

$$P(E,E_\gamma) \propto \mathscr{T}(E_\gamma)\rho(E-E_\gamma). \quad (1)$$

Here, $\mathscr{T}(E_\gamma)$ is assumed to be temperature (or excitation energy) independent according to the Brink-Axel hypothesis [7, 8].

The ρ and $\mathscr{T}$ functions are determined by an iterative procedure [3] by adjusting these two functions until a global χ^2 minimum with the experimental $P(E,E_\gamma)$ matrix is reached. It has been shown [3] that if one of the solutions for ρ and $\mathscr{T}$ is known, then the entries of the matrix $P(E,E_\gamma)$ in Eq. (1) are invariant under the transformations:

$$\tilde{\rho}(E-E_\gamma) = A\exp[\alpha(E-E_\gamma)]\rho(E-E_\gamma), \quad (2)$$

$$\tilde{\mathscr{T}}(E_\gamma) = B\exp(\alpha\, E_\gamma)\ \mathscr{T}(E_\gamma). \quad (3)$$

The parameters A, B and α are unknown and can be obtained by normalizing the Oslo data to other experimental data or systematics. The determination of A and α is discussed in the next section, and parameter B is discussed in Sect. IV.

III. NUCLEAR LEVEL DENSITY AND THERMODYNAMICS

The level density ρ extracted from our coincidence data by the use of Eq. (1) contains the fine structures, but is not normalized. The transformation generators A and α of Eq. (2), which decide the absolute value and slope of the level density, can be determined by normalizing to the discrete levels at low excitation energies [1] and to the level density determined from the available resonance spacings data of photonuclear experiments. Unfortunately, the neutron-resonance spacings data for the target nucleus ^{44}Ti are not found in literature (^{44}Ti has a half life of 67 years). We therefore use the systematics of T. von Egidy and D. Bucurescu [9], which is based on a global fitting of known neutron resonance spacing data with the back-shifted Fermi gas (BSFG) formula:

$$\rho_{\mathrm{BSFG}}(U) = \frac{\sqrt{\pi}}{12}\frac{\exp(2\sqrt{aU})}{a^{1/4}U^{5/4}}\frac{1}{\sqrt{2\pi}\sigma}, \quad (4)$$

where a is the level density parameter, $U = E - E_1$ is the intrinsic excitation energy and E_1 is the back-shifted energy parameter. The spin distribution is given by the spin cut-off parameter σ given by

$$\sigma^2 = 0.0146A^{5/3}\sqrt{a(E-E_1)}, \quad (5)$$

where A is the nuclear mass number. The level-density parameters are summarized in Table I.

In Fig. 1 the nuclear level densities deduced from the neutron resonance spacing data [10] of odd and even titanium nuclei have been compared with the BSFG level densities obtained from the systematics [9]. The systematic values $\rho(S_n)$ for the titan isotopes are seen to overestimate the experimental values determined from resonance spacing data. Thus, the systematic values from Eq. (4) are multiplied with a factor of $\eta = 0.5$ to make them more comparable with the experimental values. In this way (see Fig. 1), the unknown level density of ^{45}Ti is estimated to be $\rho(S_n) = 1400 \pm 700$ MeV^{-1}. Figure 2 shows our normalized level density for ^{45}Ti (black squares), which is adjusted (A and α) to fit the discrete levels at low excitation energy (solid lines) and the systematic value at S_n (open square).

The slope (given by α) of the measured level density may be uncertain due to the estimated level density at S_n, the upper anchor point of the normalization. Various ways of analyzing the global set of neutron resonance spacing data, may result in different $\rho(S_n)$ values within a factor of two. In order to justify our adopted level-density normalization, the experimental data of ^{47}Ti [11] are also shown in Fig. 2. The level density in ^{47}Ti is determined using proton-evaporation spectra from the ^{45}Sc(^{3}He,p)^{47}Ti reaction. In this method, the slope of the level density should be well determined, however, the absolute value is undetermined. The good agreement between the slopes of ^{45}Ti and ^{47}Ti in the energy region of 4 – 8 MeV gives confidence to the present normalization.

The level density is seen to follow very nicely the density of known levels up to $E \sim 2-3$ MeV. At higher excitation energies only a part of the levels are known, mainly from transfer reactions. The BSFG level density (dashed line of Fig. 2) is seen not to describe the fine structure of our data, but is assumed to be relevant for the extrapolation between our data and the value at S_n. This assumption is also supported by the ^{47}Ti data, which follow closely the Fermi gas level density to higher excitation energies.

The level density of ^{45}Ti shows pronounced step structures below $E \sim 6-7$ MeV. These structures are probably the results of the amount of energy needed to cross shell gaps and to break Cooper pairs. The level density of the ^{45}Ti nucleus, with $Z = 22$ protons and $N = 23$ neutrons, is close to its double magic $Z = N = 20$ core. The gap energies are around 2 – 3 MeV, which are comparable with the energy (2Δ) required for breaking Cooper pairs. Thus, it is very difficult to foresee the level-density fine structure in this case.

From the measurements of level density as a function of excitation energy, one can explore various thermodynamical properties of the nucleus like entropy and temperature. For the present analysis, the micro-canonical ensemble has been used since hot nuclei are better described statistically through such an ensemble [12]. Within this framework, the nucleus is considered to be an isolated system with a well-defined energy. The extracted level density ρ at excitation energy E is directly related to the the entropy S by

$$S(E) = k_B \ln\rho(E) + S_0, \quad (6)$$

where the Boltzmann's constant k_B is set to unity. The normalization term S_0 is adjusted to fulfill the third law of ther-

modynamics i.e., $S \to 0$ for $T \to 0$, T being temperature of the nucleus. Using the ground state band of the even-even ^{44}Ti, the normalization term is found to be $S_0 = -0.1$. Furthermore, the microcanonical temperature T can be deduced from S by

$$\frac{1}{T(E)} = \frac{\partial S}{\partial E}. \tag{7}$$

Figures 3 and 4 show the micro-canonical entropy and temperature of ^{45}Ti, respectively. The variations in entropy with excitation energy are equivalent to the variations in the level density. The fine structure of the entropy curve is seen to be enhanced for the temperature T curve due to the differentiation performed to S. The enhanced bump structures in the temperature spectra can be interpreted as the breaking of nucleon pairs. When particle pairs are broken, new degrees of freedom open up leading to dramatic increase of $\rho(E)$ and decrease in temperature $T(E)$. In the temperature plot of Fig. 4 one can notice the locations of negative slopes. First such location appear at $E \sim 2.0$ MeV which should be compared with twice the proton pairing gap parameter $2\Delta_p$ of ^{45}Ti, the minimum required energy to break a nucleon Cooper pair. By following the definition of [13], one gets $2\Delta_p = 1.784$ which is comparable to the location of the first temperature drop. The second such location of temperature drop occurs around ~ 4.2 MeV which can be interpreted as the point of four quasi-particles pair breaking.

The experimental level density is compared with the BSFG level density (shown as dashed line in Fig. 2) in the excitation region above 6 MeV. In this energy region, the comparison shows that the BSFG agrees nicely with the extracted level density of ^{45}Ti. However, the BSFG model level density does not reproduce the detailed structures in the experimental level density. In order to investigate the level density further, a microscopic model has been applied.

A. Combinatorial BCS Model of Nilsson Orbitals

The model [14] is based on combining all the proton and neutron configurations within the Nilsson level scheme and using the concept of Bardeen-Cooper-Schrieffer (BCS) quasi-particles [15]. The single-particle energies $e_{\rm sp}$ are taken from the Nilsson model for an axially deformed core, where the deformation is described by the quadruple deformation parameter ε_2. The quasi-particle excitation energies are described by

$$E_{\rm qp}(\Omega_\pi, \Omega_\nu) = \sum_{\Omega'_\pi, \Omega'_\nu} \left(e_{\rm qp}(\Omega'_\pi) + e_{\rm qp}(\Omega'_\nu) + V(\Omega'_\pi, \Omega'_\nu) \right), \tag{8}$$

where Ω_π and Ω_ν are the spin projections of protons and neutrons on to the symmetry axis, respectively, and V is the residual interaction described by a random Gaussian distribution. The single quasi-particle energy $e_{\rm qp}$, characterized by the Fermi level λ and pair-gap parameter, is defined as:

$$e_{\rm qp} = \sqrt{(e_{\rm sp} - \lambda)^2 + \Delta^2}. \tag{9}$$

The total excitation energy is the sum of the quasi-particle energy $E_{\rm qp}(\Omega_\pi, \Omega_\nu)$, rotational excitations and vibrational excitations i.e.,

$$E = E_{\rm qp}(\Omega_\pi, \Omega_\nu) + A_{\rm rot} R(R+1) + \hbar\omega_{\rm vib}\nu. \tag{10}$$

The rotational excitations are described by the rotational parameter $A_{\rm rot} = \hbar/2\mathscr{I}$, $\mathscr{I}$ being the moment of inertia and R being the rotational quantum number. The vibrational excitations are described by the phonon number $\nu = 0, 1, 2, \ldots$ and oscillator quantum energy $\hbar\omega_{\rm vib}$. At low excitation energy, the rotational parameter $A_{\rm rot}$ is for simplicity taken as the value ($A_{\rm gs}$) deduced around the ground state of even-even nuclei in this mass region. For increasing excitation energy, we let the rotational parameter decrease linearly according to

$$A_{\rm rot}(E) = A_{\rm gs} + \left(\frac{A_{\rm rigid} - A_{\rm gs}}{E_{\rm rigid}} \right) E, \tag{11}$$

where we assume $A_{\rm rot} = A_{\rm rigid}$ for excitation energies above the excitation energy $E_{\rm rigid}$. Since theoretical approaches seem to predict rigid moment of inertia at the neutron separation energy, we put $E_{\rm rigid} = S_n$. The rigid value is calculated from

$$A_{\rm rigid} = \frac{5\hbar}{4MR_A^2(1 + 0.31\varepsilon_2)}, \tag{12}$$

where M is the nuclear mass and R_A is the nuclear radius.

The spin (I) of each state is schematically calculated from the rotational quantum number (R) and the total projection (K) of the spin vector on the nuclear symmetry axis by

$$I(I+1) = R(R+1) + K^2. \tag{13}$$

The quantity K is determined by the sum of projections on the symmetry axis:

$$K = \sum_{\Omega'_\pi, \Omega'_\nu} \Omega'_\pi + \Omega'_\nu. \tag{14}$$

The Nilsson single-particle orbitals appropriate for ^{45}Ti are drawn in Fig. 5. The spin-orbit parameter $\kappa = 0.066$ and centrifugal parameter $\mu = 0.32$ are taken from Ref. [16]. The main harmonic oscillator quantum is estimated by $\hbar\omega_0 = 1.2(41A^{-1/3})$ MeV. The vibrational quantum energy $\hbar\omega_{\rm vib} = 2.611$ MeV is taken from the excitation energy of the first 0^+ vibrational state in ^{46}Ti. The fermi levels for protons and neutrons are also shown in Fig. 5 for an estimated deformation of $\varepsilon_2 = 0.25$. Other parameters employed to calculate the level density of ^{45}Ti, are listed in Table II.

Figure 6 shows that the calculated level density for ^{45}Ti describes satisfactorily the experimental level density. The general increase and the structural details of the level density are well reproduced. These structures can be understood from Fig. 7 where the average number of nucleon pairs broken $\langle N_{\rm qp} \rangle$ is plotted as a function of excitation energy. Here, the average number of pairs includes both proton and neutron pair breaking. Figure 7 shows that the first pairs break at $2\Delta \sim 2.5$ MeV of excitation energy. The pair breaking process leads to an exponential increase of level density, and the

process is also responsible for an overall increase at higher energies. Rotational and vibrational excitations are of less importance. Even the shell gaps expected at $Z = N = 20$ seem not to play a major role, probably because the gap between the $f_{7/2}$ and $d_{3/2}$ orbitals is reduced by the nuclear quadrupole deformation. Indeed, the single-particle Nilsson orbitals appear to make a rather uniform energy distribution at $\varepsilon_2 = 0.25$ in Fig. 5.

The spin distribution of our model can be compared with the commonly used spin distribution [17]:

$$g(E,I) = \frac{2I+1}{2\sigma^2}\exp\left[-(I+1/2)^2/2\sigma^2\right] \qquad (15)$$

with a spin cut-off parameter σ taken from Eq. (5). The two spin distributions (normalized to unity) are shown in Fig. 8. The comparison is made at four different excitation energy bins having an excitation energy window of 0.24 MeV. The general trend in the two distributions are surprisingly similar, however, some deviations are also obvious. This is mainly due to fluctuations originating from the low level density in this nucleus. The moment of inertia of ^{45}Ti is chosen to approach a rigid rotor at energies near and above S_n, which has been seen theoretically in the medium mass region nuclei $A \sim 50-70$ [18]. The satisfactory resemblance of the two spin distributions indicates that our simplified treatment of determining the spin of levels through Eqs. (13) and (14) works well.

The parity distribution is a quantity that also reveals the presence (or absence) of shell gaps. In the extreme case, where only the $\pi f_{7/2}$ and $\nu f_{7/2}$ shells would be occupied by the valence nucleons, just negative parity states would appear. The parity asymmetry parameter can be utilized to display the parity distribution in quasi-continuum and is defined by [19]

$$\alpha = \frac{\rho_+ - \rho_-}{\rho_+ + \rho_-}, \qquad (16)$$

where ρ_+ and ρ_- are the poisitive and negative parity level densities. An equal parity distribution would give $\rho_+ = \rho_-$, and thus $\alpha = 0$. Other α values range from -1 to +1 i.e., from more negative parity states to more positive parity states. Figure 9 shows that there are more negative parity states ($\alpha < 0$) below 4 MeV, however, at higher excitation energies the asymmetry is damped out giving an equal parity distribution. Thus, the parity calculations also confirm the absence of pronounced shell gaps in ^{45}Ti.

IV. GAMMA-RAY STRENGTH FUNCTION

The γ-ray strength function can be defined as the distribution of average decay probability as a function of γ-ray energy between levels in the quasi-continuum. The γ-ray strength function f_{XL}, where X is electromagnetic character and L is the multipolarity, is related to the γ-ray transmission coefficient $\mathscr{T}_{XL}(E_\gamma)$ for multipole transitions of type XL by

$$\mathscr{T}(E_\gamma) = 2\pi\sum_{XL} E_\gamma^{2L+1} f_{XL}(E_\gamma). \qquad (17)$$

According to the Weisskopf estimate [20], we assume the electric dipole $E1$ and the magnetic dipole $M1$ transitions are dominant transitions in a statistical nuclear decay. It is also assumed that the numbers of accessible positive and negative parity states are equal i.e.,

$$\rho(E-E_\gamma, I_f, \pm\pi_f) = \frac{1}{2}\rho(E-E_\gamma, I_f). \qquad (18)$$

The expression of average total radiative width $\langle\Gamma_\gamma\rangle$ [21] for s-wave neutron resonances with spin $I_t \pm 1/2$ and parity π_t at $E = S_n$, reduces to

$$\langle\Gamma_\gamma(S_n, I_t \pm 1/2)\rangle = \frac{1}{4\pi\rho(S_n, I_t \pm 1/2, \pi_t)}\int_0^{S_n} \mathrm{d}E_\gamma \times B\mathscr{T}(E_\gamma)\rho(S_n - E_\gamma) \times \sum_{J=-1}^{1} g(S_n - E_\gamma, I_t \pm 1/2 + J). \qquad (19)$$

As mentioned in Sect. II, we extract the level density ρ and transmission coefficient $\mathscr{T}$ from the primary γ-ray spectrum. The slope of $\mathscr{T}$ is determined by the transformation generator α (see Eq.(3)), which has already been determined during the normalization of ρ in Sect. II. However, the factor B of Eq. (3) which determines the absolute value of the transmission coefficient, remains to be determined. The unknown B can be determined using Eq. (19) if in a photonuclear experiment the $\langle\Gamma_\gamma\rangle$ at S_n is known. Unfortunately, the average total radiative width for ^{45}Ti is not measured. Instead, $\langle\Gamma_\gamma\rangle$ for ^{47}Ti has been used as guideline for the determination of the parameter B.

The normalized γ-ray strength function is shown in Fig. 10. In order to be more confident with our adopted parameters for normalization, the total photoabsorption cross-section data in ^{46}Ti(γ,abs) [22] reaction have been displayed together with our normalized data. The cross-section data has been transformed into the γ-ray strength function by employing the relation [10]

$$f(E_\gamma) = \frac{1}{3\pi^2\hbar^2c^2}\frac{\sigma(E_\gamma)}{E_\gamma}. \qquad (20)$$

The increase of the ^{45}Ti γ-ray strength function with γ-ray energy in Fig. 10 is well in line with the low energy part of the (γ,abs) data.

In order to investigate the strength functions further, the experimental data of ^{45}Ti are compared with the Generalized Lorentzian Model (GLO), described in Ref. [10]. The model is used to describe the giant electric dipole resonance (GEDR) at low γ energies and at resonace energies. In the lower energy region this model gives a non zero finite value of the dipole strength function in the limit of $E_\gamma \to 0$. The GLO model is proposed by Kopecky and Chrien [23] and describes the strength function as:

$$f_{GLO} = \frac{1}{3\pi^2\hbar^2c^2}\sigma_{E1}\Gamma_{E1} \times [E_\gamma\frac{\Gamma_k(E_\gamma,T)}{(E_\gamma^2 - E_{E1}^2)^2 + E_\gamma^2\Gamma_k^2(E_\gamma,T)} + 0.7\frac{\Gamma_k(E_\gamma=0,T)}{E_{E1}}], \qquad (21)$$

where σ_{E1}, Γ_{E1} and E_{E1} are the cross-section, width and energy of the centroid of the GEDR, respectively. The energy and temperature dependent width Γ_k is given by [24]

$$\Gamma_k(E_\gamma, T) = \frac{\Gamma_{E1}}{E_{E1}^2}(E_\gamma^2 + 4\pi^2 T^2). \quad (22)$$

The shape of the GEDR cross section obtained from (γ,abs) data [22] shows clearly a splitting of the GEDR into two or more resonances. This splitting is a signature of the ground state deformation of the nucleus. The GEDR cross sections are thus best fitted with two Lorentzians using two sets of resonances parameters. Furthermore, we assume that the γ-ray strength function is independent of the excitation energy, i.e. with a constant temperature $T = 1.4$ MeV. This constant temperature approach is adopted in order to be consistent with the Brink-Axel hypothesis in Sect. II, where the transmission coefficient $\mathscr{T}(E_\gamma)$ is assumed to be temperature independent. In Table III the two sets of GEDR parameters for the ground state deformation $\varepsilon_2 \sim 0.25$ (interpolated between the known neighboring nuclei) are listed using the systematics of Ref. [10].

The magnetic dipole $M1$ radiation, supposed to be governed by the giant magnetic dipole (GMDR) spin-flip $M1$ resonance radiation [25], is described by a Lorentzian [26]

$$f_{M1}(E_\gamma) = \frac{1}{3\pi^2\hbar^2c^2}\frac{\sigma_{M1}E_\gamma\Gamma_{M1}^2}{(E_\gamma^2 - E_{M1}^2)^2 + E_\gamma^2\Gamma_{M1}^2}, \quad (23)$$

where σ_{M1}, Γ_{M1}, and E_{M1} are the GMDR parameters deduced from the systematics given in Ref. [10].

The total model γ-ray strength function, shown by solid and dash-dotted lines in Fig. 10, is given by

$$f_{\rm tot} = \kappa\left[f_{E1,1} + f_{E1,2} + f_{M1}\right], \quad (24)$$

where the factor κ is used to scale the model strength function with the experimental γ-ray strength function. The value of κ is expected to deviate from unity, since only approximate values of the average resonance spacings D and the total average radiative width data $\langle\Gamma\rangle$ have been used for the absolute normalization of the strength function.

The comparison of Fig. 10, shows that the Oslo data are well descibed by the GLO model in the energy region $\sim 2.5-9$ MeV. However, at low γ-ray energies ($E_\gamma < 2.5$ MeV) an enhancement in the γ-ray strength function compared to the GLO model has been observed. Previously, this upbend has been seen in several nuclei with mass number $A < 100$ (see e.g. Ref. [14] and references therein). The physical origin of this enhancement has not been fully understood yet, as no theoretical model accounts for such a behaviour of the nucleus at low γ-ray energies.

V. CONCLUSIONS

The level density and γ-ray strength function for ^{45}Ti have been measured in a ^{46}Ti$(p,d)^{45}$Ti reaction, using the Oslo method. The thermodynamical quantities; entropy and temperature, in a micro-canonical ensemble are extracted from the measured level densities. The avearge temperature for ^{45}Ti is found to be 1.4 MeV. The experimental level density is also compared with combinatorial BCS model of Nilsson orbitals. The model describes satisfactorily the general increase and structural details of the experimental level density.

The generalized Lorentzian model (GLO) has been compared with the experimental γ-ray strength funcion. The GLO model describes the Oslo data well in the energy region $E_\gamma \sim 2.5-9$ MeV. However, at $E_\gamma < 2.5$ MeV an enhancement in the γ-ray strength function compared to GLO model has been observed. This is very interesting since a similar γ-decay behaviour has been observed in several other light mass nuclei, however, this observation is still not been accounted for by present theories.

[1] Data extracted using the NNDC On-Line Data Service from the ENSDF database.
[2] S.S. Dietrich and B.L. Berman, At. Data Nucl. Data Tables **38**, 199 (1988).
[3] A. Schiller, L. Bergholt, M. Guttormsen, E. Melby, J. Rekstad, and S. Siem, Nucl. Instrum. Methods Phys. Res. A **447**, 498 (2000).
[4] M. Guttormsen, A. Atac, G. Løvhøiden, S. Messelt, T. Ramsøy, J. Rekstad, T.F. Thorsteinsen, T.S. Tveter, and Z. Zelazny, Phys. Scr. **T 32**, 54 (1990).
[5] M. Guttormsen, T.S. Tveter, L. Bergholt, F. Ingebretsen, and J. Rekstad, Nucl. Instrum. Methods Phys. Res. A **374**, 371 (1996).
[6] M. Guttormsen, T. Ramsøy, and J. Rekstad, Nucl. Instrum. Methods Phys. Res. A **255**, 518 (1987).
[7] D.M. Brink, Ph.D. thesis, Oxford University, 1955.
[8] P. Axel, Phys. Rev. **126**, 671 (1962).
[9] T. von Egidy and D. Bucurescu, Phys. Rev. C **72** , 044311 (2005) and Phys. Rev. C **73**, 049901(E) (2006).
[10] T. Belgya, O. Bersillon, R. Capote, T. Fukahori, G. Zhigang, S. Goriely, M. Herman, A.V. Ignatyuk, S. Kailas, A. Koning, P. Oblozinsky, V. Plujko and P. Young. Handbook for calculations of nuclear reaction data, RIPL-2 (IAEA, Vienna, 2006), http://www-nds.iaea.org/RIPL-2/.
[11] A.V. Voinov, S.M. Grimes, A.C. Larsen, C.R. Brune, M. Guttormsen, T. Massey, A. Schiller, S. Siem, and N.U.H. Syed, Phys. Rev. C **77** , 034613 (2008).
[12] D.J. Morrissey, Annu. Rev. Nucl. Part. Sci. **44** 27 (1994).
[13] J. Doczewski, P. Magierski, W. Nazarewicz, W. Satula, and Z. Szymanski, Phys. Rev. C **63**024308 (2001).
[14] A.C. Larsen, R. Chankova, M. Guttormsen, F. Ingebretsen, S. Messelt, J. Rekstad, S. Siem, N.U.H. Syed, and S.W. Oedgaard, Phys. Rev. C **76**, 044303 (2007).
[15] J. Bardeen, L.N. Cooper, and J.R. Schrieffer, Phys. Rev. **108**, 1175 (1957).
[16] D.C.S. White, W.J. McDonald, D.A. Hutcheon, and G.C. Neil-

TABLE I: Parameters used for the back-shifted Fermi gas level density

Nucleus	S_n (MeV)	a (MeV^{-}1)	E_1 (MeV)	σ	D (keV)	$\rho(S_n)$ (10^3 MeV)	η
^{45}Ti	9.53	5.62	-0.90	3.48	-	1.4(7)[a]	0.5

[a] Estimated from the systematics of Fig. 1 (see text).

TABLE II: Level density model parameters used for calculation.

Nucleus	ε_2	Δ_π (MeV)	Δ_ν (MeV)	κ	μ	$A_{\rm rot}$ (MeV)	λ_π (MeV)	λ_ν (MeV)
^{45}Ti	0.25	0.892	1.350	0.066	0.32	0.075	54.913	56.872

son, Nucl, Phys. A **260** , 189 (1976).

[17] A. Gilbert, A.G.W. Cameron, Can. J. Phys. **43** , 1446 (1965).

[18] Y. Alhassid, S. Liu, H. Nakada, Phys. Rev. Lett. 99, 162504 (2007).

[19] U. Agvaaluvsan and G.E. Mitchell, Phys. Rev. C **67** , 064608 (2003).

[20] J.M. Blatt, V.F. Weisskopf **Theoretical Nuclear Physics** (Wiley, New York, 1952).

[21] J. Kopecky and M. Uhl, Phys. Rev. C **41** , 1941 (1990).

[22] B.S. Ishkhanov, I.M. Kapitonov, E.I. Lileeva, E.V. Shirokov, V.A. Erokhova, M.A. Elkin, A.V. Izotova, R,MSU-INP-2002-27, 711 (2002).

[23] J. Kopecky and R.E. Chrien, Nucl. Phys. **A 468** , 285 (1987).

[24] Reference Input Parameter Library IAEA, RIPL1 (IAEA-TECDOC 1998), http://www-nds.iaea.org/RIPL-1/.

[25] A. Voinov, M. Guttormsen, E. Melby, J. Rekstad, A. Schiller, and S. Siem, Phys. Rev. C **63,**044313 (2001).

[26] A. Bohr and B.R. Mottelson, Nuclear Structure (Benjamin, New York, 1975), Vol II, p.636.

TABLE III: GEDR and GMDR parameters determined using the systematics given in [10].

Nucleus	$E_{E1,1}$ (MeV)	$\Gamma_{E1,1}$ (MeV)	$\sigma_{E1,1}$ (mb)	$E_{E1,2}$ (MeV)	$\Gamma_{E1,2}$ (MeV)	$\sigma_{E1,2}$ (mb)	E_{M1} (MeV)	Γ_{M1} (MeV)	σ_{M1} (mb)	$\langle\Gamma_\gamma\rangle$ (meV)	κ
^{45}Ti	16.20	5.31	22.26	22.52	9.96	44.53	11.53	4.0	1.23	1400[b]	1.55

[b] The s-wave average total radiative width $\langle\Gamma_\gamma\rangle$ of ^{47}Ti has been used for normalization.

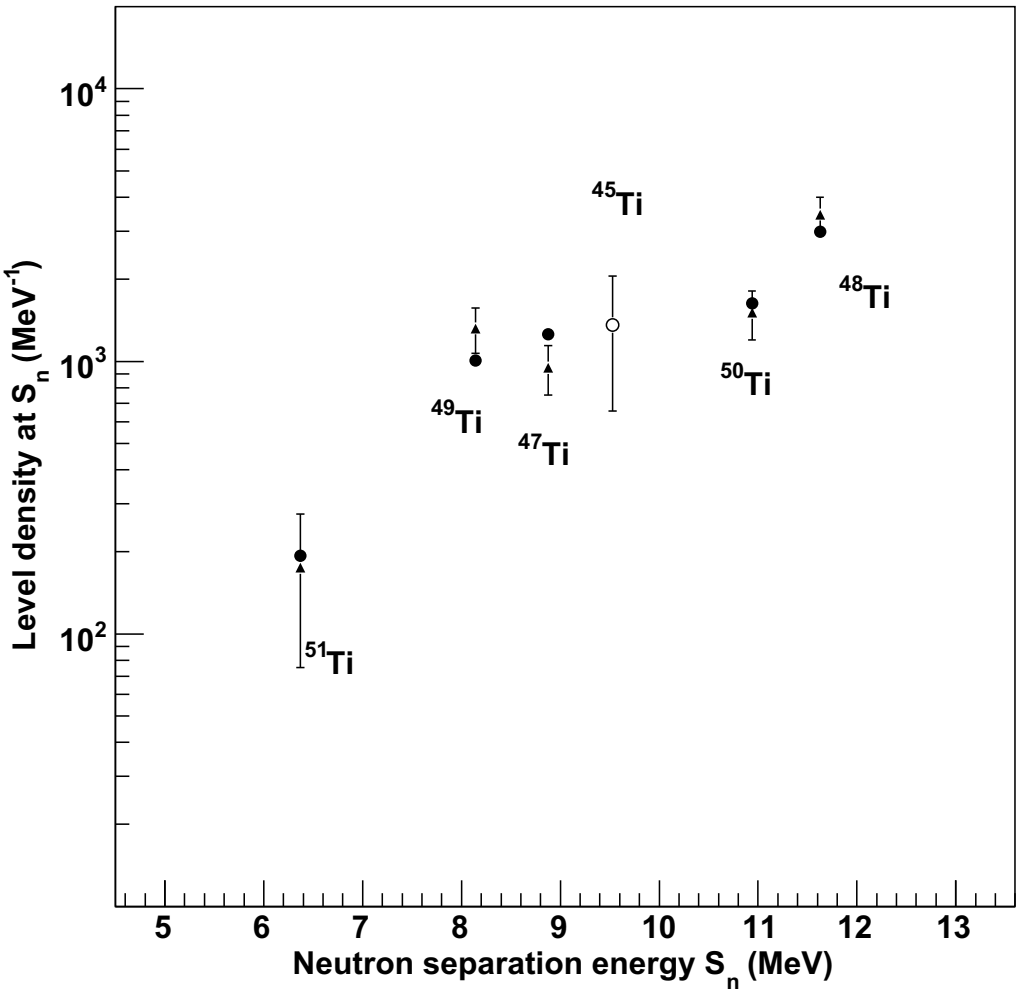

FIG. 1: The neutron resonance spacings data of [10], in a target nucleus of a (γ,n) reaction, has been used to deduce the $\rho(S_n)$ (filled triangles). The filled circles are the level densities that have been calculated using Eq. (4). The calculated level densities are multiplied with a factor of 0.75 in order to make them compareable with level densities deduced from resonance spacing data. The level density of ^{45}Ti (open circle) is calculated and scaled using the above mentioned systematics with an adopted uncertainity of 50%.

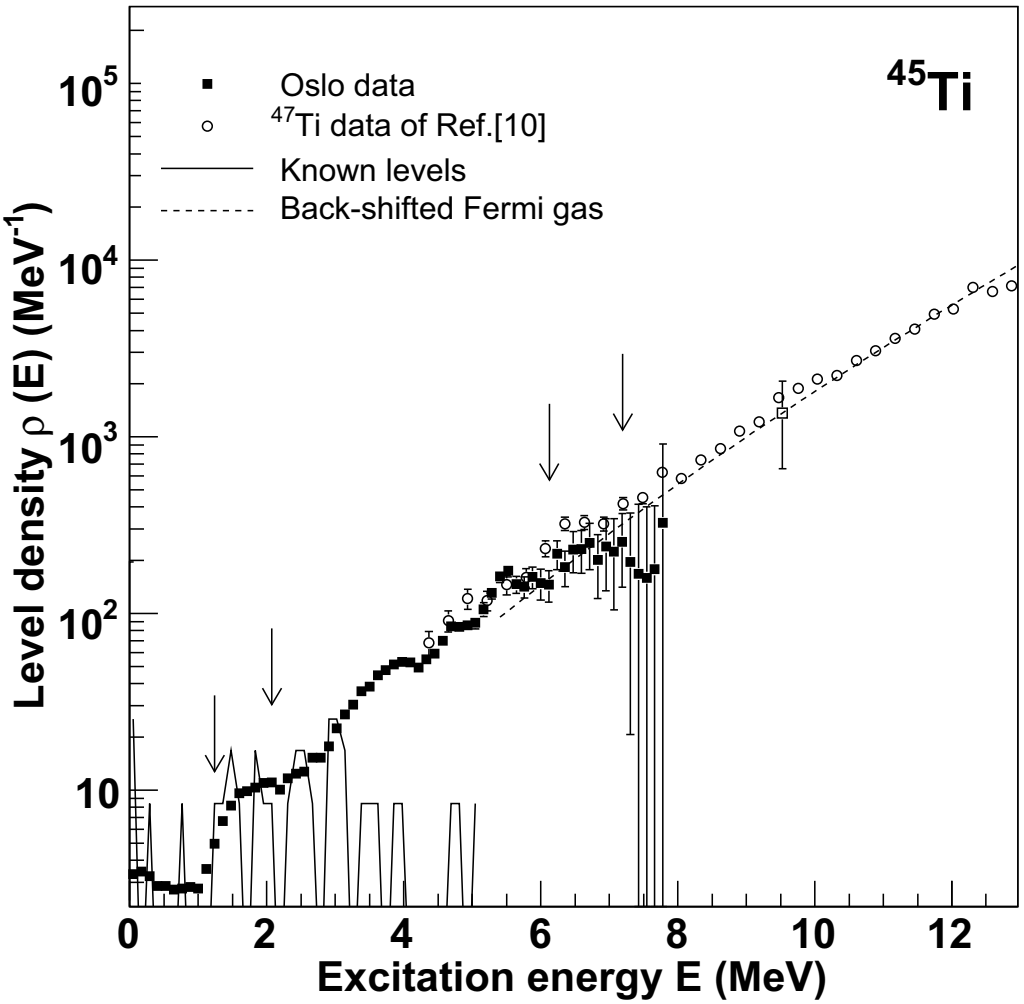

FIG. 2: Normalization proceedure of the nuclear level density (data points) of ^{45}Ti. At low excitation energies the data points are normalized between the arrows, to known levels (solid line). At higher excitation energies, the data points are normalized to the BSFG level density (dotted line). The open square is the level density at S_n estimated from the systematics of Fig. 1. Open circles are data from particle-evaporation spectra [11].

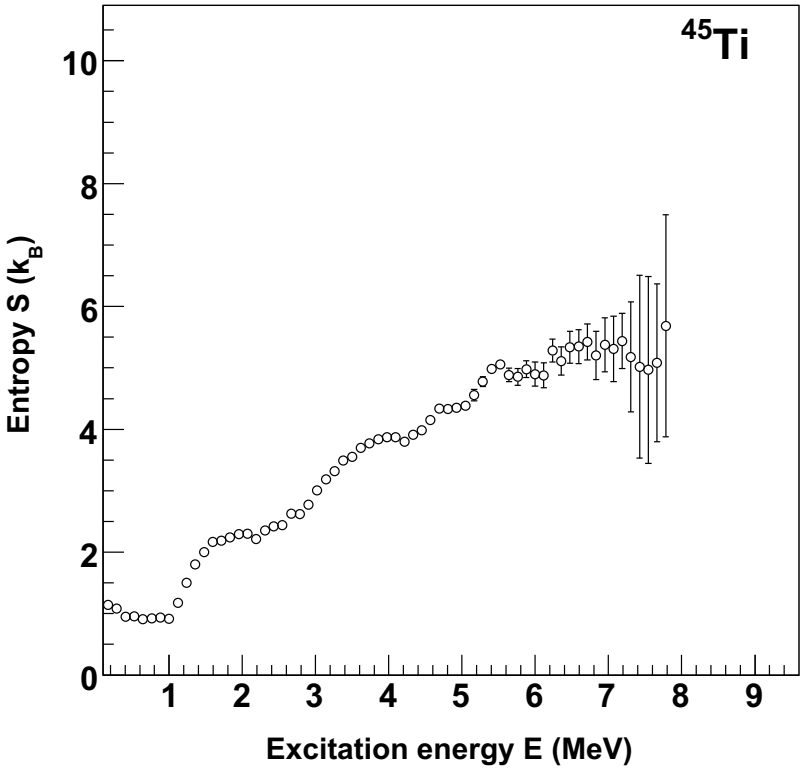

FIG. 3: Microcanonical entropy in ^{45}Ti.

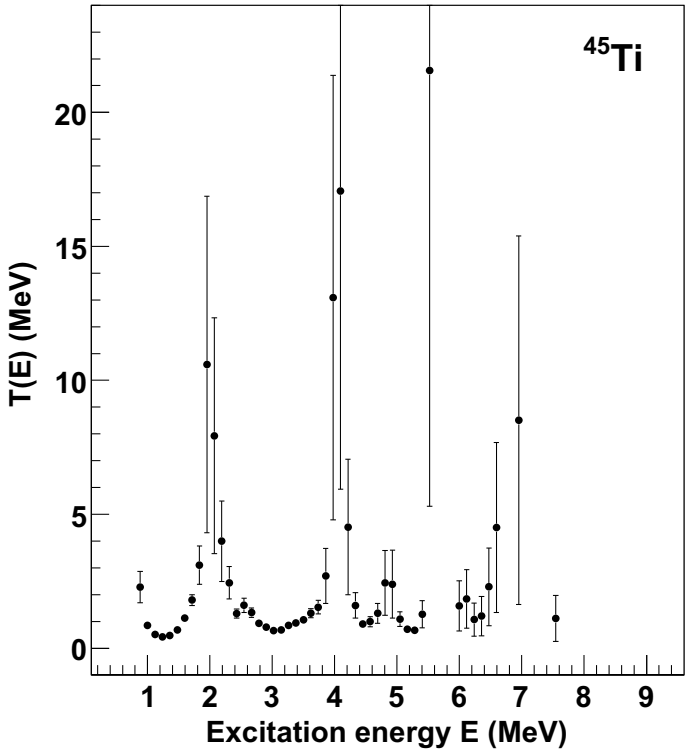

FIG. 4: The micro-canonical temperature as a function of excitation energy in ^{45}Ti.

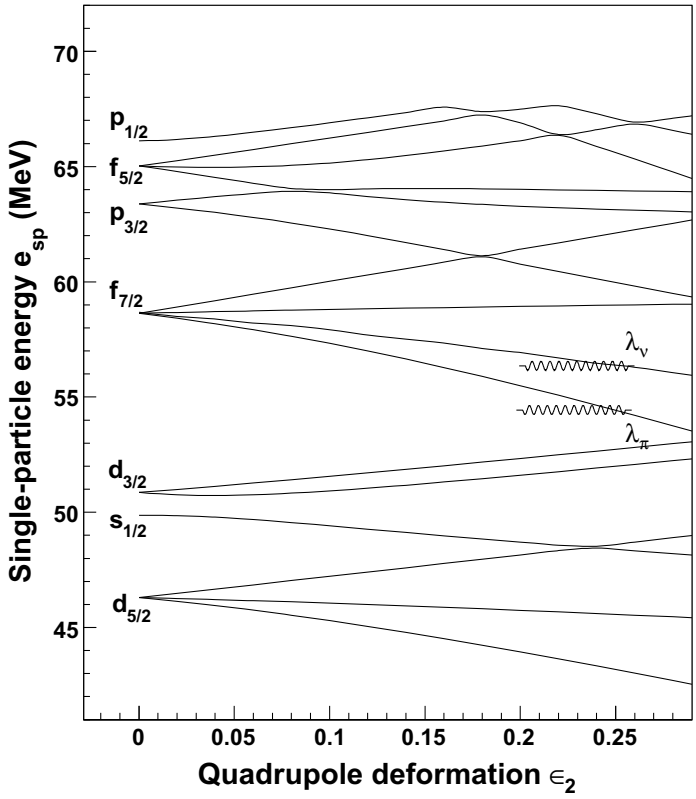

FIG. 5: Nilsson level scheme for ^{45}Ti.

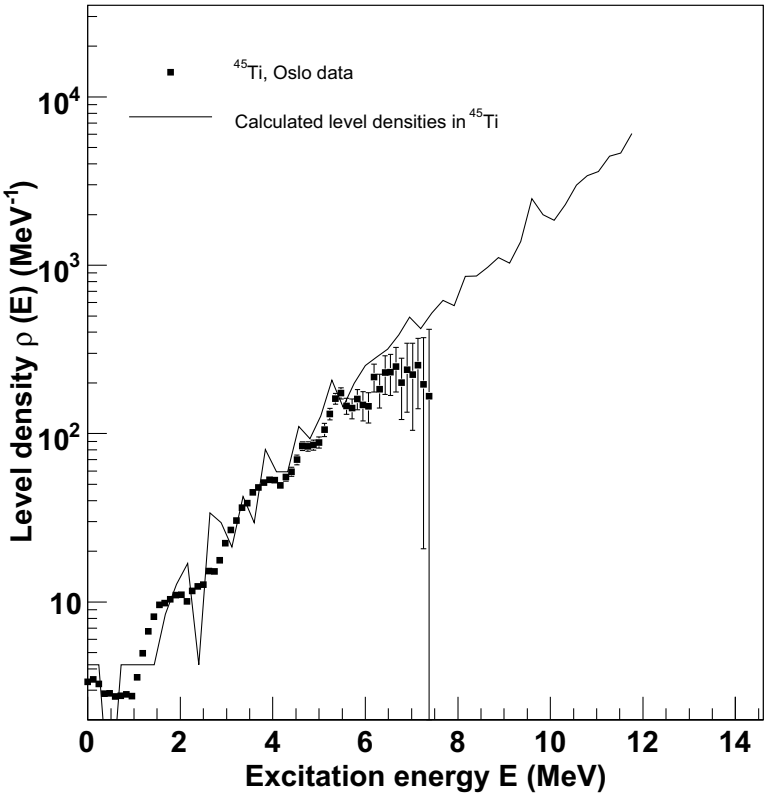

FIG. 6: Comparison between the experimental (filled squares) and calculated (solid line) level densities in ^{45}Ti.

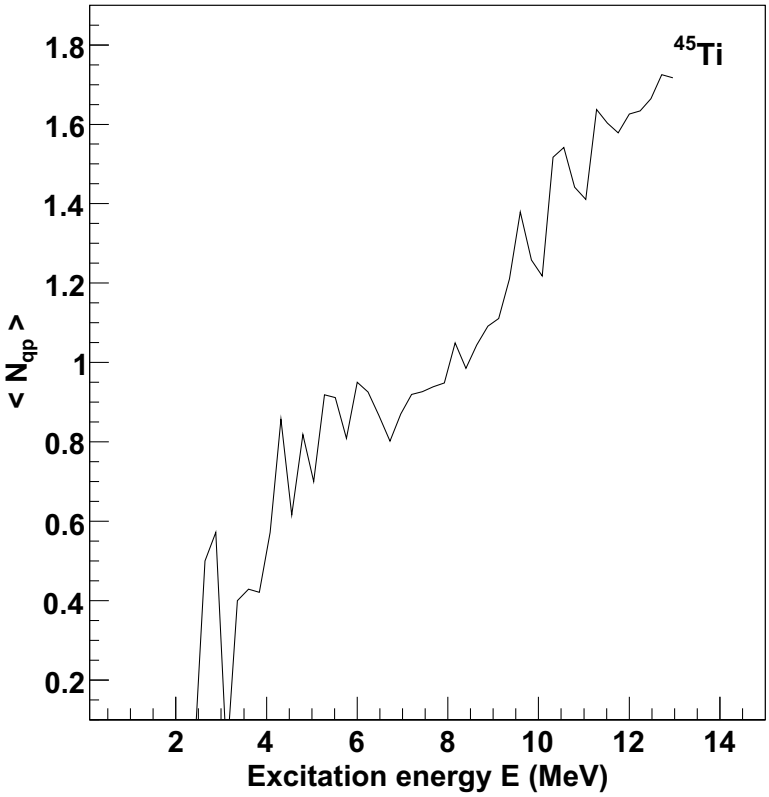

FIG. 7: Average number of broken Cooper-pairs in ^{45}Ti.

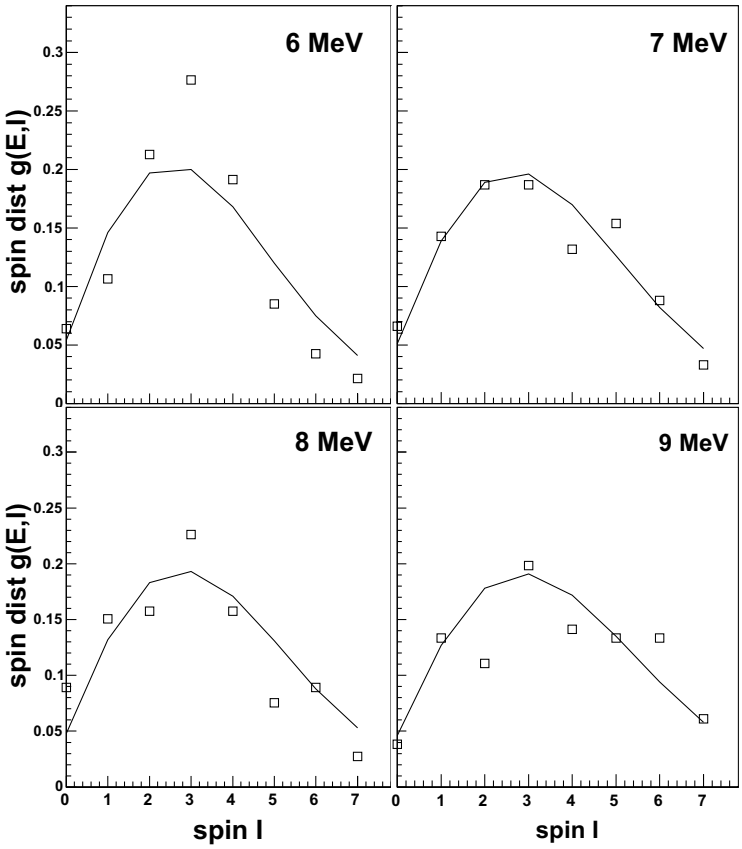

FIG. 8: Comparison of spin distributions in ^{45}Ti determined by Eq. (13) (open squares) with that determined by Eq. (15) (solid lines) at different excitation energy bins.

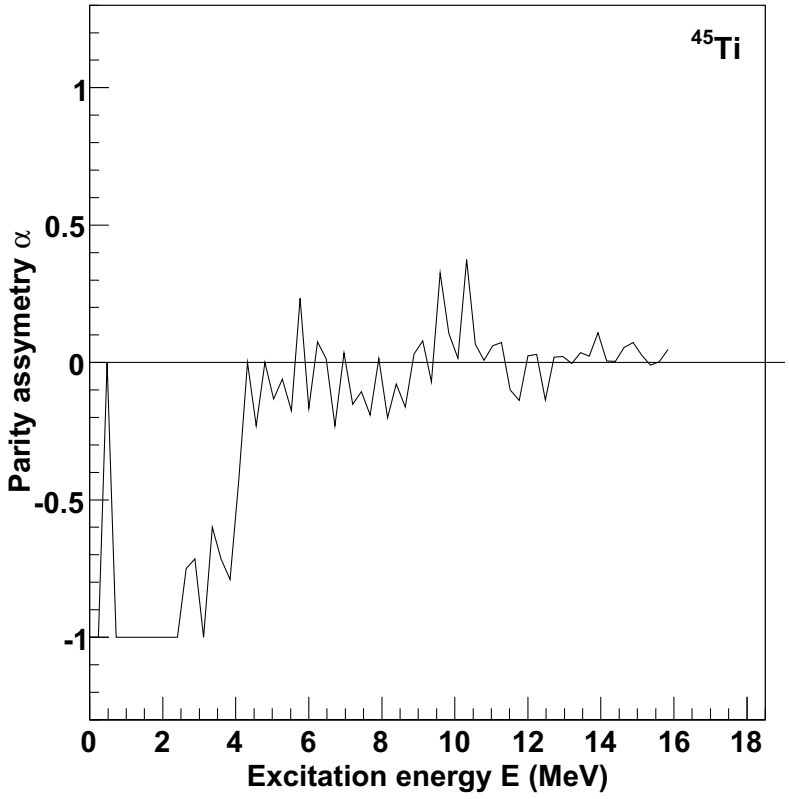

FIG. 9: Parity asymmetry in ^{45}Ti.

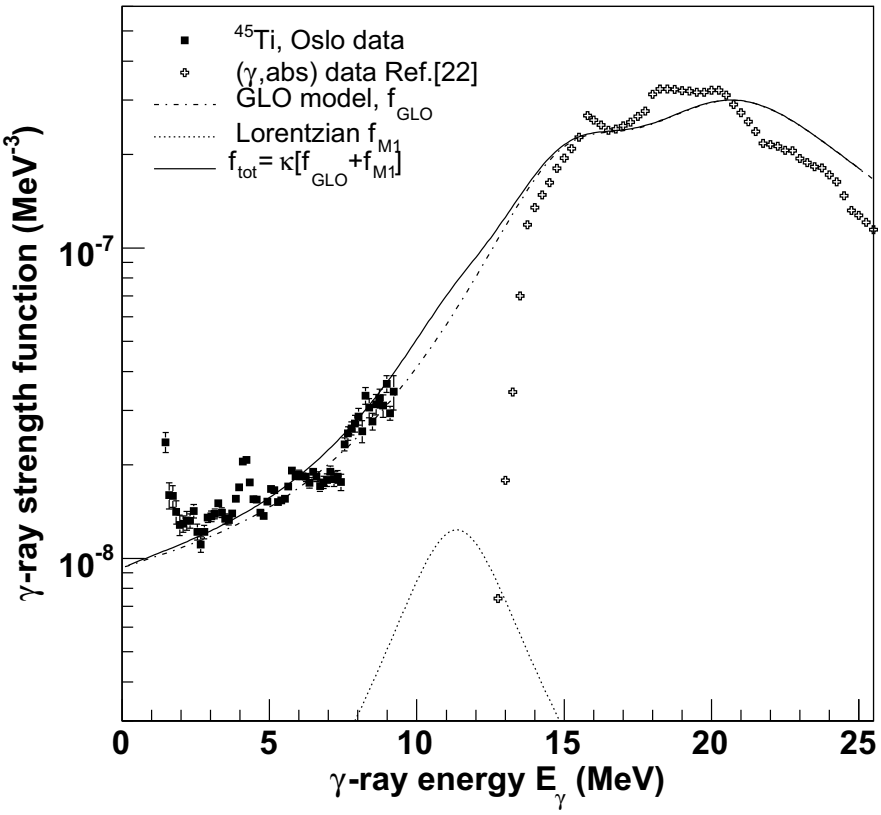

FIG. 10: Normalized γ-ray strength function for ^{45}Ti nuclei shown as a function of γ-ray energy. The Oslo data (filled squares) are compared with the GLO model [23] (solid line). In addition the data of (γ,abs) reaction [22] (crosses) for ^{46}Ti nucleus have also been drawn at γ-ray energies above the particle treshold.

Chapter 8

Summary and Conclusions

8.1 Summary of experimental results

The Oslo method has been used to extract the energy distribution of the first generation γ-ray spectra in the ^{44,45}Sc, ^{45}Ti, ^{50,51}V, and $^{205-208}$Pb nuclei. In these nuclei, the excited states at and below the neutron separation energy are populated by inelastic scattering or neutron pick-up reactions. The primary γ-ray spectra in the region of quasi-continuum contain the information of two important statistical quantities, level density and γ-ray strength function.

The level densities are normalized with the known discrete levels at low excitation energies and neutron resonance spacing data at the neutron separation energy. The slope of the γ-ray strength function is fixed by the level density normalization. However, the absolute normalization of the strength function is achieved either from the average total radiative width of neutron resonances or by scaling our data with other photonuclear reaction data. A great advantage of the Oslo method is the simultaneous determination of the level density and the strength function. Therefore, in a specific energy region these quantities are extractable independently with little model dependency.

The invested nuclei in this thesis are situated in the vicinity of closed or near closed shells. For these nuclei the statistical properties are less favorable as compare to mid-shell nuclei. It is known that the level densities for light or closed shell nuclei are generally low. In the previous findings by the Oslo physics group, the level densities extracted in the rare-earth region for the excitation energies near S_n were around 10^6 MeV^{-1}. However, in the present thesis we are reporting level densities for light and/or closed shell nuclei, around $10^3 - 10^4$ MeV^{-1}.

In papers I, II, IV, and V prominent bump structures have been observed in the experimental level densities. The origin of these structures is partly due to shell closure effects and breaking of Cooper pairs. These structures were most

prominent in ^{207,208}Pb and less prominent in ^{45}Ti, ^{44,45}Sc and ^{51}V. In Paper IV the effect of moving away from the doubly closed shell ^{208}Pb to the single closed $^{205-207}$Pb isotopes has been described. One prominent effect is that the level densities of ^{205,206}Pb become a smoother function of excitation energies, compared to ^{207,208}Pb, as valance neutrons come into play.

In papers I, IV, and V the measured level densities are used to explore the thermodynamic properties like entropy and temperature. Here, the micro-canonical ensemble has been used to determine thermodynamic quantities of the nuclei. The results of paper I and V show a sudden increase in entropy at the pair breaking energies, which appears as a sudden drop in temperature. In paper IV the micro-canonical entropy difference ΔS between ^{205}Pb and ^{206}Pb is found to be $0.9k_B$ for excitation energies $2 \leq E \leq 5$ MeV. This difference in entropy is close to that observed in paper I between ^{50,51}V ($\Delta S \sim 1.2k_B$), and is nearly one half of the value observed in the rare earth nuclei ($\Delta S \sim 2k_B$). The relative smooth entropy function in ^{205}Pb makes its temperature function sufficiently smooth such that one can fit a straight line between $0.4 \leq E \leq 5.0$ MeV. In this way, an average temperature of 0.9(1) MeV is obtained, which is in good agreement with the proposed temperature of 0.81(4) MeV for ^{205}Pb in Ref. [34].

The level densities of ^{207,208}Pb show large fluctuations giving that the entropies fluctuate in the same manner. The temperature extraction for these nuclei due to strong entropy fluctuations is therefore not reliable.

In Paper III the level densities of ^{44}Sc extracted by the Oslo method and by particle-evaporation technique are compared. The slope of the extracted level densities of ^{47}Ti by proton-evaporation spectra is found to be similar to the level density of ^{45}Ti from the Oslo method. The consistency in level densities by the two approaches in Sc and Ti nuclei strengthens the reliability of the results obtained by the Oslo method.

The average electromagnetic nature of γ-transitions are studied in papers I, II, IV, and V by the determination of the γ-ray strength functions. Furthermore, the strength functions obtained for the lead nuclei show large bump structures at $E_\gamma < S_n$. These intermediate structures are more prominent for ^{206,208}Pb than for ^{205,207}Pb. In general, the strength functions in the lead nuclei are poorly described by the SLO and EGLO models of the $E1$ strength functions. However, the strength functions for ^{44,45}Sc, ^{45}Ti, and ^{50,51}V are satisfactorily described by the KMF and GLO models at the tail of GEDR, except for γ-ray energies lower than 2 – 3 MeV.

The previous results for the γ-ray strength functions in ^{56,57}Fe, and ^{93,98}Mo nuclei show an enhancement at low γ-ray energies. This enhancement (upbend) has now been confirmed to be present in the γ-ray strength functions for the ^{44,45}Sc, ^{45}Ti, and ^{50,51}V isotopes. In paper II it has been shown that the upbend is independent of the excitation energy region chosen to extract the strength functions. The physical origin of this low-energy upbend is not yet fully understood. However,

the present studies suggest that this upbend structure is more likely to occur in a certain mass region $A < 100$ caused by some sort of collective motions.

A general problem that has been encountered in the ^{44,45}Sc, ^{45}Ti, and ^{206,208}Pb nuclei were the absolute normalizations of their γ-ray strength functions due to the lack of average total radiative width in these nuclei. Scaling our strength functions with the available photonuclear cross-section data above the particle threshold has been used in these cases. However, this way of normalizing the data, especially in the Pb region, introduces large uncertainties in the absolute values of the γ-ray strength function.

8.2 New experimental setup

The old silicon particle detectors are now replaced by modern, segmented silicon detectors. Eight detectors are joined together in the form of a ring, called SiRi system. Each detector, shown in Fig. 8.1, consists of eight front detector pads with a common end detector, joined in the form of a trapezoid. The SiRi telescopes can

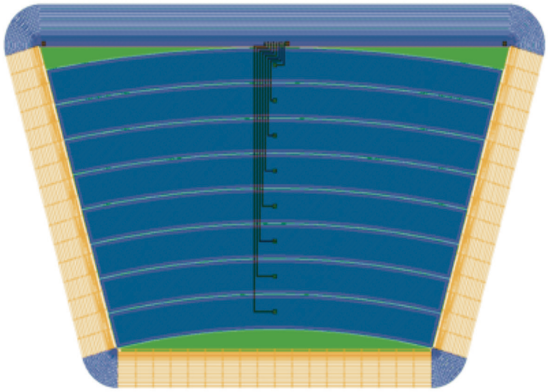

Figure 8.1: Layout of segmented SiRi detector, showing the eight front ΔE counters and the guard ring. The wafer covers about 4 cm^2.

be arranged both in the forward and backward angles covering a total solid angle fraction 6% of 4π. This is roughly 30 times higher solid angle than previously. Therefore, one would expect better statistics in the future experiments. Moreover, the segmented front telescopes will give better particle energy resolution due to better angular resolution.

The group has plans to replace the NaI(Tl) γ-ray detectors with the $LaBr_3$(Ce) scintillation detectors. With $LaBr_3$(Ce) crystals one can achieve the energy resolution of the 662 keV photopeak of ^{137}Cs to be 3% full width half maximum (FWHM), compared to 6.5% in NaI(Tl) scintillators. The light output yield of NaI(Tl) detectors is relative non-proportional to the energy. However, in $LaBr_3$(Ce) detectors a proportional response has been observed. Over the energy range from 60 to 1275 keV, the non-proportionality in the light yield is about 6% for $LaBr_3$(Ce), which is better than for NaI(Tl) where 20% non-proportionality has been observed [35]. In addition to the good energy resolution and proportional response these detectors show good timing resolution and fast response allowing high count rates. Therefore, $LaBr_3$(Ce) is a promising scintillator detector. The future prospect is therefore to replace all the NaI(Tl) detectors of the CACTUS array with the $LaBr_3$(Ce) detectors.

Bibliography

[1] H. A. Bethe, Phys. Rev. **50**, 332 (1936).

[2] M.G. Mayer and G.H.D. Jensen, *Elementary Theorey of Nuclear Shell Structure*, (John Wiley & Sons, New York Inc., and Chapman and Hall Ltd., London, 1995).

[3] W. Hauser and H. Feshbach, Phys. Rev. **87**, 366 (1952).

[4] Data extracted using the NNDC On-Line Data Service from the ENSDF database. URL: http://www.nndc.bnl.gov/ensdf/

[5] RIPL-1: Handbook for calculations of nuclear reaction data, IAEA, Vienna, Report No. IAEA-TECDOC-1024 (1998); RIPL-2: Handbook for calculations of nuclear reaction data, IAEA, Vienna, Report No. IAEA-TECDOC-1506 (2006). URL: http://www-nds.iaea.org/RIPL-2/

[6] M. Guttormsen, T.S. Tveter, L. Bergholt, F. Ingebretsen, and J. Rekstad, Nucl. Instrum. Methods Phys. Res. A **374**, 371 (1996).

[7] M. Guttormsen, T. Ramsøy, and J. Rekstad, Nucl. Instrum. Methods Phys. Res. A **255**, 518 (1987).

[8] A. Schiller, L. Bergholt, M. Guttormsen, E. Melby, J. Rekstad, and S. Siem, Nucl. Instrum. Methods Phys. Res. A **447**, 498 (2000).

[9] E. Melby, L. Bergholt, M. Guttormsen, M. Hjorth-Jensen, F. Ingebretsen, S. Messelt, J. Rekstad, A. Schiller, S. Siem, and S. W. Ødegård, Phys. Rev. Lett. **83**, 3150 (1999).

[10] A. Schiller, A. Voinov, E. Algin, J. A. Becker, L. A. Bernstein, P. E. Garrett, M. Guttormsen, R. O. Nelson, J. Rekstad, S. Siem, Phys. Lett. B **633** 225 (2006).

[11] A. Schiller, M. Guttormsen, E. Melby, J. Rekstad, S. Siem, and A. Voinov, nucl-ex/0011018; Los Alamos preprint server: http://xxxlanl.gov/abs/nucl-ex/0011018.

[12] A. Voinov, E. Algin, U. Agvaanluvsan, T. Belgya, R. Chankova, M. Guttormsen, G.E. Mitchell, J. Rekstad, A. Schiller and S. Siem, Phys. Rev. Lett **93**, 142504 (2004).

[13] M. Guttormsen, R. Chankova, U. Agvaanluvsan, E. Algin, L.A. Bernstein, F. Ingebretsen, T. Lönnroth, S. Messelt, G.E. Mitchell, J. Rekstad, A. Schiller, S. Siem, A.C. Sunde, A. Voinov and S. Ødegård, Phys. Rev. C **71**, 044307 (2005).

[14] A. C. Larsen, M. Guttormsen, R. Chankova, F. Ingebretsen, T. Lönnroth, S. Messelt, J. Rekstad, A. Schiller, S. Siem, N. U. H. Syed, and A. Voinov, Phys. Rev. C **76**, 044303 (2007).

[15] N.U.H. Syed submitted to the Oslo collaboration.

[16] A. C. Larsen, R. Chankova, M. Guttormsen, F. Ingebretsen, T. Lönnroth, S. Messelt, J. Rekstad, A. Schiller, S. Siem, N. U. H. Syed, A. Voinov, and S. W. Ødegård, Phys. Rev. C **73**, 064301 (2006).

[17] N.U.H. Syed, M. Guttormsen, F. Ingebretsen, A.C. Larsen, T. Lönnroth, J. Rekstad, A. Schiller, S. Siem, and A. Voinov., submitted to Phys. Rev. C (2008).

[18] M. Guttormsen, A. Atac, G. Løvhøiden, S. Messelt, T. Ramsøy, J. Rekstad, T.F. Thorsteinsen, T.S. Tveter, and Z. Zelazny, Phys. Scr. **T 32**, 54 (1990).

[19] J.F. Mollenauer, Phys. Rev. 127 (1962) 867.

[20] D. M. Brink, Ph.D. thesis, Oxford University, 1955.

[21] P. Axel, Phys. Rev. **126**, 671 (1962).

[22] A. Gilbert and A. G. W. Cameron, Can. J. Phys. **43**, 1446 (1965).

[23] T. von Egidy and D. Bucurescu, Phys. Rev. C **72**, 044311 (2005); Phys. Rev. C **73**, 049901(E) (2006).

[24] A. Bohr and B. Mottelson, *Nuclear Structure*, (Benjamin, New York, 1969), Vol. I, p. 169, p. 184-185.

[25] J. Kopecky and M. Uhl, Phys. Rev. C**41**, 1941 (1990).

[26] D.J. Morrissey, Annu. Rev. Nucl. Part. Sci. **44**, 27 (1994).

[27] J. M. Blatt and V. F. Weisskopf, *Theoretical Nuclear Physics* (John Wiley & Sons, New York, 1952).

[28] A. Bohr and B. Mottelson, *Nuclear Structure*, (Benjamin, New York, 1969), Vol. I, p. 169, p. 636.

[29] Y.P. Popov, Fiz. Elem. Chastits At. Yadra **13**, 1165 (1982) [Sov. J. Part. Nucl. **13**, 482 (1982)].

[30] S.G. Kadmenskiĭ, V.P. Markushev, and V.I. Furman, Yad. Fiz. **37**, 277 (1983) [Sov. J. Nucl. Phys. **37**, 165 (1983)].

[31] J. Kopecky and R. E. Chrien, Nucl. Phys. **A 468**, 285 (1987).

[32] J. Kopecky and M. Uhl, Phys. Rev. C **41**, 1941 (1990).

[33] M. Uhl and J. Kopecky, Proc. Int. Conf. Nuclear Data for Science and Technology, Gatlinburg, 1994. p. 438.

[34] T. von Egidy, and D. Bucurescu, Phys. Rev. C **72**, 044311 (2005).

[35] K.S. Shah et al. "LaBr3:Ce Scintillator for Gamma Ray Spectroscopy" submitted to IEEE, Trans. Nucl. Sci. , pre-print LBNL-51793, 2002.